University of Basilicata

PhD in
Applied Biology and Environmental Safeguard

THESIS TITLE

CITRATE PATHWAY AND NF-κB: ROLE IN IMMUNOMETABOLISM AND CRITICAL TARGETS FOR MODULATION OF MACROPHAGE FUNCTION INDUCED BY *AGLIANICO DEL VULTURE* RED WINE

Scientific Disciplinary Sector
BIO/13 – Applied Biology

PhD coordinator

Prof. FALABELLA PATRIZIA

PhD student

Dr. SANTARSIERO ANNA

Tutor

Prof. INFANTINO VITTORIA

XXXIII cycle

INDEX

ABSTRACT

Pro-inflammatory stimuli, such as lipopolysaccharides (LPS), induce a metabolic reprogramming in macrophages. Of note is the broken Krebs cycle which allows for the export of citrate from the mitochondria and its accumulation in the cytosol. The mitochondrial citrate carrier (CIC) transports citrate that, once in the cytosol, is broken by ATP citrate lyase (ACLY) into acetyl-CoA and oxaloacetate, precursors for the biosynthesis of chemical mediators of inflammation, namely reactive oxygen species (ROS), nitric oxide ($NO^{\bullet}$) and prostaglandin E2 (PGE2). Citrate also acts as signaling molecule in the inflammatory cascade. The citrate pathway is one of the main players in immunometabolism, an emerging frontier at the interface between immunity and metabolism. We observed that ACLY, even if is downstream of CIC, is upregulated earlier than CIC and its protein and mRNA levels as well as activity fluctuate over time in the first moments of LPS stimulation. We demonstrated that the short-term activation of ACLY is necessary to sustain histone acetylation and transcription of *IL-1β*, *IL6* and *PTGS2* proinflammatory genes. We identified the citrate pathway as a target of *Aglianico del Vulture* red wine in carrying out its anti-inflammatory and immunomodulatory activities. In LPS-activated human macrophages, phenolic compounds of *Aglianico del Vulture* red wine powder (RWP) reduce the secretion of pro-inflammatory cytokines IL-1β, IL-6 and TNF-α and increase the release of IL-10 anti-inflammatory cytokine. Noteworthy, RWP acts on NF-κB signaling pathway by lowering NF-κB protein levels, promoter activity, and p65 nuclear translocation. Because of NF-κB inhibition, reduced promoter activities of *SLC25A1* – encoding CIC - and *ACLY* metabolic genes have been detected. RWP downregulates CIC and ACLY, decreases ACLY activity, the cytosolic citrate concentration, and in turn ROS, $NO^{\bullet}$, PGE_2 and H3 histone acetylation levels. In addition, RWP restores Annexin A1 levels, involved in the resolution of inflammation. All the evidence suggest that the powder of *Aglianico del Vulture* potentially restores the homeostasis of LPS-triggerd macrophages by suppressing inflammatory pathways and activating pro-resolutive processes.

1 INTRODUCTION

1.1 Inflammation

Inflammation occurs when tissues are injured by pathogens (bacteria, viruses, parasites) and/or toxins released by pathogens, trauma, foreign bodies, heat, other stimuli and noxious conditions [1]. Despite the numerous damaging agents, inflammation consists of a dynamic sequence of vascular and cellular events that have constant features, since they are not determined only by the damaging agent, but also by the release of endogenous substances, the chemical mediators of inflammation. Regardless of the trigger, inflammation is as an adaptive response to restore homeostasis, even if there is a transient loss of tissue function, which may in turn contribute to pathogenesis of diseases [2, 3]. Inflammation is a protective response involving the cells of the immune system, capillaries, and molecular mediators. The aim of inflammation is to eliminate the initial cause of cell damage, necrotic cells, and damaged tissues, and to initiate the tissue repair process. Therefore, inflammation is not a negative phenomenon, but a natural and non-specific process, a physiological response to something that the organism considers as "non-self" and wants to eliminate in order to restore homeostasis.

1.1.1. Chemical mediators of inflammation

During the inflammatory response, plasma-derived mediators (the liver is the main source) and cellular mediators of inflammation are released, which exert their activity after binding to specific receptors on target cells. A mediator can induce the release of other mediators with consequent effect of amplification, modulation, or regulation. Chemical mediators of inflammation can exert their action on one or more cell types, on which they can have different effects and they have a short half-life. Almost all mediators are potentially harmful. Plasma-derived mediators include bradykinin and some complement factors.

Cellular mediators of inflammation are divided into two groups:

- ***Preformed mediators***, which include vasoactive amines: histamine released by mast cells and basophils and serotonin secreted by platelets. They cause vasodilation, increase vascular permeability and prostaglandin production.
- ***De-novo synthesized inflammatory mediators***, which in turn are classified into:

- Arachidonic acid metabolites: they are produced by phospholipases that act on phospholipids of cell membranes: leukotrienes via 5-lipoxygenase; prostaglandins and thromboxane A2 via cyclo-oxygenase (COX), COX-1 and COX2. COX-1 is ubiquitous, while COX2 is induced by activating stimuli such as platelet activating factor (PAF), Interleukin 1 (IL-1) and Tumor Necrosis Factor α (TNFα). Arachidonic acid is converted into prostaglandin G2 (PGG2), which in turn, through PGH2, gives life to prostacyclin (PGI2: supports vasodilatation and inhibits platelet aggregation), to thromboxane A2 (TXA2: vasoconstricting and promotes platelet aggregation) and prostaglandins, specifically PGD2 and PGE2 (they support vasodilation and increase vascular permeability). In addition, PGE2 acts on type C nerve fibers (usually in response to bradykinin) by causing pain associated with inflammation and on the hypothalamus causing fever. Non-steroidal drugs (NSAIDs) inhibit COX2 by blocking the synthesis of prostaglandins. Via 5-lipoxygenase, leukotrienes LTC4, LTD4 and LTE4 induce vasoconstriction, bronchospasm and increase permeability, while LTB4 is a chemotactic factor.
- PAF: it is produced by mast cells, neutrophils, endothelium, platelets, monocytes/macrophages; its main proinflammatory actions are to increase vascular permeability, vasodilation, leukocyte adhesion, chemotaxis, and platelet activation and to stimulate other mediators such as leukotrienes and superoxide anion. PAF is stronger than histamine in inducing vasodilation and increasing vascular permeability.
- Reactive oxygen species (ROS): free oxygen radicals are released by leukocytes into the extracellular environment following exposure to chemotactic agents, immune complexes or during phagocytosis. ROS kill viruses and bacteria, but their release can damage the host. Among ROS there are the superoxide anion O_2^-, the hydrogen peroxide H_2O_2 and the hydroxyl radical $OH^{\bullet}$. Superoxide anion is generated from molecular oxygen (O_2) and nicotinamide adenine dinucleotide phosphate (NADPH) by NADPH oxidase according to the following reaction:

$$NADPH + 2O_2 \rightarrow NADP^+ + H^+ + 2O_2^-.$$

Phagocytes, such as neutrophils, eosinophils, monocytes, and macrophages have NADPH oxidase.

- Nitric oxide (NO•): soluble gas produced in immune system cells, especially macrophages, by inducible nitric oxide synthase (iNOS). NO• is synthesized from L-arginine. The conversion of L-arginine to NO• and L-citrulline requires NADPH and molecular oxygen (**Figure 1.1**. NO• has a short half-life, is a powerful vasodilator, reduces platelet aggregation and the adhesion of leukocytes to blood vessels. It is a bactericidal agent. However, under increased oxidative stress, excessive superoxide anion produced is converted into peroxynitrite, a toxic radical form [4].

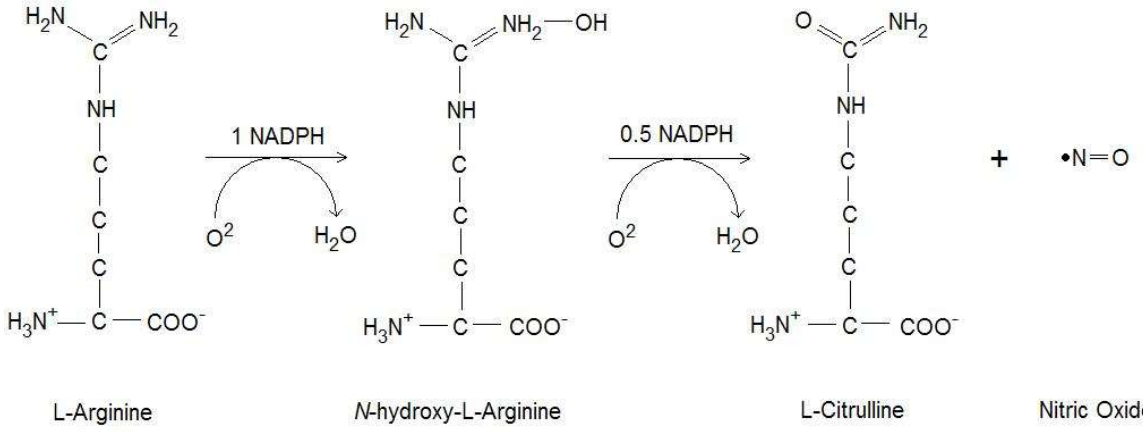

Figure 1.1: Biosynthesis of nitric oxide by nitric oxide synthase from L -arginine. NO• is produced from L-arginine, O_2 and NADPH. Oxidation of L-arginine to L-citrulline requires two successive monooxygenation reactions producing N-hydroxy-L-arginine as intermediate.

- Cytokines: small secreted proteins released by different cell types which modulate the function of other cells and are involved in immunity and inflammation. According to kind of cell that release them, cytokines could be classified in lymphokines (cytokines released by lymphocytes), monokines (cytokines made by monocytes), chemokines (cytokines with chemotactic activities), and interleukins (cytokines secreted by a leukocyte and acting on other leukocytes). Cytokines may be autocrine if they act on the cells that secrete them, paracrine if they act on nearby cells, or may have endocrine action if their activity is on distant cells. Both pro-inflammatory and anti-

inflammatory cytokines exist. Pro-inflammatory cytokines are mainly produced by activated macrophages and have crucial roles in the up regulation of inflammatory reactions. The main pro-inflammatory cytokines are IL-1β, IL-6, TNFα and interferons (especially interferon γ – IFNγ -, which induces phagocytosis in macrophages and granulocytes, induces the production of IL-1 and TNFα and ROS release).

IL-1β is released predominantly by monocytes and macrophages but also by nonimmune cells (fibroblasts and endothelial cells) during cell or tissue injury, infection, invasion, and inflammation. It is pyrogenic and promotes activation, costimulation, and secretion of other cytokines and acute-phase proteins.

TNFα is involved in the regulation of a wide spectrum of biological processes including cell proliferation, differentiation, apoptosis, lipid metabolism, and coagulation. It is produced mainly by macrophages, and large amounts of this cytokine are released in response to lipopolysaccharide (LPS) and IL-1.

IL-6 is mainly secreted by macrophages, T cells, and fibroblasts. It has costimulatory action and induces cell proliferation and differentiation. Additionally, it synergizes with transforming growth factor-beta (TGFβ) to drive toward the phenotype of T helper 17 (Th17) cells.

IL-10 is one of the best-known anti-inflammatory cytokines. It is produced by T-cells, monocytes, mast cells, and to a lesser extent by lymphocytes. It could be released by macrophages but also by T helper cells, Tregs, B cells, dendritic cells. IL-10 has pleiotropic effects in immunoregulation and inflammation. IL-10 causes immune suppression; decreases antigen presentation and MHC (major histocompatibility complex) class II expression of dendritic cells; down- regulates pathogenic Th1, Th2, and Th17 responses. It also enhances B cell survival, proliferation, and antibody production. IL-10 can block NF-κB (nuclear factor kappa-light-chain-enhancer of activated B cells) activity and is involved in the regulation of the Janus kinase (JAK)-signal transducer and activator of transcription (STAT) signaling pathway. IL-10 is important for counteracting excessive immunity

in the human body. IL-10 inhibits the synthesis of IFNγ, IL-2, IL-3, TNF, and GM-CSF secreted by activated macrophages and by T - helper cells.

1.1.2. Inflammatory response: triggers and transcription factors

The process of acute inflammation is initiated by resident immune cells in the damaged tissue, mainly resident macrophages, dendritic cells, and mast cells. These kinds of cells have cell surface receptors, known as pattern recognition receptors (PRRs), which recognize two types of molecules: pathogen-associated molecular patterns (PAMPs) and damage-associated molecular patterns (DAMPs). PAMPs are highly conserved structures of some microorganisms that are not specific to the host organism, such as LPS, a component of the wall of gram-negative bacteria, viral double-stranded RNAs, unmethylated CpG sequences, the terminal mannose residue, that typically lacks in mammalian glycoproteins [5].

DAMPs are host molecules that can induce and perpetuate a non-infectious inflammatory reaction and include intracellular proteins, such as Heat shock proteins (HSP) or proteins deriving from the extracellular matrix following tissue damage, such as fragments of hyaluronic acid, but also DNA, RNA, ATP and uric acid [6, 7].

Following the recognition of the PAMP or DAMP by the PRR (the PRRs also include the Toll-like receptors: TLRs), an intracellular signaling is triggered which has as final event the activation of transcription factors, mainly activator protein 1 (AP-1), STAT and NF-κB [8].

AP-1 is a ubiquitous protein complex formed by the Fos and Jun subunits. It mediates the release of some inflammatory mediators, such as IL-8 [9].

STAT (signal transducers of activated transcription) transcription factors are activated by phosphorylation by cytosolic tyrosine kinases, JAK (Janus kinase), induced, in turn, by the binding of a pro-inflammatory cytokine to its receptor (for example, IFNγ). STAT phosphorylation causes its dimerization (homodimers or heterodimers) and subsequent translocation to the nucleus.

NF-κB transcription factors have a central role in modulating innate and adaptive immune functions. In mammals the family of NF-κB transcription factors comprises five members: NF-κB1 (p105/p50), NF-κB2 (p100/p52), RelA (p65), RelB, and c-Rel. Both NF-κB1 and NF-κB2 are synthesized as large polypeptides that, after translation, are cleaved to generate subunits p50 and p52, respectively. The best characterized member of this family is NF-κB1

(originally defined as NF-κB) which consists of a 50 kDa protein (p50), derived from a 105 kDa precursor, and a 65 kDa protein (RelA). The members of the NF-κB family are characterized by the presence of a highly conserved N-terminal region, which is called Rel homology domain (RHD), that contains a nuclear localization sequence and is involved in sequence-specific DNA binding, dimerization, and interaction with the inhibitory IκB proteins [10]. NF-κB1 and NF-κB2 lack transcriptional activation domains which instead Rel-A, Rel-B, and c-Rel own. The balance between different NF-κB homo- and heterodimers determine which dimers are bound to specific κB sites and thus regulate the level of transcriptional activity. Moreover, the expression of these transcription factors shows a cell- and tissue-specific pattern that provides another level of regulation: NF-κB1 and p65 are ubiquitously expressed, and the p50/p65 heterodimer is the most common inducible NF-κB binding activity. On the other hand, NF-κB2, Rel-B, and c-Rel are found specifically in lymphoid cells and tissues. The p65 subunit also has a transactivation domain at the C-terminus [11].

The main localization of inactive NF-κB complexes is cytoplasmatic due to the masking of their nuclear localization signals (NLS) by κB inhibitors (IκB, IκB-α in p50/p65) [5, 11]. Specifically, IκBα (inhibitor of nuclear factor kappa B) inactivates p50/p65 by masking the NLS of NF-κB proteins and keeping it sequestered in an inactive state in the cytoplasm. All members are structurally related and promote the expression of more than 150 genes, involved in a variety of cellular processes, including genes encoding for cytokines, chemokines, growth factors, immunoregulatory molecules, cell adhesion molecules, acute phase proteins, stress response genes, surface receptors, apoptosis regulators and many others.

Latent NF-κB/IκB cytoplasmic complex is activated in response to different stimuli, such as pro-inflammatory cytokines (TNFα, IL-1 and IL-6), LPS, double-stranded RNA, pathogens, stress-inducing agents [11] (**Figure 1.2**). The mechanism of activation provides the phosphorylation of IκBα by IκB kinase (IKK) and its subsequent ubiquitination and degradation by the proteasome (**Figure 1.2**). Active NF-κB translocates from cytosol to the nucleus and binds to DNA in the promoter or enhancer regions of specific genes, determining their transcription [5] (**Figure 1.2**). NF-κB is a critical regulator of several genes involved in inflammation.

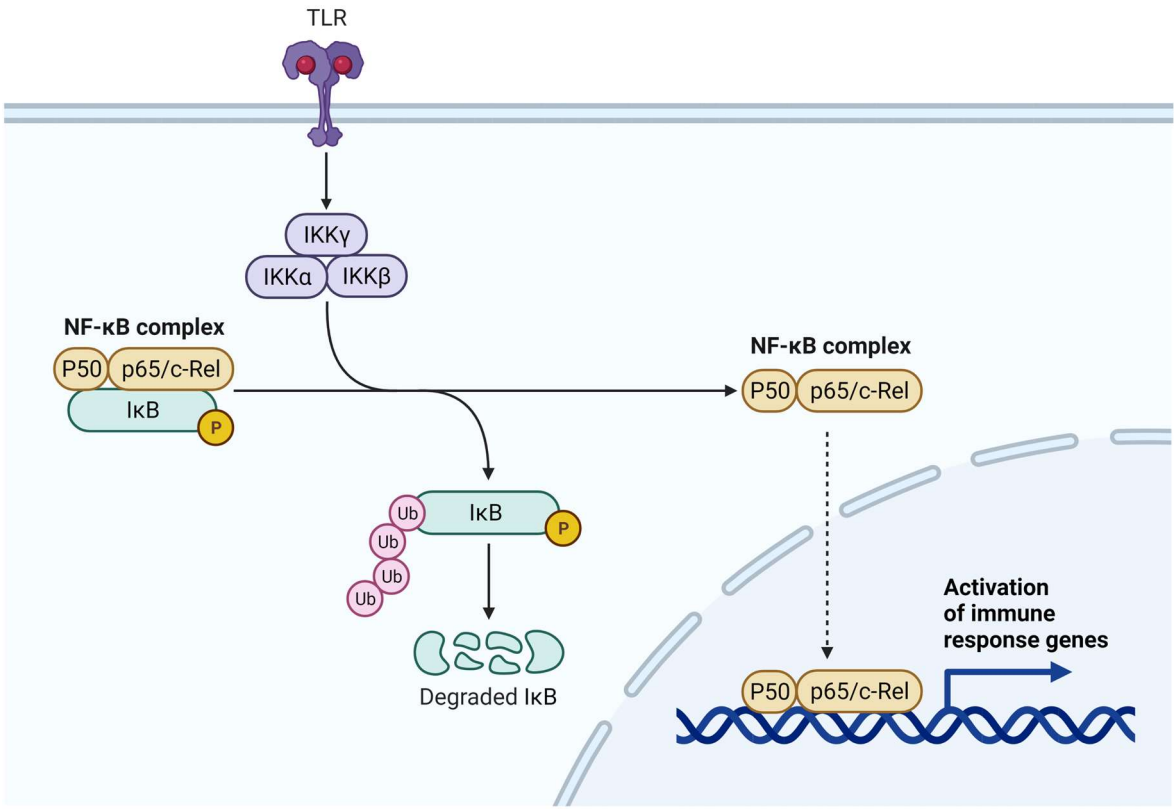

Figure 1.2: The canonical NF-κB signaling pathway. The canonical NF-κB pathway responds to different stimuli which binds TLR, including various cytokines, growth factors, mitogens, microbial components, and stress agents. The primary mechanism is the degradation of IκBα triggered through its site-specific phosphorylation by IKK, made of two catalytic subunits, IKKα and IKKβ, and a regulatory subunit, IKKγ. Upon activation, IKK phosphorylates IκBα and, thereby, triggers ubiquitin-dependent IκBα degradation in the proteasome, resulting in rapid and transient nuclear translocation of NF-κB members (predominantly the p50/p65 and p50/c-Rel dimers). In the nucleus, NF-κB complex induce the transcription of immune response genes.

1.1.3. Macrophages: role in inflammation and classification

All blood cells originate within the bone marrow from a single type of unspecialized cell called stem cell. The monoblast represents the first stage of monocyte-macrophages: once mature, the monoblast pours into the bloodstream as a monocyte. Monocytes have a diameter of 10-15 μm, a bean shaped nucleus and a finely granular cytoplasm containing lysosomes, vacuoles, and cytoskeletal filaments. Monocytes migrate from the bloodstream into other tissues where they differentiated into resident macrophages or dendritic cells. At the migration site, macrophages acquire different cytomorphological feature according to the tissue in which they are. Macrophages are called microglia cells in the central nervous system, Kupffer cells in the liver, alveolar macrophages in the lung, osteoclasts in the bone. In connective tissues, macrophages could be in a quiescent state or in an activated one. In

the first case they are resident macrophages: they are attached to the extracellular matrix with their cytoplasmic extensions, reason for which they have a star shape. In inflammatory processes, macrophages undergo structural and functional changes and become activated.
The term "macrophages" derives from Greek (μακρός (makrós) = large, φαγεῖν (phagein) = to eat) and means big eaters. In fact, macrophages are white blood cells that defend the host against infection and injury carrying out phagocytosis. Indeed, they are highly heterogeneous phagocytic cells which engulf and digest anything that is "non-self" including cancer cells, microbes, cell debris, extraneous substances. Macrophages, together with dendritic cells (DCs), belong to the innate immune system that is the first line of defense against infection. These cells have pathogen recognition receptors that allow for the recognition of PAMPs and DAMPs from damaged tissues or cells [12]. Macrophages and DCs are crucial for the initiation and resolution of the immune response since they both produce inflammatory mediators, carry out phagocytosis and release chemokines useful for the recruitment of other immune cells to the site of infection [13]. DCs have a key role also in the initiation of adaptive immune response since they activate naive T cells as they can present antigen to the T cells [14].
Macrophages stood throughout the body to guarantee tissue homeostasis; thus, they are found in all tissues and they can adopt distinctive phenotypes to adapt to specific environmental cues. Thanks to this strong plasticity, macrophages display great anatomical and functional diversity what makes them have roles in immunity, homeostasis, development, and tissue repair [15]. Emerging evidence in the last decade revealed that these different functions are convoyed by specific reprogramming of macrophages metabolism.
According to their inflammatory nature, macrophages are commonly classified as per the dichotomous categorization M1 or M2, that is classic *vs.* alternative activated macrophages (**Figure 1.3**). The M1 and M2 paradigm of macrophage activation is used to mimic T helper (Th) cell nomenclature founded on the different cytokines released by Th1 and Th2 cells [16, 17]. Th1 cells are triggered by the polarizing cytokine interleukin (IL)-12 and secrete IFNγ, a cytokine that activates macrophages and dendritic cells enhancing their ability to kill intracellular bacteria and protozoa. Th1 cells also release TNF and IL-2, which contribute to antimicrobial defense. On the other hand, Th2 cells triggered by the polarizing

cytokines IL-4 and IL-2, produce as main effector cytokine IL-4 and are linked to allergic responses and protection against extracellular protozoa such as helminths.

In the 1960s the term "macrophage activation" was coined by Mackaness after discovering that in mice the resistance to infection was linked to enhanced antimicrobial mechanisms because of the activation of macrophages [18]. Twenty years later, IFNγ was identified as responsible for the induction of such classical macrophage activation and consequent antimicrobial response [19]. IFNγ, the main cytokine released by Th1 cells, was found to increase the synthesis of pro-inflammatory cytokines in macrophages and inhibit the expression of the mannose receptor on macrophages. Conversely Th2 cells-derived IL-4 reduced pro-inflammatory cytokine secretion and enhanced the mannose receptor expression [20]. The last opposing reaction to the classical form of activation was considered as an "alternative" form of macrophage activation.

The M1/M2 terminology was introduced after the observation of Mills who discovered that LPS and IFNγ elicit divergent effects and distinct metabolic programs on macrophages isolated from different prototypical Th1 and Th2 mouse strains. In macrophages isolated from so-called Th1 strains (C57BL/6) LPS and IFNγ stimulate NO production in large quantities and induce Th1 driven inflammatory responses, whereas the same triggers prompt arginine metabolism to ornithine in macrophages isolated from Th2 strains (Balb/c) and stimulate Th2 responses [21].

Over time, M1 macrophages became incorrectly synonymous with classical activated macrophages and M2 with alternative activated macrophages [22]. Generally, M1 are macrophages stimulated with TLR ligands such as LPS from Gram-negative bacteria and lipoteichoic acid (LTA) - typical of Gram-positive bacteria, IFNγ, a combination of INFγ and LPS, granulocyte-macrophage colony-stimulating factor (GM-CSF) (**Figure 1.3**). M1 macrophages express specific transcription factors: NF- κB, STAT and interferon regulatory factors (IRFs), AP-1 which control inflammatory profiles characterized by secretion of pro-inflammatory cytokines (e.g. IL-6, TNFα, IL-12 and IL-1β), chemokines (e.g. chemokine (C-C motif) ligand 2 (CCL2) and chemokine (C-X-C motif) ligand 10 (CXCL10)) and antigen presentation molecules including major histocompatibility complexes (**Figure 1.3**) [23]. Moreover, M1 macrophages secrete large quantities of ROS and NO• – as consequence of iNOS upregulation - to ensure effective killing of pathogens.

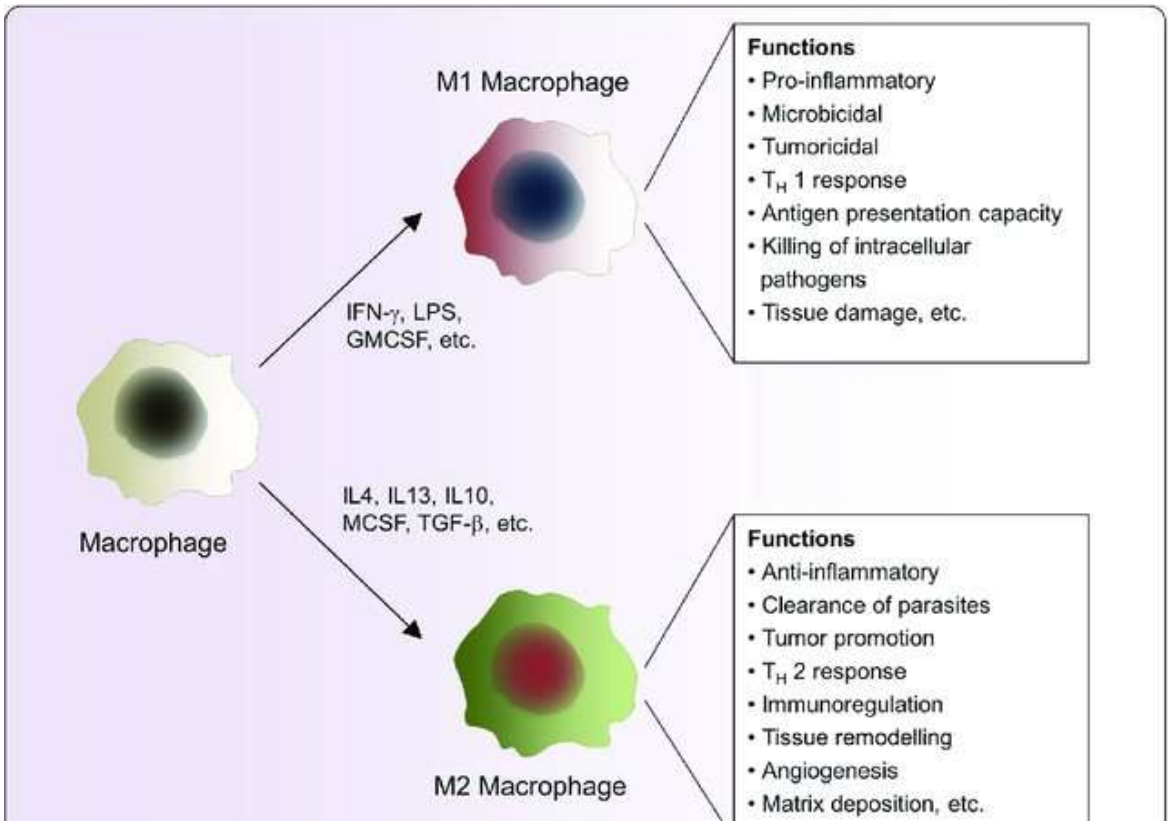

Figure 1.3: M1 and M2 paradigm of macrophage activation. Different stimuli polarize toward M1 and M2 macrophages. M1 and M2 macrophages have opposite functions, different phenotypes, and release pro-and anti-inflammatory cytokines respectively [24].

Conversely, IL-4 is the main stimulus associated with M2 macrophages and induces activation of STAT6, accompanied by inhibition of pro-inflammatory signals production, increased arginase activity, elevated expression of the mannose receptor and a specific set of genes and surface makers. Different activation signals may induce M2 polarization: as consequence distinct phenotypes exist. More in detail, M2 macrophages can be divided in regulatory or wound-healing macrophages. Prostaglandins, apoptotic cells, and IL-10 can trigger differentiation in regulatory macrophages which are important in resolutive phases of inflammation. They release the immunosuppressive cytokine IL-10. On the other side, wound-healing macrophages regenerate the damaged tissue thanks to the production of IL-4 and upregulation of arginase activity, that is the enzyme responsible for the production of polyamines and collagen (**Figure 1.3**) [25].

In conclusion, M1 and M2 macrophages show opposite functions: while M1 macrophages have a key role in the host defense being phagocytic cells, M2 macrophages resolve

inflammation and are associated with healing powers to support tissue integrity (**Figure 1.3**) [26]. However, recent transcriptomic analyses evidenced multiple distinct macrophage activation states [27]. Therefore, the M1/M2 paradigm of macrophages activation is rather an oversimplified *in vitro* model that cannot represent the complex *in vivo* environment that determines macrophage polarization. Nevertheless, the dichotomy M1/M2 macrophages provides a reductive tool to analyze the functions of macrophages and their roles in diseases.

1.2 Metabolism

The term metabolism is used to describe the set of reactions typical of each organism that determine its growth, renewal, and maintenance. Metabolism includes catabolic processes, which, through the demolition of molecules, allows for obtaining energy and anabolic processes, which lead to the synthesis of new compounds. Metabolism is based on the production and the use of energy in the form of adenosine triphosphate (ATP). Energy is obtained thanks to the oxidation of nutrients. Therefore, metabolism is the process that allows the generation of energy in the form of ATP by breaking down sugars (50-55% energy needs), lipids (40-45% energy needs) and proteins (5% energy needs). Foods have not only an energetic role but also a plastic role, since they provide the substances for the growth, and maintenance of structural integrity of the organism.

The cell factories of energy are mitochondria: they are involved in the Krebs cycle and oxidative phosphorylation (OXPHOS), to generate a proton gradient which is exploited by ATP synthetase for ATP production.

Catabolism includes all metabolic processes that allow for the breakdown and oxidation of the molecules adsorbed with food: proteins, polysaccharides, and lipids. Macromolecules such as polysaccharides (starch and cellulose) and proteins are digested, respectively, by glycosidases into monosaccharides and by proteases into amino acids. In the cell, sugars, such as glucose and fructose, are converted by glycolysis into pyruvate and two ATP molecules. Under anaerobic conditions, glycolysis produces lactate: through the enzyme L-lactate dehydrogenase, NADH is oxidized to NAD^+ and reused in glycolysis to obtain energy (2 ATP per glucose molecule).

Pyruvate is an intermediate in several metabolic pathways, but most of it crosses the mitochondrial membranes and in the mitochondrial matrix is transformed into acetyl-coenzyme A (acetyl-CoA) in the reaction known as oxidative decarboxylation of pyruvate. Acetyl-CoA fuels the Krebs cycle (**Figure 1.4**), also known as the citric acid cycle and the tricarboxylic acid (TCA) cycle, whose most important product, besides ATP, is NADH. A molecule of FADH2 (flavin adenine dinucleotide) is also produced. This reaction releases carbon dioxide (CO_2). TCA cycle is an amphibolic metabolic pathway because, in addition to being involved in the catabolism of sugars, proteins and fatty acids, it supplies α-ketoglutarate and oxaloacetate for the biosynthesis of amino acids (aspartate and glutamate, respectively) while oxaloacetate is converted to phosphoenolpyruvate during gluconeogenesis.

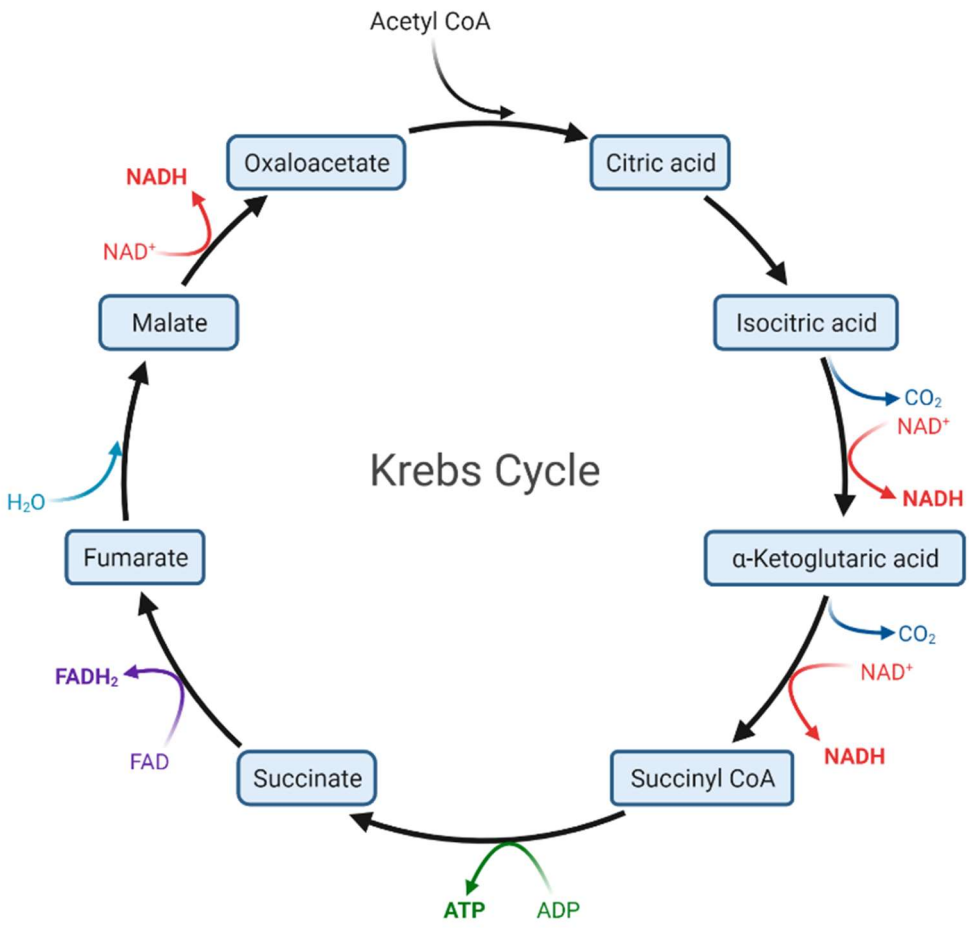

Figure 1.4: Krebs cycle. The Krebs cycle consists of eight reactions that allow the oxidation of acetyl-CoA to CO2 and the production of energy molecules: NADH, FADH2 and ATP.

An alternative pathway for glucose degradation is the pentose phosphate pathway (PPP), which occurs in the cytoplasm and generates pentoses such as ribose and NADPH, necessary for anabolic processes.

The ingested lipids, especially triglycerides, are hydrophobic and are converted into micelles by bile salts to increase the surface exposed to water-soluble lipases, whose action produces fatty acids, mono-di-triglycerides, and glycerol. Fatty acids have more atoms of oxygen, compared to carbohydrates for which more energy is obtained from their complete oxidation (sugars provide 4.2 kcal/g, lipids 9.3 kcal/g and proteins 4.4 kcal/g). While glycerol is converted to dihydroxyacetone, and then glyceraldehyde, and enterprises the glycolysis, fatty acids are degraded by sequential removals of acetate units. This process, which takes place in the mitochondria, is the β-oxidation of fatty acids and involves the release of acetyl-CoA which can enter the citric acid cycle.

Amino acids are used either for the synthesis of proteins or they could be oxidized to urea and CO_2 to obtain energy. The oxidation begins with the removal of the amino group by aminotransferases and its transfer to a keto acid to form glutamate. Glutamate can undergo oxidative deamination and give ammonium ions and α-ketoglutarate, which can enter the Krebs cycle or be used for glucose synthesis or in transamination reactions.

The carbon skeleton of some amino acids can be converted into pyruvate or other intermediates of the Krebs cycle (α-ketoglutarate, succinyl-CoA, fumarate, oxaloacetate). These amino acids are called glucogenic to differentiate them from ketogenic ones, which can be used for the synthesis of fatty acids and the production of ketone bodies because their carbon skeleton is converted into acetyl-CoA and acetoacetyl-CoA.

It is possible to identify three phases in metabolism:

1. Glucose, fatty acids, and amino acids are degraded to acetyl-CoA (**Figure 1.5**).
2. The Krebs cycle (**Figures 1.4-1.5**), which consists of eight reactions that allow for the oxidation of the two carbon atoms of acetyl-CoA to CO_2 and the production of three molecules of NADH, one of $FADH_2$ and one of ATP. In addition to this catabolic role, TCA cycle also has an anabolic role since it produces metabolic intermediates used in different biosynthetic pathways.
3. The coenzymes NADH and $FADH_2$, produced by both glycolysis and the Krebs cycle, are oxidized, with the transfer of reducing equivalents to molecular oxygen,

through the components of the electron transport chain. Oxidation is coupled with the synthesis of ATP in the process of oxidative phosphorylation (**Figure 1.5**).

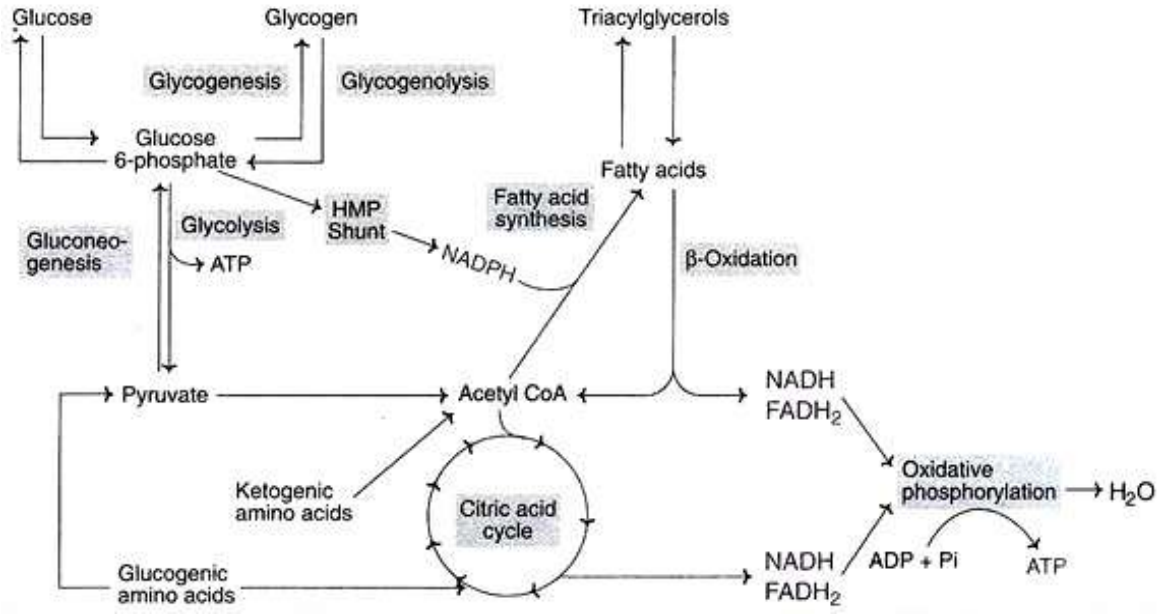

Figure 1.5: Overview of the integration and interaction of metabolic pathways.

1.3 Immunometabolism

In the last decades, different studies have been evidenced that immune cells undergo intense metabolic reprogramming following environmental changes, such as hypoxia and nutrient alterations, but also in response to activating stimuli such as LPS and cytokines. This evidence has been determined the birth of the immunometabolism, a branch of biology which deals the interplay between metabolism and immunology.

The term “immunometabolism” first appeared 10 years ago, in 2011, when Mathias and Shoelson defined it as "an emerging field of investigation at the interface between the historically distinct disciplines of immunology and metabolism" [28]. In 2016 O'Neill, Kishton and Rathmell described immunometabolism as "the changes that occur in intracellular metabolic pathways in immune cells during activation" [29].

The term "immunometabolism" gives the idea that changes in metabolism determine the phenotype of the cells of the immune system by controlling the transcriptional and post-transcriptional events that are central to their activation.

This convergence between metabolism and the immune system is becoming evident especially in macrophages, but it is also a feature of T lymphocyte polarization and activation of dendritic cells (and maybe of all other immune cells) [30].

1.3.1. Metabolism dictates macrophage activation

The foundation of the dichotomous M1/M2 macrophages classification is the different way to metabolize arginine. In M1 macrophages iNOS, the enzyme that convert arginine into NO and citrulline, is upregulated while M2 macrophages exhibit increased arginase activity to form urea and ornithine. The last one is the precursor for polyamines and collagen important for supporting repair processes. On the other hand, NO released by M1 macrophages inhibits cell proliferation and is useful in the fight against pathogens. M1 macrophages kill speedily pathogens which are able to proliferate very quickly and this function is crucial since adaptive immunity is relatively slow to act as first line of defense [26]. Therefore, M1 macrophages need energy and biosynthetic products rapidly to supply the short-lived antimicrobial and inflammatory responses [31]. Conversely, M2 macrophages require a more sustained source of energy since they are involved in more long-lasting repair processes. Changes in intracellular metabolism during macrophage activation happen and recent emerging evidence in the field of immunometabolism have increased our understanding of processes. Upon activation stimuli, immune cells undergo the reprogramming of their metabolic pathways also to produce metabolites that can act as signaling molecules.

Macrophages as well as DCs must be able to switch quickly from a resting to an activated state. In M1 macrophages glycolysis and the pentose phosphate pathway are upregulated, the Krebs cycle has two breakpoints and the fatty acid oxidation and oxidative phosphorylation are downregulated [31] (**Figure 1.6**).

Likewise, TLR-activated DCs show increased aerobic glycolysis and decreased OXPHOS and FAO [32]. M2 macrophages display also upregulate glycolysis, but the Krebs cycle is complete and OXPHOS works well [31].

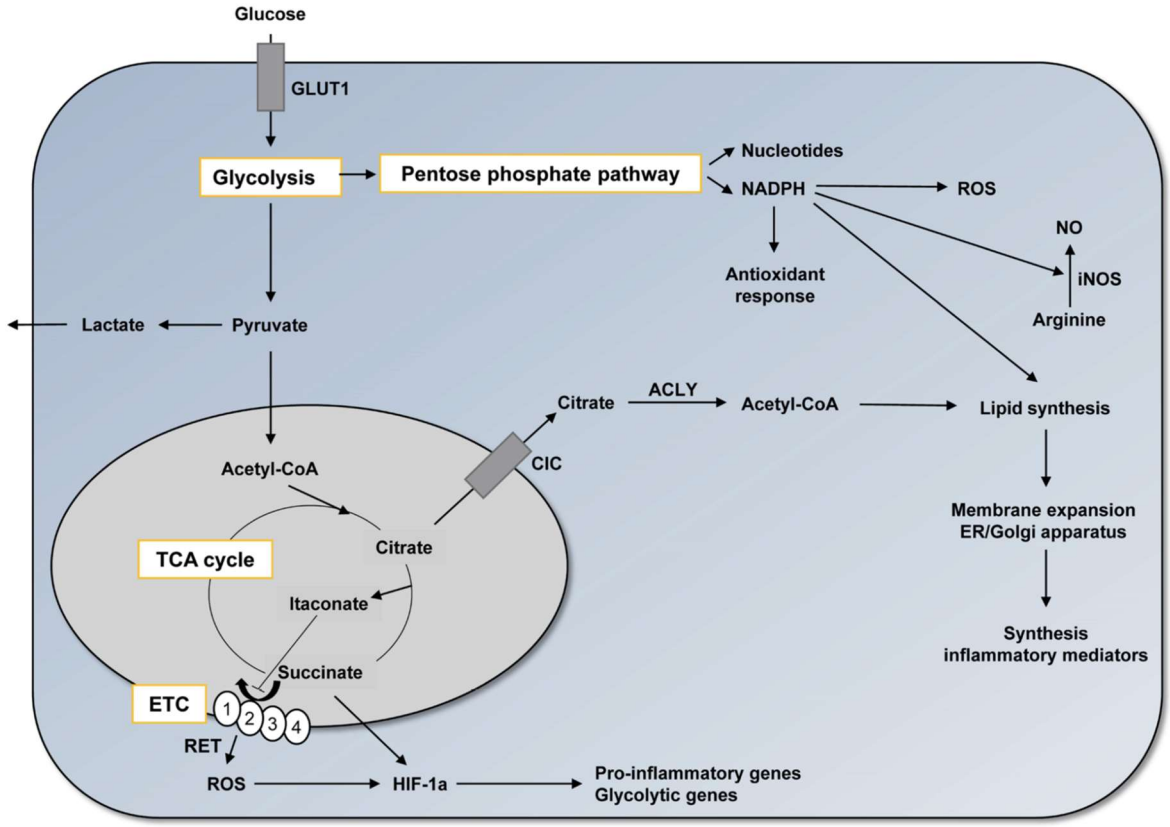

Figure 1.6. Schematic representation of the interplay between cellular metabolism and inflammatory responses in macrophages.

1.3.1.1. Glycolysis

M1 macrophages show a higher production of lactate and a decreased oxygen consumption. A similar phenomenon is typical of tumor cells which predominantly utilize glycolysis even in the abundance of oxygen. This phenomenon is well-known as the Warburg effect [33]. In this metabolic scenario, most glycolysis-derived pyruvate is reduced to lactate, instead of been oxidized in the Krebs cycle to feed the electron transport chain (ETC) and oxidative phosphorylation. The switch from OXPHOS towards aerobic glycolysis is the main energy source in M1 macrophages. This could seem faulty since in OXPHOS 36 molecules of ATP are generated per glucose molecule while glycolysis produces only two molecules of ATP. Indeed, although less efficient in ATP production, glycolysis can be induced rapidly instead of OXPHOS that requires the induction of mitochondrial biogenesis, a longer and more complex process. Moreover, glycolysis guarantees the reduction of NAD^+ to NADH, which is co-factor of different enzymes. Furthermore, glycolytic intermediates can support

biosynthetic processes during macrophage activation fueling other anabolic pathways such as the pentose phosphate pathway. Therefore, glycolysis upregulation supplies energy and biosynthetic products, crucial for inflammatory macrophages that must act rapidly being the first line of host defense.
Glucose transporter 1 (GLUT1) is overexpressed during polarization to M1 macrophages to boost rapid glucose uptake and glycolysis [34].

1.3.1.2. Pentose phosphate pathway

Glycolysis supplies glucose-6-phosphate that can be diverted to the pentose phosphate pathway. During inflammatory responses, in M1 macrophages the glucose flux towards the PPP is elevated to satisfy the increased cellular demands of energy and biosynthetic products [35]. Pentose phosphate pathway is made of two phases: a first oxidative one that provides NADPH and the non-oxidative phase which generates ribose sugars. NADPH is used as co-factor by NADPH oxidase and iNOS for ROS and NO production, respectively. Moreover, NADPH counteracts the increased oxidative stress when is reduced to glutathione and, acting as a reducing equivalent, is required for different biosynthetic reactions, such as fatty acids synthesis. Fatty acids are important during inflammatory responses both to expand the membranes of the endoplasmic reticulum and the Golgi apparatus for cytokines synthesis and as precursor of prostaglandins. On the other side, ribose sugars serve as precursors for the synthesis of nucleotides and induce specific transcriptional programs during macrophage activation [36].

1.3.1.3.Krebs cycle

M1 macrophages show several breaks in the tricarboxylic acid cycle, resulting in the accumulation of metabolites succinate, itaconate and citrate [37, 38]. Isocitrate dehydrogenase, the enzyme responsible for the conversion of citrate to alpha-ketoglutarate, was downregulated with consequent accumulation of citrate. Citrate could be used for the synthesis of itaconic acid, which has anti-microbial properties [39] or for fatty acid biosynthesis or channeled into the citrate pathway, that will be discuss further on. The second breakpoint occurred after succinate: in the TCA cycle, succinate is converted to fumarate from which derives malate. Oxidation of accumulated succinate via succinate

dehydrogenase (SDH) drives inflammatory responses [40] since it leads to reverse electron transport (RET) in complex I driving the production of ROS, which in turn activate HIF1α, transcription factor that promotes aerobic glycolysis. Increased levels succinate in the cytosol inhibit the prolyl hydroxylase domain enzymes, potentiating the stabilization of HIF1α [41]. Among HIF-target genes there are those encoding for glycolytic enzymes, the glucose transporter GLUT1, lactate dehydrogenase (LDH) [42, 43] and the pro-inflammatory cytokine interleukin-1β [44]. Itaconate is a competitive inhibitor of SDH [45] and is required for activation of transcription factor NRF2 (nuclear factor erythroid 2–related factor 2) involved in antioxidant and anti-inflammatory responses [46]. Thus, while succinate acts as a pro-inflammatory metabolite, itaconate has anti-inflammatory function.

1.3.1.4.Electron transport chain and oxidative phosphorylation

NADH and FADH2 generated in the Krebs cycle furnish high-energy electrons which are transferred to molecular oxygen thanks to the electron transport chain made of a series of protein complexes embedded in the mitochondrial inner membrane (complex I-IV) that transfer electrons from electron donors to electron acceptors via redox reactions. The transfer of electrons across the ETC releases energy employed to pump positively charged protons from the mitochondrial matrix to the intermembrane space. The consequence is the generation of an electrochemical proton gradient (ΔΨm) across the mitochondrial membrane responsible for a proton-motive force that drives ATP synthase (complex V) to phosphorylate ADP to ATP in the process known as oxidative phosphorylation.

The switch from OXPHOS to glycolysis as the main source of ATP generation is one of the most relevant metabolic hallmarks of M1 macrophages. High levels of nitric oxide produced during polarization to M1 macrophages damage the ETC and the synthesis of ATP and contribute to the switch toward glycolysis [47]. As consequence of the metabolic switch to glycolysis, the protons buildup in the intermembrane space accompanied by an increased ΔΨm occurs [40]. In M1 macrophages the elevated ΔΨm contributes, together with the accumulated succinate, to mitochondrial ROS production that induces HIF-1α stabilization and IL-1β secretion.

In M1 macrophages succinate is rapidly oxidized by complex II (succinate dehydrogenase). However, because of the high ΔΨm, complex III cannot accept the excessive electrons

supplied by complex II and they are forced back to complex I (Reverse electron transport) with consequent ROS production [48]. Thus, mitochondria upon M1 activation produce ROS rather than energy.

1.3.1.5. Fatty acid synthesis and oxidation

In M1 macrophages increased pentose phosphate pathway provides NADPH while TCA cycle furnishes citrate which both support the synthesis of fatty acids [49]. TCA-cycle derived citrate is exported from the mitochondria into the cytosol by the mitochondrial citrate carrier (CIC) where it is converted by ATP citrate lyase (ACLY) to acetyl-CoA which acts as precursor for fatty acid synthesis. Moreover, the enhanced activation of sterol regulatory element binding protein 1a (SREBP-1a) upon M1 polarization contributes to augmented fatty acid biosynthesis [50]. Fatty acids are essential to produce membranes necessary for the expansion of the ER and Golgi to facilitate increased secretion of pro-inflammatory proteins such as cytokines and for antigen presentation. Additionally, acetyl-CoA derived from ACLY is linked to the production of pro-inflammatory prostaglandin E2 [51].

M1 macrophages exhibit increased fatty acid synthesis and decreased fatty acid oxidation (FAO) [49]. FAO is the opposite to fatty acid synthesis so that during this metabolic process, fatty acids are broken down to NADH, FADH2 and acetyl-CoA in the mitochondria. Carnitine palmitoyltransferase I (CPT1) is one of the crucial regulatory enzymes involved in FAO and mediates the transport of long-chain fatty acids to the mitochondria for oxidation. CPT1 and FAO are repressed in M1 macrophage but boosted in M2 macrophages.

1.3.2. Metabolic rearrangement in dendritic cells upon immunogenic stimulation

Resting dendritic cells are characterized by a catabolic metabolism that shows active OXPHOS, driven by TCA cycle fueled via fatty acid oxidation and glutaminolysis [14]. Resting DCs use intracellular glycogen, apart from glucose, to support glycolysis and obtain metabolic substrates for mitochondrial respiration [52]. Upon immunogenic stimulation, DCs often switch to an anabolic metabolism that allows for the generation of substrates useful for cell growth and biosynthesis [13]. Activated DCs switch to glycolysis and lactic

fermentation that provide energy and glycolytic intermediates fuels the PPP. Although increased glucose uptake by DCs in the first stages after activation is linked to lactate production, Warburg metabolism is not used as a mechanism for ATP production because OXPHOS provides ATP during this time [47]. Rather, glycolysis fulfills a need of activated DCs for citrate, important after his export into the cytosol by CIC for fueling fatty acid synthesis, thus support the biosynthesis of *de novo* lipids, necessary for the expansion of the endoplasmic reticulum and Golgi apparatus and to increase the biosynthetic capacity essential for the functions of mature DCs. Moreover, NO• production is induced with consequent inhibition of ETC. The TCA cycle is rewired, leading to accumulation of TCA intermediates that act as immunomodulatory signals, support FAS and ROS and NO• production [13, 14, 29]. Succinate also induces DCs chemotaxis to allow for antigen presentation to T lymphocytes. The second phase occurs after eighteen hours when the activated dendritic cells pass to glycolysis and inactivate OXPHOS: this metabolic change is important for regulating responses of T lymphocytes, partly due to the fact that it thus increases the cell half-life for the time it takes for the dendritic cell to activate the T lymphocyte [53].

1.4 Citrate metabolism

Citrate has crucial and multiple roles in cellular metabolism. Citrate is synthesized in the first reaction of Krebs cycle by citrate synthase (CS) from the aldol condensation of oxaloacetate (OAA), produced from a previous turn of the cycle, and acetyl-CoA. Acetyl-CoA may be derived from pyruvate, the end product of glycolysis, or from fatty acids that have undergone β-oxidation [54]. In the TCA cycle, citrate is converted into cis-aconitate, which in turn is converted in isocitrate [54]. Isocitrate is the substrate of IDH that convert it to α-ketoglutarate (αKG) in a decarboxylation reaction [54]. The complete oxidation of citrate in the TCA represents the major source of ATP in cell.

Citrate has a regulatory role in the metabolism since it blocks or activates enzymes of glycolysis, Krebs cycle, gluconeogenesis, and fatty acids synthesis (**Figure 1.7**). Citrate inhibits citrate synthase by product inhibition. High concentration of citrate in the cytosol can directly inhibit specific enzymes of glycolysis: phosphofructokinase (PFK) 1 and PFK2 and pyruvate kinase (PK). PFK1 and PFK2 are directly inhibited by citrate while PK

inhibition is due to decreased levels of fructose-1,6-bisphosphate, which is a PK activator [55]. High levels of citrate can block the Krebs cycle since citrate inhibits pyruvate dehydrogenase (PDH) and SDH. On the contrary, citrate triggers anabolic pathways such as gluconeogenesis and fatty acid synthesis. By activating Acetyl Coenzyme A Carboxylase (ACC), citrate leads to production of malonyl-CoA which can block FAO by CPT1 inhibition. Citrate can activate the gluconeogenesis since it regulates fructose 1,6-bisphosphatase (FBPase1) and stimulates fatty acid synthesis acting on ACC.

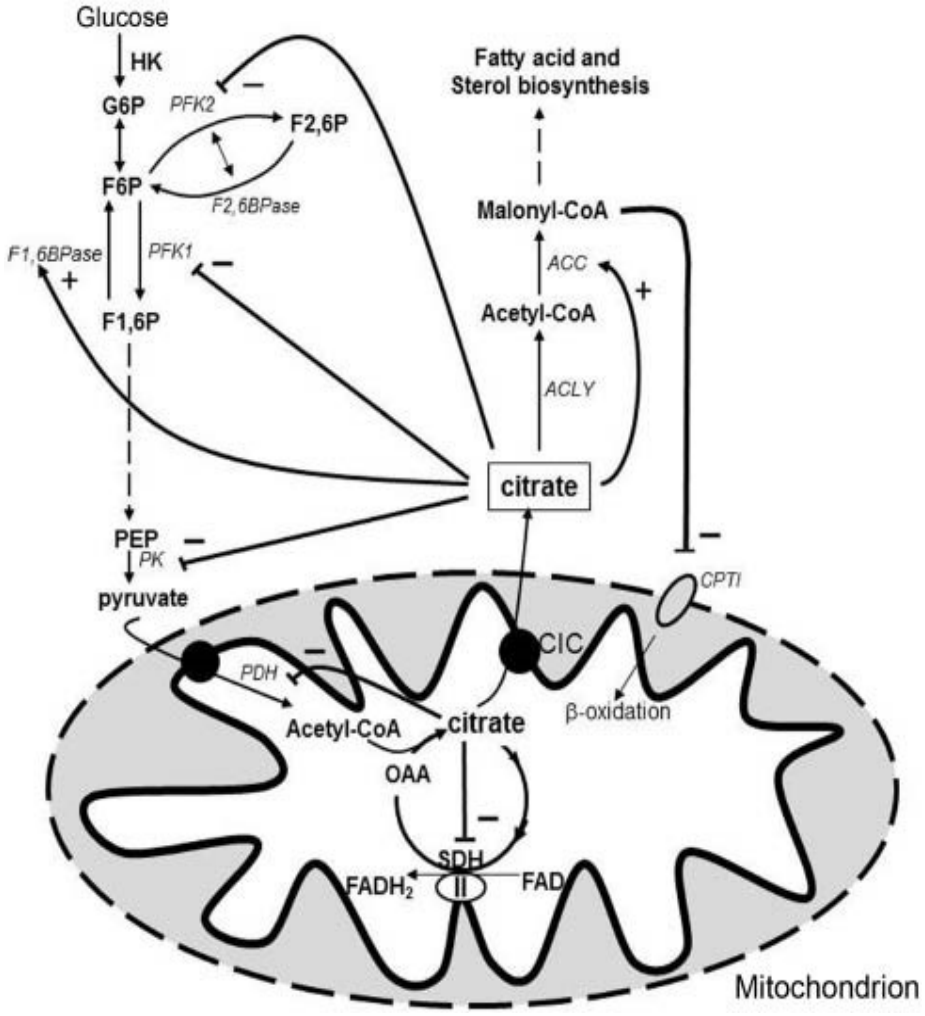

Figure 1.7: Regulatory role of citrate in metabolism. Citrate is synthesized in the first reaction of Krebs cycle by citrate synthase (CS) from acetyl-CoA and oxaloacetate (OAA). CIC exports citrate from mitochondria to cytosol. Citrate inhibits PFK1, PFK2, PK, PDH, and SDH. Citrate supports lipid biosynthesis through ACC, which produces malonyl-CoA, the first product of lipid biosynthesis, which, in turn, inhibits the CPT-1, the first enzyme of β-oxidation reaction. Through fructose 1,6 bisphosphatase (F1,6BPase), citrate stimulates gluconeogenesis. Abbreviations: ACC, acetyl-CoA carboxylase; G6P, glucose-6-phosphate; F6P, fructose-6-phosphate; HK, hexokinase; PEP, phosphoenolpyruvate [54].

Citrate is exported from the mitochondria to cytosol via the mitochondrial citrate carrier. CIC is encoding by solute carrier family 25 member 1 (*SLC25A1*) gene. As all mitochondrial carriers, whose function is known, the citrate carrier belongs to the protein family SLC25 (solute family carrier 25) [56]. Mitochondrial carriers are integral membrane proteins, responsible for the specific transport of substrates across the inner mitochondrial membrane from the cytosol to the mitochondria and vice versa [57]. As driving force for transport they exploit the concentration gradient of the solutes and/or an electrochemical gradient of protons ($\Delta\mu H^+$) [58].

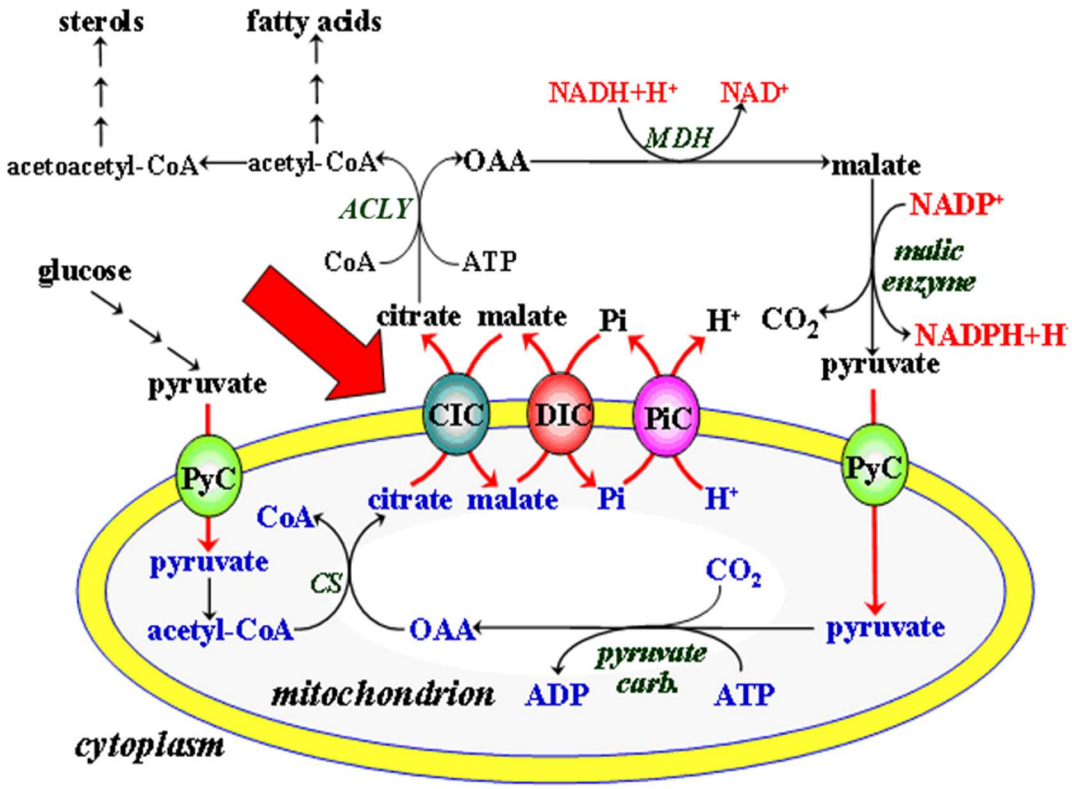

Figure 1.8: Mitochondrial and cytoplasmic fate of citrate. Glycolysis derived pyruvate enters the mitochondrion via PyC (pyruvate carrier) and is converted into acetyl-CoA which condenses with OAA to generate citrate through CS (citrate synthase). CIC catalyzes the electroneutral exchange between the citrate and the malate. The citrate in the cytosol is cleaved by ACLY into acetyl-CoA and OAA, both of which are involved in the biosynthesis of sterols and fatty acids. OAA, through MDH (malate dehydrogenase) and the malic enzyme is converted into pyruvate which re-enters the mitochondrion through PyC. The activity of CIC is closely associated with DIC (carrier of dicarboxylic acids) and PiC (carrier of phosphate) for malate recycling.

CIC catalyzes the electroneutral exchange between citrate and malate [58] (**Figure 1.8**). Once in the cytosol, in the presence of ATP and CoA, citrate is cleaved by ATP-citrate lyase (ACLY), into OAA and acetyl-CoA, which lead to the biosynthesis of sterols and fatty acids

(**Figure 1.8**). OAA is reduced by malate dehydrogenase (MDH) to malate and, in turn, converted into pyruvate by the malic enzyme with consequent production, in the cytosol, of NADPH $^{+}$/ H^{+} ($NADPH^{+}$ contributes to the synthesis of sterols and fatty acids) (**Figure 1.8**). At this point pyruvate re-enters the mitochondria, through the citrate-pyruvate shuttle (PyC), and malate, necessary for the release of the citrate, is recycled by the dicarboxylate carrier (DIC) in exchange for inorganic phosphate, which enters in the mitochondrion thanks to phosphate carrier (PiC) (**Figure 1.8**). On the other hand, acetyl-CoA is carboxylated by ACC into malonyl-coenzyme A. Malonyl-CoA can be incorporated into cholesterol or fatty acids (**Figure 1.8**). Acetyl-CoA can be used as substrate for acetylation of both histone and non-histone proteins [59]. The metabolism of citrate represents a link between glucose metabolism, fatty acid metabolism, and epigenetic reprogramming. Therefore, citrate has key role and changes in flux through this pathway may have different consequences and effects.

1.4.1. Citrate carrier

The human genome contains a single gene encoding CIC (*SLC25A1*) located on chromosome 22q11.21 in the Di George critical region (DGCR), and two pseudogenes [60, 61]. Mitochondrial citrate carrier is an integral protein of the inner mitochondrial membrane of 298 amino acids (32.557 KDa) [62-65]. CIC precursor protein from mammals has a short N-terminal presequence of 13 amino acids that is absent in other organisms and acts as intramolecular chaperone, increasing the solubility of the CIC precursor in the cytosol [62-65]. Like other members of the mitochondrial carrier family, CIC consists of three homologous, tandem-repeated transmembrane domains approximately 100 amino acids in length organized in the form of 2α-helices across the inner mitochondrial membrane (**Figure 1.9**). In total, CIC has 6 hydrophobic α-helices connected by short hydrophilic loops exposed to both the intermembrane space and the matrix [66] (**Figure 1.9**). Therefore, within each domain, there are two hydrophobic tails that cross the membrane as α-helices separated by hydrophilic regions. These amphipathic helices parallel to the membrane plane on the matrix side (**Figure 1.9**). Both the N-terminal and the C-terminal ends protrude into the intermembrane space [66] (**Figure 1.9**). The citrate carrier, like all mitochondrial carriers

identified so far, contains a short characteristic sequence called the carrier signature [PX(D/E)XX(K/R)], at the end of the first, third, and fifth α-helices [66] (**Figure 1.9**).

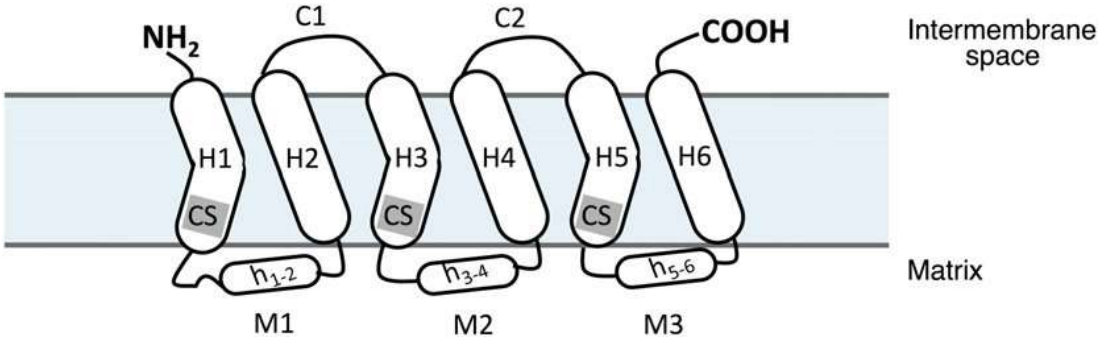

Figure 1.9: Secondary structure of the citrate carrier. CIC consists of 6 transmembrane helices (H1-H6), connected by 3 loops on the matrix side (M1-M3) and 2 loops on the intermembrane space (C1, C2). Matrix loops contain short amphipatic helices (h 1-2 , h 3-4 , and h 5-6). With CS is indicated the carrier signature [66].

In human CIC is highly expressed in liver, adipocytes, prostate, lung, and thyroid. Although in less amount CIC is expressed also in heart, skeletal muscle, brain, pancreas, and kidney [66].

1.4.2.ATP citrate lyase

ATP-citrate lyase is a key metabolic enzyme that, in humans, links carbohydrate metabolism to fatty acid biosynthesis. ACLY catalyzes the ATP-dependent conversion of citrate and coenzyme A (CoA) to oxaloacetate and acetyl-CoA, substrate for *de novo* biosynthesis of fatty acids and cholesterol [67]. Additionally, acetyl-CoA could be used for acetylation of cytosolic and nuclear proteins (*i.e.* histones) thus connecting metabolism with epigenetic control of gene expression proteins [59]. In mammals, high expression levels of ACLY are in lipogenic tissues, such as adipose tissue, liver or lactating mammary glands [68]. Furthermore, ACLY is overexpressed and correlated with poor prognosis in many kinds of cancer where it supports proliferation through *de novo* lipogenesis. Human ACLY is a ubiquitous homo-tetrameric protein of 1101 amino acid residues localized both in the cytosol and the nucleus [59]. The mammalian ACLY has a N-terminal citrate-binding domain, followed by a CoA binding domain and CoA-ligase domain and finally a C-terminal citrate synthase domain. The cleft between the CoA binding and citrate synthase domains represents the active site of the enzyme, where both citrate and acetyl-coenzyme A bind. More in detail, ACLY contains six domains: domains 3 and 4 form the ATP-grasp fold for

binding ATP, domain 5 represents the citrate-binding site, domain 1 is the putative CoA-binding site, and domain 2 contains the catalytically phosphorylated His760 residue (**Figure 1.10**) [69]. The C-terminal domain has weak sequence homology to citrate synthase (**Figure 1.10**) [69]. The citrate synthase homology domain is involved in CoA binding.

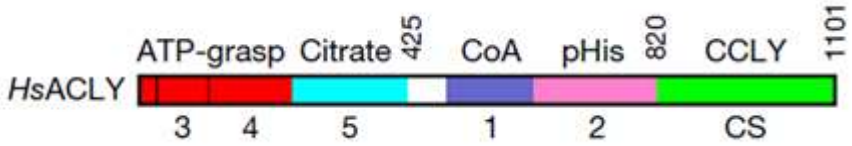

Figure 1.10: Domain organization of human ACLY. The domains are indicated with different colors, named numerically on the bottom while their functions are indicated on the top [69].

1.5 Citrate metabolism in cells of innate immunity and inflammation

In the last few years, the immunomodulatory role of citrate has been emerging. Indeed, citrate represents a key signal for the activation and function of immune cells and has a central role in inflammatory cascade. It is involved in the synthesis of inflammatory mediators, namely ROS, NO• and PGE2, and can impact cytokine production. Moreover, citrate-derived itaconate promotes an anti-inflammatory response while citrate-derived acetyl-CoA provokes acetylation of both histone and non-histone proteins contributing to epigenetic modifications.

1.5.1. Citrate metabolism in M1 macrophages: the citrate pathway

The fragmented Krebs cycle is a metabolic hallmark of M1macrophages. The breakpoint at isocitrate dehydrogenase allows for the withdrawal of citrate from mitochondria to cytosol. Indeed, in M1 macrophages the isocitrate: α ketoglutarate ratio is increased and *Idh1* is downregulated [37]. Increased levels of citrate were detected in both mouse (LPS-stimulated) and human (LPS, TNFα or IFNγ-triggered) macrophages [44, 70]. The increase in citrate runs parrel with the upregulation of both CIC and ACLY [1, 51, 70]. The term "citrate pathway" was coined to refer to the export of citrate into the cytosol via CIC and its breakdown by ACLY in acetyl-CoA and OAA.

An *in silico* analysis evidenced the presence of two NF-κB-responsive elements in *SLC25A1* human gene promoter [1]. In has been demonstrated a NF-κB dependent mechanism for LPS and TNFα-driven CIC induction, therefore *SLC25A1* is a NF-κB target gene required for LPS or TNFα-driven inflammation through citrate pool availability [1, 70]. On the other hand, IFNγ induces CIC and ACLY via STAT1 [51]. In M1 macrophages the export of citrate has a key role for the synthesis of fatty acids and pro- and anti-inflammatory mediators [1, 45], namely NO•, ROS, PGE2 [1, 51, 70]. Oxaloacetate, via cytosolic malate dehydrogenase and malic enzyme, produce NADPH, which can be used by NADPH oxidase and iNOS to produce ROS and NO• respectively (**Figure 1.11**) [1, 51, 70]. The second metabolic product of citrate, acetyl-CoA, provides units for lipid synthesis, including arachidonic acid, precursor of prostaglandins (**Figure 1.11**). Acetyl-CoA could have also other fates: it can be used for cholesterol formation and fatty acid synthesis for membrane biogenesis or it can be used in acetylation reactions, thus participating in epigenetic modifications [59, 71] and this is relevant in inflammation since different genes involved in inflammatory cascade, also those encoding for inflammatory mediators, are regulated via acetylation and methylation in their promoter regions and on histones [72, 73]. Furthermore, acetyl-CoA is required for macrophage maturation [74].

Inhibition of CIC by benzenetricarboxylate (BTA) or -Chloro-3-[[(3-nitrophenyl)amino]sulfonyl]-benzoic acid (CNFASB) or its genetic silencing with siRNA leads to a marked reduction in NO•, ROS, and PGE2 production in LPS and cytokine-stimulated macrophages (**Figure 1.11**) [1, 70]. Similar results were obtained when ACLY was silenced or inhibited by hydroxycitrate (HCA) or SB 204990 or radicicol (**Figure 1.11**) [51]. The effect of CIC inhibition on PGE2 production was rescued by adding exogenous acetate that can be converted to acetyl-CoA by acetyl-CoA synthase (ACSS): this fact confirms that citrate-derived acetyl-CoA is used for PGE2 synthesis [70]. Citrate may be critical to IL1β synthesis since endogenous PGE2 is essential to produce LPS-induced pro-IL1β [75].

Interestingly, the citrate pathway upregulation has been found in children affected by Down syndrome, a genetic disorder characterized by permanent oxidative stress and inflammatory facets [76], and is involved in the metabolic reprogramming of Behçet's syndrome [77].

Similarly, the hydrosol of *Pistacia lentiscus* exerted anti-inflammatory activity acting through the citrate pathway [78].

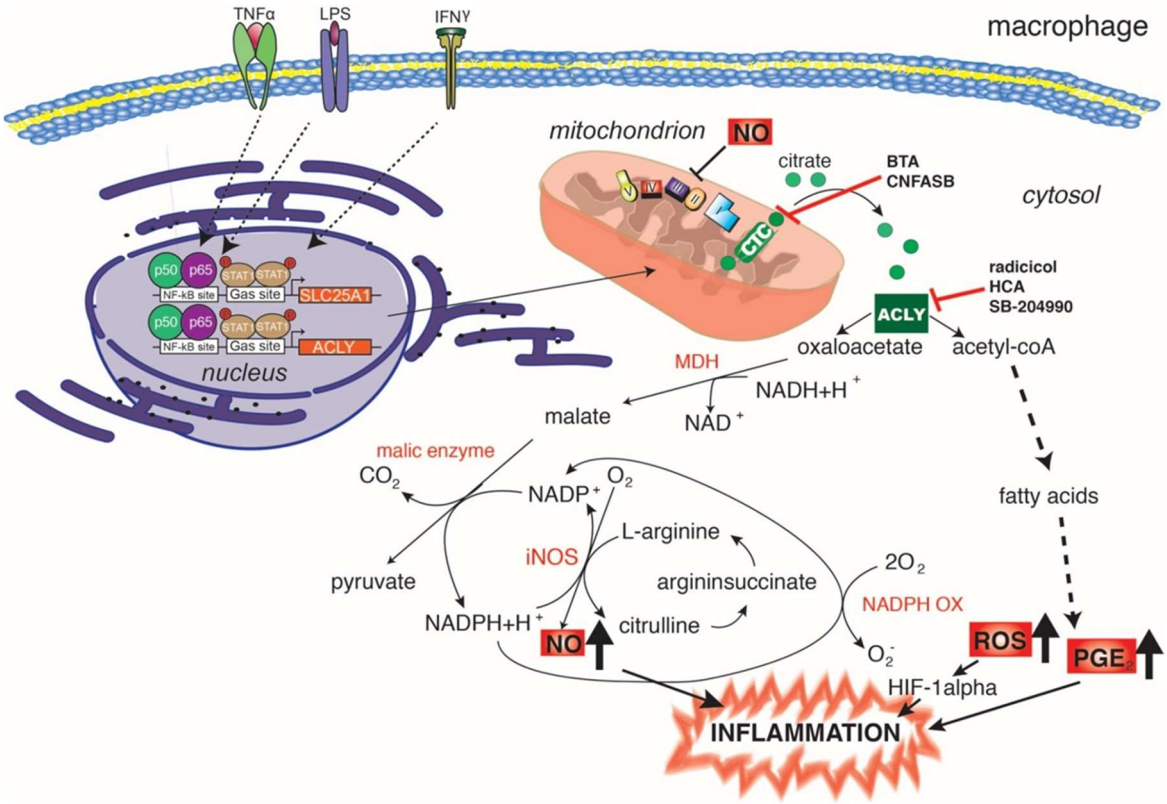

Figure 1.11: Citrate pathway in macrophages triggered by LPS or TNFα and/or IFNγ. LPS and TNFα, via NF-κB, and IFNγ, through STAT1, induce *SLC25A1* and *ACLY* upregulation. The citrate is exported from mitochondria from CIC and once in the cytosol it is cleaved by ACLY in acetyl-CoA and oxaloacetate, precursors for inflammatory mediators ROS, NO and PGE2.

A study of Lauterbach et al. in 2019 confirmed the crucial role of citrate metabolism and ACLY induction in macrophage activation, underling their role in cytokine production control. They showed that LPS increased the extracellular acidification rate (ECAR) in bone marrow derived macrophages within 2 hours after stimulation, with consequent increasing in the rate of glycolysis [79]. Eight hours after LPS exposure the maximal respiration in macrophages was reached. In contrast, LPS activation for 24 hours led to decreased basal OXPHOS [79]. These data suggested that mitochondrial metabolism changes rapidly when LPS binds to TLR4 and the early response, relevant for gene transcription, is different from that obtained after 24 hours [79]. They also found that LPS increased the synthesis of succinate, lactate, and citrate. The change in citrate encouraged them to analyze ACLY expression and when ACLY was inhibited increased mRNA expression of IL-10 and IL-1R

antagonist (IL1- RA) and decreased mRNA expression of IL-6, IL-18, IL- 27 were observed [79].

Tan et al. demonstrated that CIC inhibition or complete knockout of *SLC25A1* gene lead to lowering of IL-6 levels and increased IL-10 and IL-4 [80]. CIC impairment significantly reduced inflammatory M1 macrophage polarization and tissue infiltration, TNF-α and iNOS expression were downregulated [80]. When CIC was inhibited, alternative pathways compensate for citrate deficiency. Enzymes as IDH1, IDH2 and acetyl-CoA synthetases (ACSS 1 and 2), that synthetize acetyl-CoA from acetate, were downregulated by CIC inhibitor while increased mRNA and protein expression of SLC13A5, a transporter which takes up citrate from the extracellular environment, were observed [80]. Therefore, extracellular citrate can be the only source of cytosolic acetyl-coA in absence of CIC.

The last aspect concerning citrate is itaconate. Itaconate derives from the decarboxylation of cis-aconitate, the intermediate product of citrate conversion to isocitrate by aconitase in the second step of TCA cycle. One of the most prominent consequence of LPS and IFNγ - triggered activation in macrophages is the shift in Krebs cycle towards itaconate production [81, 82]. Itaconate has antimicrobial and growth inhibition activity towards different microorganisms and anti-inflammatory properties. Succinate dehydrogenase is one of itaconate target in macrophages activated by LPS and IFNγ [83]. Succinate levels in macrophages are strictly linked to itaconic acid metabolism. Itaconate reduces ROS/RNS (reactive nitrogen species) lowering IL1-β production [83]. Furthermore, itaconate modulates NRF2 transcriptional factor, essential in driving anti-oxidant and anti-inflammatory responses [46].

1.5.2. Citrate metabolism in dendritic cells

Citrate has been demonstrated to be important also for the activation of dendritic cells. Mitochondrial respiration collapses in TLR-activated DCs 6 hours after receiving activating stimuli. Up until the 6 hours, DCs show increased rate of glycolysis while OXPHOS is downregulated. The breakpoint at isocitrate dehydrogenase is also a feature of DCs [84].

Instead, citrate exits from the TCA cycle and support *de novo* fatty acid synthesis [84]. Inhibition of ACC or fatty acid synthase or blocking expression of *Slc25a1* diminished the early activation of DCs. Augmented lipids production is required for membrane synthesis

necessary for the expansion of both the endoplasmic reticulum and Golgi, in turn useful for increased synthesis and secretion of various proteins following TLR-activation. The PPP is also upregulated and generates NADPH, required as a cofactor for lipogenesis.

1.5.3. Citrate metabolism in natural killer cells

In activated natural killer cells (NK cells), the citrate–malate shuttle is important in the metabolic reprogramming occurring after activation [85]. With the term "the citrate–malate shuttle" is indicated the export of citrate into the cytosol via CIC, and its breakdown by ACLY and MDH1 yielding malate. In activated NK cells *Slc25a1* and *ACLY* mRNA are upregulated under transcriptional control of SREBP [85]. NK cells once activated show increased glycolysis and OXPHOS which are critical for their activation and growth. Inhibition of the citrate–malate shuttle reduced IFN-γ production. Citrate itself has been shown to inhibit the HIF asparaginyl hydroxylase [factor inhibiting HIF (FIH)] [86]. FIH hydroxylates asparagine residues on HIF1α, preventing it from interaction with transcriptional coactivators such as CRE binding protein/p300 [86]. Therefore, increased citrate is important in the activation of macrophages, DCs, and NK cells.

1.6 *Aglianico del Vulture* red wine

Aglianico del Vulture is one of the most important varieties of Italian wines. *Aglianico del Vulture* is deeply pigmented and tannic wine obtained from the vinification in purity of Aglianico grapes which are nearly black in color and thick-skinned. The production is allowed in the Vulture area, in Potenza (Basilicata, Italy), where volcanic soils are particularly suitable for this variety. In this area Aglianico is cultivated up to 800 meters above sea level, but best conditions are between 200 and 600 AMSL (above mean sea level). This early-budding grape thrives in dry climates with a lot of sunshine. The grape ripens slowly, and harvests can take place as late as November.

Aglianico del Vulture red wines are full-bodied and tannic, balanced with good acidity. Consequently, they have the potential to age for an exceptionally long time. In fact, they cannot be put on the market before one year after the harvest and it is preferable to consume *Aglianico del Vulture* wine from the third year of age. To indicate the aging time two terms are used: "Vecchio", for a minimum of three years, and "Riserva" for five years. The alcohol

content of *Aglianico del Vulture* ranges from 11.5 to 15 degrees. The yield of grapes into wine must not exceed 70%.

About organoleptic characteristics, the color is intense ruby red, with aging it takes on orange reflections; the smell is harmonious and increases in intensity and pleasantness with age; the flavor is dry, mineral, savory, warm, harmonious, rightly tannic, with aging it becomes more and more velvety. It has earthier notes, like mushroom, leather, and forest floor.

1.7 Health-promoting properties of moderate red wine consumption

An increasing body of evidence has shown the health benefits of red wine consumption since red wines are rich in polyphenols, natural compounds widely distributed in plants responsible of pigmentation, growth, reproduction, radical scavenging, signaling and defense from pathogen and parasitic attack. Different kind of polyphenols are present in wines, more abundant in red wines than in white ones. They include resveratrol, a non-flavonoid polyphenol and the main stilbene found in grape skin cells and red wines, flavonols (e.g., quercetin, myricetin), phenolic acids (e.g. caffeic and coumaric acids), condensed tannins and flavan-3-ols (e.g., epicatechin, catechin) and their polymeric derivatives).

Each wine has its unique profile of phenolic compounds; therefore, the identification and quantification of secondary metabolites present in wine and in grapes may also contribute to winegrape taxonomic characterization and it is necessary for certifying wine quality and origin. Quality and quantity of polyphenols in red wines are dependent on different vineyard factors such as variety, climate, geographical origin, quality, temperature, rain, sun exposure, vinification factors, and the time of grape skin contact with solid parts of the grape.

These compounds are often released by grapes during winemaking, in particular during the maceration period, and contribute to define the characteristics to grape varieties and wines. Anthocyanins, that could appear red, purple, or blue according to pH, are water-soluble pigments located in grape skins and seeds. Flavonols are yellow pigments important for UV protection and free-radical scavenging. Resveratrol is involved in the plant's defense system; thus, it is synthesized in response to invading fungus, stress, injury, infection, or UV irradiation.

Even if phenolic compounds represent only 1% of an average wine composition, in which water and ethanol are the major components (**Figure 1.12**), benefits from drinking moderate quantity wine derived derive mainly from the phenolics.

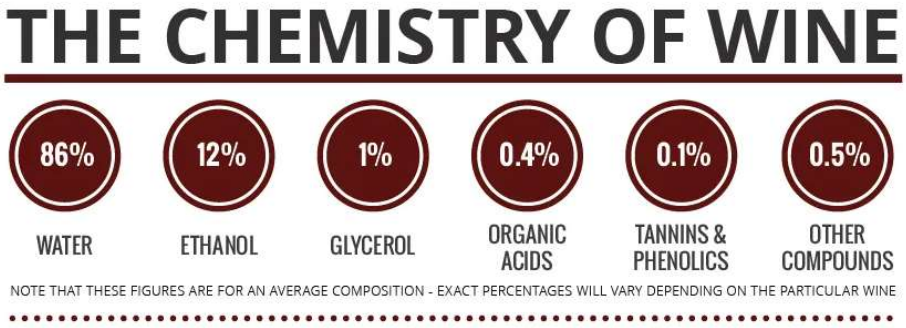

Figure 1.12: The average composition of a wine. Water and ethanol are the major components of a wine. Secondary metabolites represent about 1% of wine composition but they are critical in defying characteristics and proprieties of a wine.

Several studies demonstrated the protective role of moderate wine drinking in cardiovascular disease, atherosclerosis, hypertension, certain types of cancer, type 2 diabetes, neurological disorders, and the metabolic syndrome. These health benefits of red wine derive from its antioxidant, anti-inflammatory – by modulating inflammatory pathway and blocking the secretion of pro-inflammatory cytokines [87] – and lipid-regulating properties (**Figure 1.13**). Phenolic compounds from wines act as immunomodulators: they can interact with the immune system to modulate different biological aspects of the host response. For example, resveratrol counteracts the production of pro-inflammatory cytokines, while anthocyanidins downregulate the expression of COX2 in LPS-triggered macrophages [88].

Cyanidin-3-O-glucoside, petunidin 3-O-glucoside and delphinidin 3-O-glucoside inhibit NF-κB [89, 90]. Cyanidin 3-O-glucoside has great oxygen radical absorbance capacity *in vitro* [91] and delphinidin is one of the most active scavenger against superoxide anion [92]. Compounds found in red wine can also upregulate the transcription factor that control the expression of antioxidant and detoxifying enzymes in mammalian cells, determining an improved cytoprotection against several types of stress [92]. Interestingly, resveratrol colud dampen inflammation and induce apoptosis in immune cells by triggering pro-resolutive mediator Annexin A1 (AnxA1) pathway [93, 94].

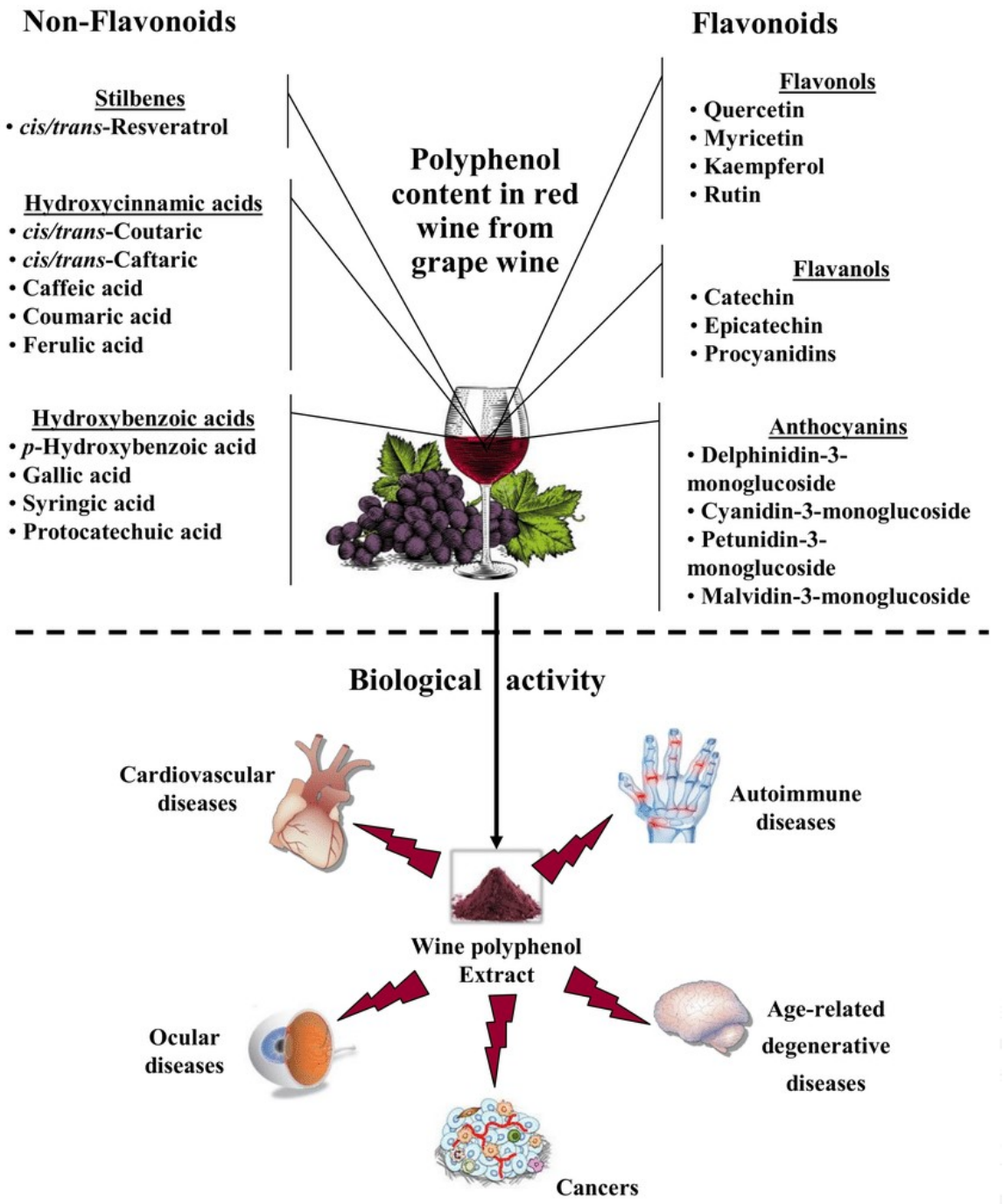

Figure 1.13: Polyphenol content in red wines and health-promoting proprieties exerted by polyphenols. Phenolic compounds from red wine have protective role in different pathologies such as cardiovascular disease, atherosclerosis, hypertension, cancer, type 2 diabetes, and autoimmune diseases.

1.8 Aims

During inflammation immune cells undergo a metabolic reprogramming to meet the new energetic and biosynthetic demands. Metabolites produced can both act as immune signaling molecules and supply substrates for pro-inflammatory mediators [29, 30]. Upon certain inflammatory stimuli macrophages as well as dendritic cells switch rapidly from a resting to an activated state with a different metabolic profile. More in detail, M1 macrophages, among which there are LPS-triggered macrophages, have high rates of glycolysis and pentose phosphate pathway, the Krebs cycle is broken, and fatty acid oxidation and oxidative phosphorylation are downregulated [29, 30]. Succinate dehydrogenase and isocitrate dehydrogenase, two enzyme of TCA cycle, are downregulated with consequent withdrawals of succinate and citrate from the cycle.

Most of the citrate is channelled into the citrate pathway, made of the mitochondrial transporter citrate carrier and the enzyme ATP citrate lyase [1, 51, 70, 95]. The citrate pathway contributes to production of inflammatory mediators, namely ROS, $NO^{\bullet}$ and PGE2 [1, 51] and could be involved in epigenetic modifications since acetyl-CoA derived from citrate could be used as substrate for protein and histone acetylation [96]. Moreover, citrate is implied in the synthesis of itaconate, that have anti-inflammatory proprieties [71]. The citrate pathway has a key role also in diseases with a strong inflammatory component such as Down syndrome and Behçet syndrome [76, 77]. Natural extract such as *Pistacia lentiscus* hydrosol [78] as well as new synthesized polyoxygenated diarylheptanoids [97] exhibit anti-inflammatory activity by suppressing the citrate pathway.

In the light of all this emerging evidence, the citrate pathway is increasingly assuming a central role in immunometabolism and in the inflammatory response. However, there is still a lot to investigate, about molecular mechanism, regulation, and implication of the citrate pathway. Therefore, one of the objectives of my PhD research project was the study of the molecular mechanisms related to immunometabolism with particular attention to mitochondrial metabolism and to the export of citrate from mitochondria resulting from the activation of macrophages with LPS.

The second objective was the evaluation of the effect of *Aglianico del Vulture* red wine on the modulation of mitochondrial activity and energy metabolism during the inflammatory

response, with particular interest in the involvement of the citrate export pathway in macrophages activated with LPS, giving attention to rapid metabolic and gene expression changes both in the absence and in the presence of *Aglianico del Vulture* red wine powder. Molecular mechanisms through which RWP modulates the expression of these genes were also investigated.

The choice to focus on immunomodulatory and anti-inflammatory proprieties of *Aglianico del Vulture* red wine was driven by the fact that *Aglianico del Vulture* is a wine produced in our land, Basilicata region, one of the best Italian wines, prized with many awards, but its biological proprieties have never been investigated. The red wines have become popular in the last few years for their antioxidant, hypolipidemic and anti-inflammatory effects due to their content of phenolic compounds. Although most of studies investigated only the chemical composition, the biodiversity, the pedigree reconstitution, and the general antioxidant properties of red wines. After obtaining a powder rich in phenolic compounds from *Aglianico del Vulture* red wine we investigated its immunomodulatory and anti-inflammatory effects, analyzing the secretion of pro-inflammatory and anti-inflammatory cytokines, NF-κB signaling pathway, the citrate pathway and epigenetic modifications in LPS-activated human macrophages.

2 MATERIALS AND METHODS

2.1 Prediction of transcription factor binding sites

The promoter sequence of human *ACLY* gene was obtained from “Gene” database of the National Center for Biotechnology Information (NCBI, https://www.ncbi.nlm.nih.gov/) clicking on the reference sequences (RefSeq) of *ACLY* gene in *Homo Sapiens*. The sequence was present as mRNA and downloaded in the FASTA format. The entire "Consensus CDS" was retrieved by clicking on "reference sequence details".

To search for the promoter region, the sequence of the genomic DNA in the FASTA format was downloaded 3000 base pairs upstream of the ATG start codon of Coding Sequence (CDS). The entire sequence obtained (-3145/+3 bp) was subjected to AliBaba2.1 program (http://gene-regulation.com/pub/programs/alibaba2/) for computational analysis.

AliBaba2.1 is a program developed to predict the binding sites of transcription factors in an unknown DNA sequence and is currently the most specific tool for this kind of analysis. In general, predictions are made by comparing predefined matrices, using binding sites collected in the TRANSFAC database which provides data on eukaryotic transcription factors, their experimentally proven binding sites, consensus binding sequences and regulated genes.

2.2 Polymerase chain reaction (PCR)

PCR is a technique employed for the amplification of DNA *in vitro* through the enzyme Taq polymerase. In our experiments, we used the nested PCR method, which uses two PCR of 30 cycles each at different concentrations of the primers.

For the first reaction the mix was:

Water	43,5 µL
Buffer (10X)	7 µL
dNTP (1,25 mM)	11 µL
Forward primer (0,5 µM)	3,5 µL
Reverse primer (0,5 µM)	3,5 µL
DNA (200 µg/µL)	1 µL
Taq polymerase	1 µL

The amplification program was:

	1° step	**1° step**	**2° step**	**3° step**	**1° step**	**2° step**
Temperature	94°C	94°C	55°C	68°C	68°C	4°C
Time	2:00	0:30	0:30	2:00	7:00	∞
Cycles	1	30				1
	Hot start	Denaturation	Annealing	Primers Extension		

For the second reaction the mix was:

Buffer (10X)	3 µl
dNTP (1,25 mM)	16 µl
Forward primer (20 µM)	5 µl
Reverse primer (20 µM)	5 µl
Taq polymerase	1 µl

The amplification program was:

	1° step	**1° step**	**2° step**	**3° step**	**1° step**	**2° step**
Temperature	94°C	94°C	55°C	68°C	68°C	4°C
Time	2:00	0:30	0:30	2:00	7:00	∞
Cycles	1	30				1
	Hot start	Denaturation	Annealing	Primers Extension		

Each PCR reaction was checked on 1% agarose gel: 20 µl were loaded; after about 30 minutes of electrophoretic stroke (100 V, 150 mA) the image was acquired. PCR fragments were then purified from nucleotides and enzymes, primers, salts, and oligonucleotides.

2.3 Cloning in PGL3-Basic Vector

Following the computational analysis of human *ACLY* promoter gene, different promoter deletion fragments were cloned into pGL3-Basic Vector (Promega) (**Figure 2.1**). This vector lacks the eukaryotic promoter so it allows the cloning of sequences, thus promoter sequence,

that can potentially regulate gene expression. It contains the region *luc*+, which has been optimized to monitor transcriptional activity in transfected eukaryotic cells (**Figure 2.1**). Each fragment derived from *ACLY* promoter contained at the ends the sites recognized by restriction enzymes Bgl II and Hind III and by using these enzymes fragments were cloned into the pGL3 Basic vector upstream of the luciferase (LUC) reporter gene that will be used to test the activity of the promoter. To verify the exact orientation of the fragment and the absence of errors during the amplification PCR, each fragment was subjected to automatic sequencing.

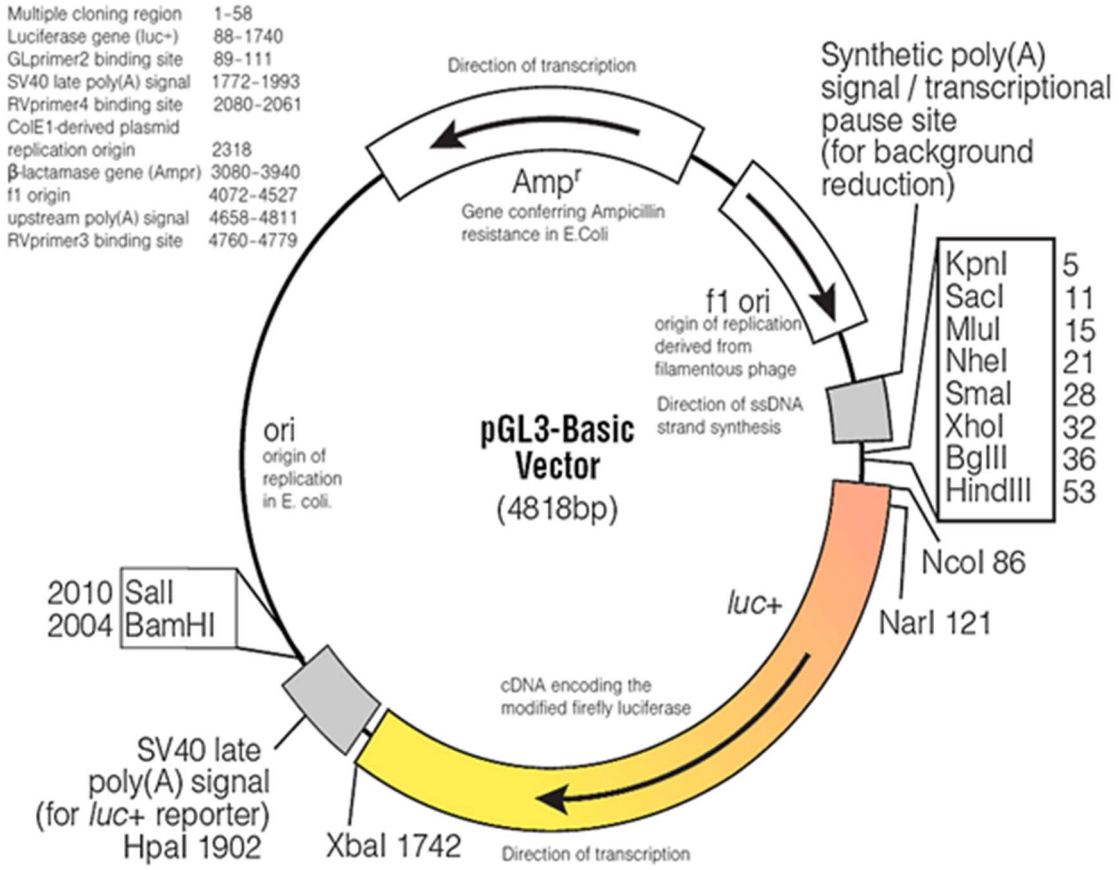

Figure 2.1: pGL3-Basic Vector map.

For restriction enzyme digestion, the reaction mix was:

Water	15 µL
Hind III (10U)	1 µL
Bgl II (10U)	1 µL
Buffer H	3 µL
DNA fragment (Removal)	10 µL

The reaction mix was incubated for 2 hours at 37 ° C. Following the enzyme denaturation for 30 minutes at 70 ° C, the DNA was purified and eluted in 30 µL of sterile water.

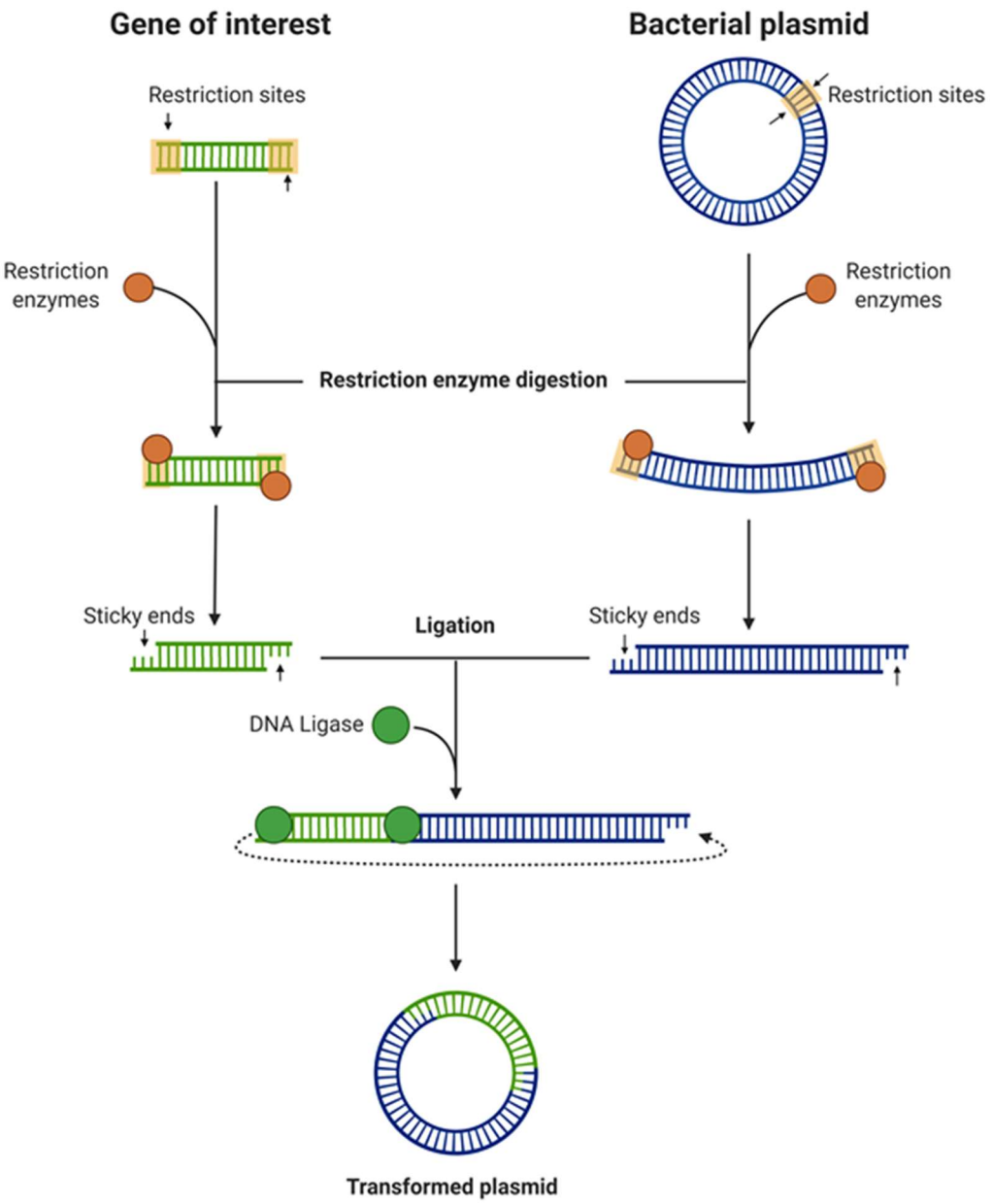

Figure 2.2: Cloning by using restriction enzymes. Gene of interests and plasmid are digested by using restriction enzymes. In this way, sticky ends are obtained and transformed plasmid are generated by DNA ligase in ligation reaction.

For vector digestion, the protocol was the same as the previous one, but the reaction mix was different:

Water	20 µL
Hind III (10U)	1 µL
Bgl II (10U)	1 µL
Buffer H	3 µL
pGL3 Basic Vector	5 µL

For dephosphorylation of the end of the digested vector, alkaline phosphatase (10U) and dephosphorylation buffer (3 µL) were added to the digestion. After an incubation of 30 minutes at 37 ° C, the purification was carried out.
For the ligation reaction, digested DNA and vector were put together in presence of 10x ligase buffer, ligase (10 U/µL) and water. At the end of two hours incubation, DNA constructs were obtained (**Figure 2.2**).

2.4 Bacterial transformation and selection

Bacterial transformation and selection are key steps in DNA cloning to increase the amount a specific piece of DNA, in our case the DNA constructs contained fragments of *ACLY* promoter. The transformation consists in the incorporation of the plasmid vector by bacteria, which can take up foreign DNA. It is not a spontaneous process, but cells need to become "competent", that means capable of incorporating the DNA added to the cell suspension during a short thermal shock. Subsequently, the ampicillin, contained in the plates and in the growth broth, serves to select the transformed cells that survive because they have the gene that carries resistance to the antibiotic, present in the plasmid vector. Transformation was performed on TOP10F ' bacterial cells after making them competent. One µL of DNA was added to 100 µL of competent cells and put on ice. After 30 minutes, the thermal shock was completed and cells at were maintained at 42° C for 90 minutes. Then 100 µL of broth (LURIA-BERTANI liquid culture medium (LB medium) - Yeast Extract, Tryptone, NaCl in proportion 5: 10: 5 in distilled water at pH 7.4-7.5) were added the samples and left at 37°C for about 45 minutes. Cells were plated on solid culture medium plates, obtained by adding 1.5% bactoagar to the LB medium. Colonies were collected from plates with a sterile toothpick are transferred to bacteriological tubes containing 1.5 ml of broth and ampicillin (0.15 µg). Colonies were incubated at 37 ° C for approximately 7 hours and then DNA was extracted.

2.5 Plasmid DNA extraction

The extraction of plasmid DNA required 3 steps:

1. Preparation and washing of the bacterial lysate.
2. Adsorption of DNA on silica-gel columns.
3. Washing and elution of the plasmid DNA.

For extraction, the columns capable of retaining DNA and the following solutions were purchased from Qiagen.

1. Buffer P1 (RNase, to degrade any traces of RNA).
2. Lysis Buffer (SDS and salts, to denature membranes).
3. Binding Buffer (CH_3COOK, to restore the pH to neutral values and increase the salt concentration, in order to denature the proteins and precipitate the bacterial DNA).
4. Washing Buffer 1 and 2 (to remove endonucleases).

Bacterial broth was centrifuged at 12000 rpm for 5 minutes and the pellet resuspend in 250 µL of buffer P1 by vortexing. To ensure the lysis, 250 µL of Lysis buffer (gently inverting to obtain a clear solution) and then 350 µL of binding buffer were added. Following centrifugation for 10 minutes at 12000 rpm, the supernatant was transferred to a column and centrifuged again for 1 minute at 12000 rpm. Column was washed with Washing Buffer 1 and 2 and DNA was eluted in 40 µL of sterile water.

2.6 Cell culture and treatments

Human embryonic kidney 293 cells (HEK293, Sigma–Aldrich) and immortalized bone marrow-derived macrophages (iBMDM, produced in the laboratory of Prof. Luke O'Neill, Trinity College Dublin, Ireland) were grown in Dulbecco's Modified Eagle Medium (DMEM, Thermo Fisher Scientific) supplemented with 10% fetal bovine serum, 2 mM L-glutamine, 100 U/mL penicillin, and 100 µg/mL streptomycin in a humidified chamber with 5% CO_2 at 37°C. HEK293 cell splitting was performed by using trypsin-EDTA solution: cells were washed once with phosphate buffered saline (PBS), incubated with trypsin-EDTA solution for 5 minutes at 37°C to detach adherent cells from flasks and complete medium was added to inactivate trypsin. iBMDM cells were detached by gentle scraping.

Inflammation was induced by 1 μg/mL of lipopolysaccharide isolated and purified from *E. coli* strain EH100 (AdipoGen Life Sciences, Inc., San Diego, USA).

2.7 Transient transfection

For monitoring the activity of the NF-κB signaling pathway, HEK293 cells were transiently transfected with a NF-κB reporter plasmid containing a firefly luciferase gene driven by five copies of NF-κB response element (5'-GGGACTTTCC-3') located upstream of the minimal TATA box promoter (pGL3–5xNF-κB). To measure *SLC25A1* gene promoter activity, HEK293 cells were transfected as previously described [98] using pGL3 basic-LUC vector (Promega, Madison, WI, USA) containing the −1785/−20 bp region of the SLC25A1 gene promoter (SLC25A1pGL3) upstream of the luciferase reporter gene [99]. For ACLY gene promoter activity, in pGL3 basic-LUC vector were cloned the −3116/−20 bp region of the ACLY gene promoter (called "3000") or a deletion fragment of this region (called "1000") [100]. To normalize the extent of transfection, cells were transfected with 10 ng of pRL-CMV (Promega).

Transfection were performed by using lipofectamine 3000 transfection reagent, according to manufacturer's instructions. Lipofectamine 3000 is a formulation that allows to transfect eukaryotic cells with high efficiency and low toxicity. DNA constructs are joined to the cationic liposomes of lipofectamine 3000 and these, attracted to the cell membrane of the cells, are internalized. Twenty-four hours after transfection, HEK293 cells were triggered with LPS in the presence or absence of RWP 20 or 200 μg/mL. The day after, cells were lysed and assayed for LUC activity by using the Dual-Luciferase® Reporter Assay System (Promega), according to the manufacturer's protocol.

The firefly luciferase, in the presence of ATP and oxygen, catalyzes the oxidation of luciferin and bioluminescence can be revealed (**Figure 2.3**) by using a luminometer. The reaction and measurement run together, as soon as the luminogenic substrate, represented by a solution of luciferin, is added to the cell lysate. The activity of luciferase is measured by reading the counts per second (cps) produced in the light reaction by each extract. Using a photomultiplier as a light detector, which acts as an ultra-fast photon counter, the instrument guarantees maximum sensitivity. Cells were lysed and Steady-Glo Reagent was added. Luminometer readings were acquired at 420 nm using a Glomax plate reader.

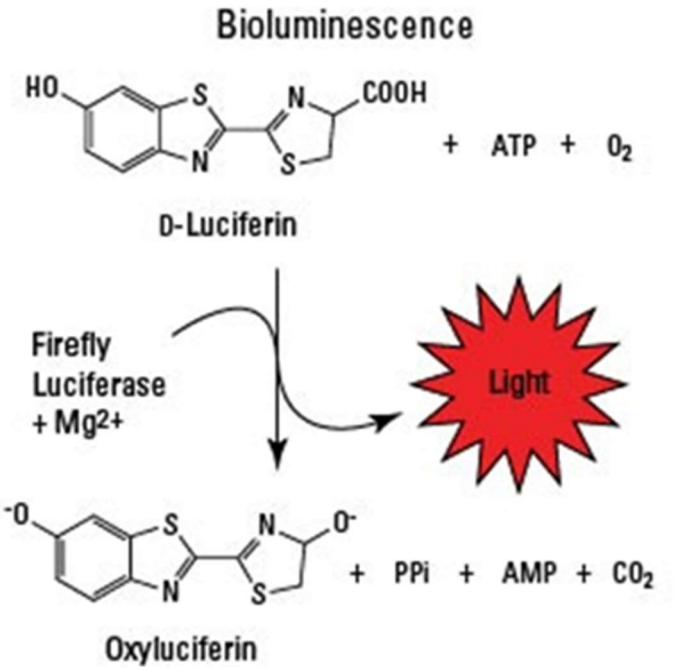

Figure 2.3: Mechanism of bioluminescence. Firefly luciferase, in the presence of ATP and oxygen, catalyzes the oxidation of luciferin and allows bioluminescence measurements.

2.8 Isolation of peripheral blood mononuclear cells

Primary human monocytes were isolated from healthy donors after obtaining written informed consent. The study was performed in agreement with the Declaration of Helsinki and in accordance with the Committee on Human Research approved procedures. Venous blood was collected into K2 EDTA-coated BD vacutainer tubes (Becton, Dickinson and Company, Franklin Lakes, NJ, USA). Peripheral blood mononuclear cells (PBMCs) were separated by Histopaque-1077 (Sigma-Aldrich, St Louis, MO) density gradient centrifugation: whole blood was mixed with Hanks' Balanced Salt solution (HBSS, Sigma-Aldrich) at a ratio of 1:2 (v/v), layered on the top of Histopaque-1077 (Sigma-Aldrich) and centrifuged at 1000 x g for 15 minutes (**Figure 2.4**). The layer of PBMCs at the interphase was recovered and washed twice in HBSS (**Figure 2.4**). PBMCs were incubated with CD14 antibody conjugated to magnetic beads (MACS®, Miltenyi Biotech GmbH, Bergisch Gladbach, Germany) for 15 minutes at 4°C. After washing, cells were loaded onto MACS® column (Miltenyi Biotech) placed in a magnetic field and CD14 positive ($CD14^+$) and negative ($CD14^-$) populations were divided. The $CD14^+$ monocytes were seeded in 6-well plates Ultra-low attachment (Thermo Fischer Scientific) at a density of 1.5 x 10^6 and

differentiated to macrophages by using 100 ng/mL human M-CSF (**Figure 2.4**). Cell were grown in Roswell Park Memorial Institute (RPMI) 1640 medium (Thermo Fisher Scientific, San Jose, CA, USA) supplemented with 10% fetal bovine serum, 2 mM L-glutamine, 100 U/mL penicillin, and 100 µg/mL streptomycin at 37°C in a humidified atmosphere of 5% CO_2.

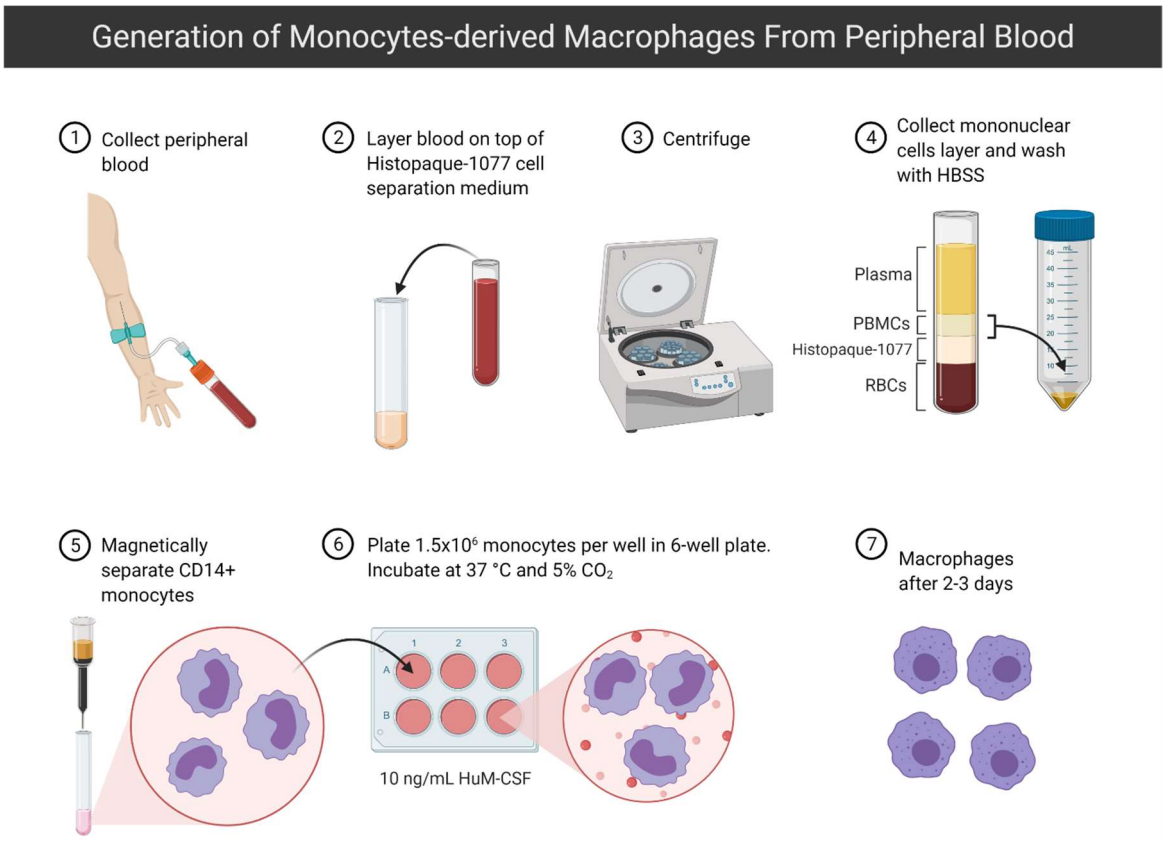

Figure 2.4: Generation of human macrophages from peripheral blood. To generate human monocyte-derived macrophages, peripheral blood was collected from healthy donors, layered on top of a density gradient cell separation medium, and centrifuged. Peripheral blood mononuclear cells were collected and washed with HBSS. Subsequently, CD14+ monocytes were isolated using magnetic separation and plated in a 6-well plate with 10 ng/mL Hu M-CSF.

2.9 RNA extraction

Total RNA was extracted from PBMCs by using *RNeasy Plus mini Kit* (Qiagen Inc., Valencia, CA, USA) according to manufacturer's instructions. 2 x 10^6 cells were lysed and homogenized in 350 µL of Buffer RLT Plus added with β-mercaptoethanol (β-ME). Buffer RLT Plus contains highly denaturing guanidine-isothiocyanate, which, together with β-ME,

immediately inactivates RNases to ensure the isolation of undegraded RNA. The same volume (350 µL) of 70% ethanol solution was then added to the cell lysate to provide the appropriate binding conditions for RNA and the sample was loaded onto a RNeasy MinElute spin column, that has a silica membrane that specifically binds the RNA from lysed cells. Contaminants were washed away by using Buffer RW1 and RPE (containing ethanol). RNA was eluted in 30 µL of RNase free water.

2.10 RNA quantification and quality assessment

Quantification and quality assessment of isolated RNAs were performed by using the Thermo Scientific™ GO 3.2 (Thermo Fisher Scientific) Multiskan™ GO Microplate Spectrophotometer, compatible with Thermo Scientific™ µDrop plate (Thermo Fisher Scientific), and SkanIt ™ RE software (Thermo Fisher Scientific). This system allows the simple and fast quantification of nucleic acids in 2 µL sample volume exploiting the feature of RNA and DNA to absorb UV light at a wavelength of 260 nm. The instrument was set to measure the absorbance at three wavelengths 230, 260 and 280 nm and then to calculate RNA concentration and 260nm/280nm and 260nm/230nm ratios. 260/280 nm ratio allows to identify contamination by proteins, which absorb at 280 nm. Pure RNA should have a ratio of about 2. Absorbance at 230 nm reflects contamination from substances such as carbohydrates, phenols, peptides, or aromatic compounds. For pure samples, the 260/230 nm ratio should be about 2.2.

2.11 cDNA synthesis (RT-PCR)

One microgram of RNA was converted to cDNA through reverse transcription PCR (RT-PCR) reaction using *GeneAmp RNA PCR core kit* (Applied Biosystem) and random primers. The mix of reaction was:

25 mM $MgCl_2$ Solution	4 µL
10X PCR Buffer II	2 µL
dNTP mix (10 mM)	2 µL
RNase Inhibitor	1 µL

MuLV Rever.TRascriptase	1 μL
Random Hexamers	1 μL
H_2O *	… μL
RNA (1 μg) *	… μL

* Volume of RNA to add depends on its quantification. The sum of volumes of RNA and H_2O must be 9 μL.

In Thermo Cycler samples were put and subjected to the following program:

15 minutes at 42°C
5 minutes at 99°C
5 minutes at 4°C

2.12 Real-time PCR

Real-Time PCR is a method for accurate quantification of DNA in real-time with a high degree of sensitivity, specificity, and reproducibility. The Real-time PCR system is based on the detection and quantification of the fluorescence emitted by a reporter molecule. This signal increases proportionally to the amount of DNA. By recording the intensity of fluorescence emitted at each cycle, the PCR reaction is monitored during the exponential phase of amplification. In this phase there is a quantitative relationship between the target DNA and the amplified product. In our experiments we used TaqMan probes as fluorescent probes for quantification of human *ACLY* and *β-actin* (4326315E, Life Technologies) genes. TaqMan assay exploits the 5' exonuclease activity of DNA polymerase to hydrolyze the TaqMan probe that specifically hybridizes an internal amplicon sequence during the annealing/extension phase of the PCR. The TaqMan probe is an oligonucleotide that has a melting temperature of about 10° C higher than the primers and contains a fluorescent reporter at the 5' end and a quencher (fluorochrome capable of absorbing the radiation emitted by the reporter) at the 3' end (**Figure 2.5**). The close proximity of the reporter and the quencher prevents the emission of fluorescence until the probe is intact. During the extension phase of the PCR, the DNA polymerase extends the primers, once it reaches the probe, it removes the nucleotides from the 5' end. The break of the probe causes the

separation of the reporter and the quencher; therefore, the reporter emits fluorescence when hit by a laser beam at a specific wavelength (**Figure 2.5**).

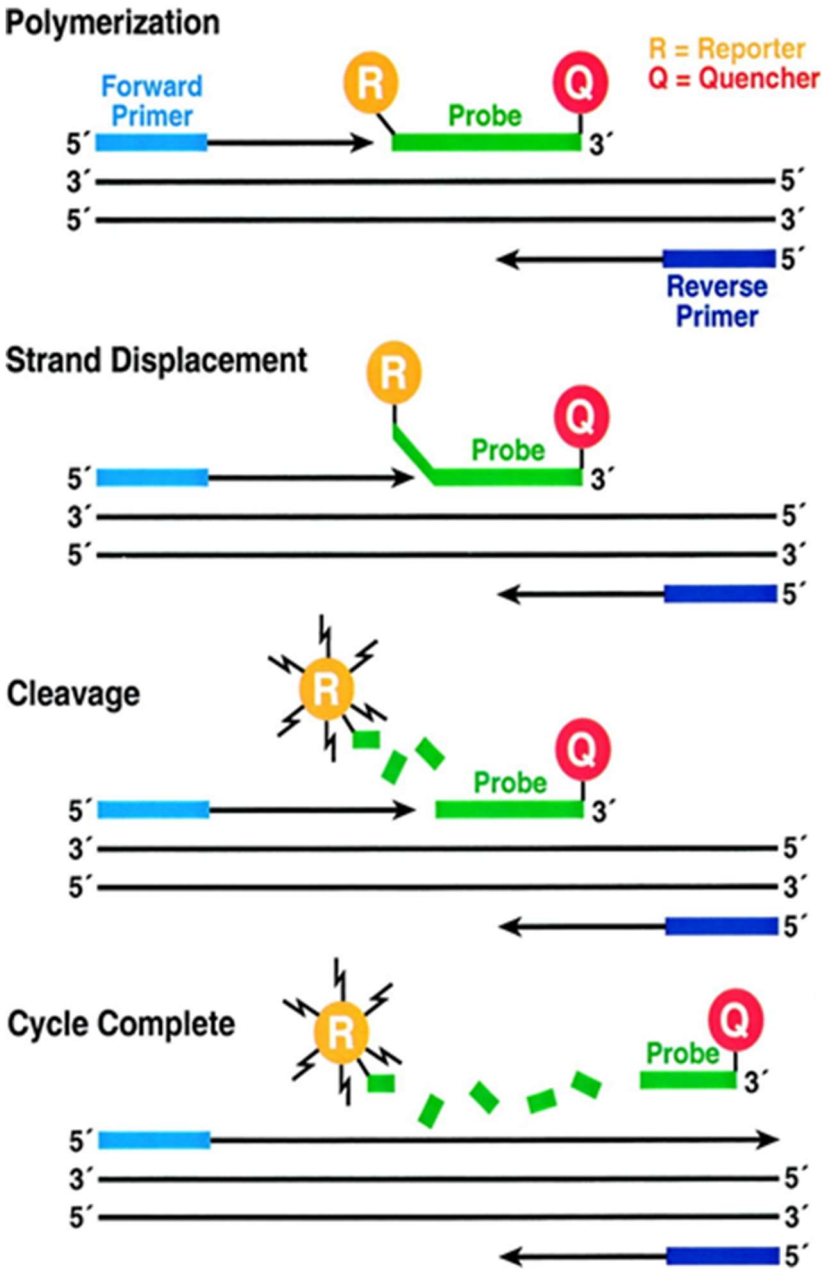

Figure 2.5: Schematic representation of the TaqMan assay to monitor the Real-time PCR reaction. Real-time PCR involves the binding of a forward primer and a reverse primer and a Taqman probe specific to the gene of interest, which hybridize to the cDNA. The Taqman probe contains a fluorescent reporter at the 5' end and a quencher at the 3' end. During the extension phase of the PCR, the DNA polymerase extends the primers in the 3'-5' direction and, due to its 5' exonuclease activity, once it reaches the probe, it removes the 5' nucleotides. This causes the separation of the reporter from the quencher; therefore, the reporter emits fluorescence if hit by a laser beam of a certain wavelength.

The following is the mix of reaction:

cDNA	3 µL
2x Master mix	10 µL
20x Taqman Probe	1 µL
20x β-actina	1 µL
Nuclease free water	5 µL

Each sample was analyzed in triplicate in 7500 Fast Real-Time PCR System instrument (Applied Biosystems), which consists of a thermal cycler and a spectrograph that records the fluorescence spectrum. The fluorescence data were collected by a computer interfaced with the device using 7500 Software v2.3 (Applied Biosystems).

The PCR program was:

1. 95°C for 10 minutes (activation of the polymerase).
2. 95°C for 15 seconds (denaturation).
3. 60°C for 1 minute (annealing and extension).

The steps 2 and 3 of denaturation and annealing and extension, respectively, were repeated for 40 cycles (**Figure 2.6**).

At the end of the reactions, the fluorescence data collected by the software were normalized against the fluctuation of the fluorescence background. Normalization was obtained by dividing the intensity of emission of the reporter with respect to that of a passive reference, the ROX (Carboxy-X-rhodamine) fluorochrome, present in the Master Mix. The output of the PCR reaction is an amplification plot in which the increase of fluorescence is reported as function of the threshold cycle (Ct). In Ct the fluorescence signal reaches the threshold level identified by a line that is set automatically by the instrument and that is at least 3 times higher than the ratio indicated as Rn. The first part of amplification plot is indicated as baseline and corresponds to signals determined by the aspecific fluorescence; the second one is the exponential phase in which fluorescence is proportional to initial target amount; the third one is the linear phase in which there is no increase in fluorescence proportional to initial target amount. The fluorescence data are analyzed above the Ct. The number of cycles required for a sample to reach the threshold level is referred to as the threshold cycle and is inversely correlated to the amount of cDNA present in the mix of reaction. Ct is determined during the exponential phase where no reaction-limiting conditions are present.

The relative quantification of ACLY expression levels was performed using the comparative method, in which ΔCt is calculated as the difference between Ct of target gene and Ct of housekeeping gene (β-actin) in each sample. The obtained value of ΔCt is inversely proportional to the amount of relative gene. Then, ΔΔCt is calculated as difference between ΔCt of a target gene in each sample (such as treated-cells) and ΔCt of the same gene in the calibrator sample (such as untreated-cells). Finally, $2^{-\Delta\Delta Ct}$ was calculated. $2^{-\Delta\Delta Ct}$ is also known as Fold Change and indicates how many times a gene is expressed in a sample with respect to calibrator sample in which 1 is the expression of the gene of interest. Therefore, $2^{-\Delta\Delta Ct}$ colud be:

- equal to 1 if is the same in the sample and in the calibrator;
- minor to 1 if the gene was less expressed in the sample than in the calibrator;
- major to 1 if the gene expression was increased with respect to calibrator.

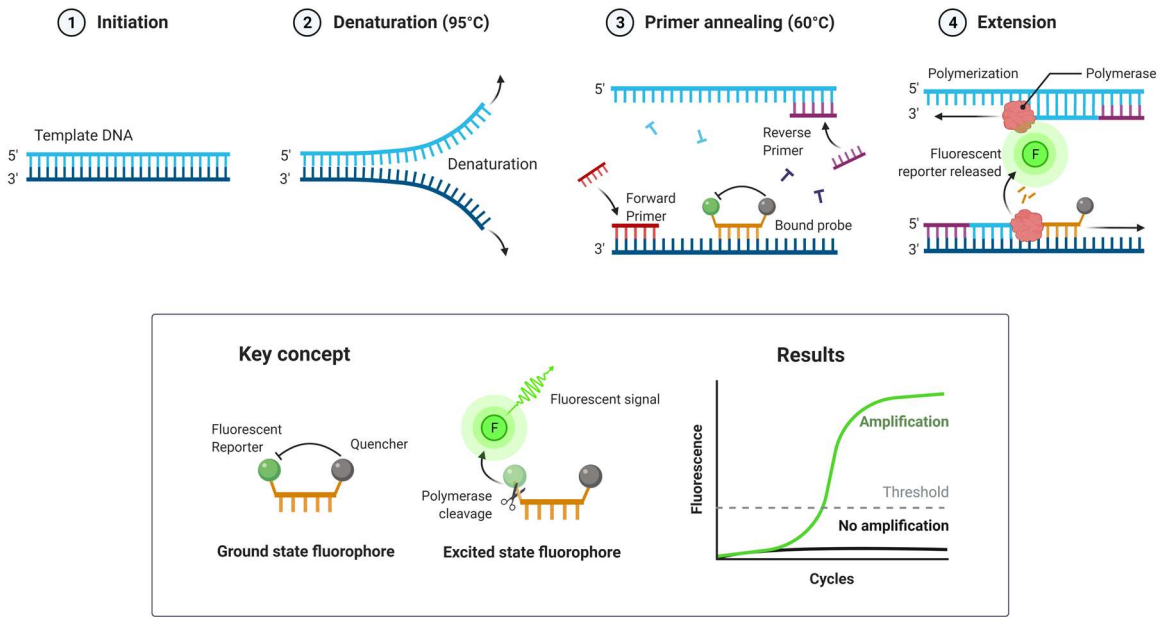

Figure 2.6: Overview of Real-time PCR. Phases of Real Time PCR reaction are reported in upper panel while schematic representation of probes and amplification plot obtained as output in Real time PCR experiment are reported in lower panel.

2.13 Western blotting

The cellular pellets were lysed in Laemmli sample buffer (60 mM Tris-HCl pH 6.8, 10% glycerol, 1% β-mercaptoethanol and 0.002% of bromophenol blue), boiled for 5 minutes at 95°C and centrifuged at 10000 rpm for 5 minutes (**Figure 2.7**). The proteins were resolved on 8%-5% or 10%-5% or 15%-5% SDS-PAGE (sodium dodecyl sulfate - polyacrylamide gel electrophoresis) gels and then electroblotted onto nitrocellulose membranes (**Figure 2.7**).

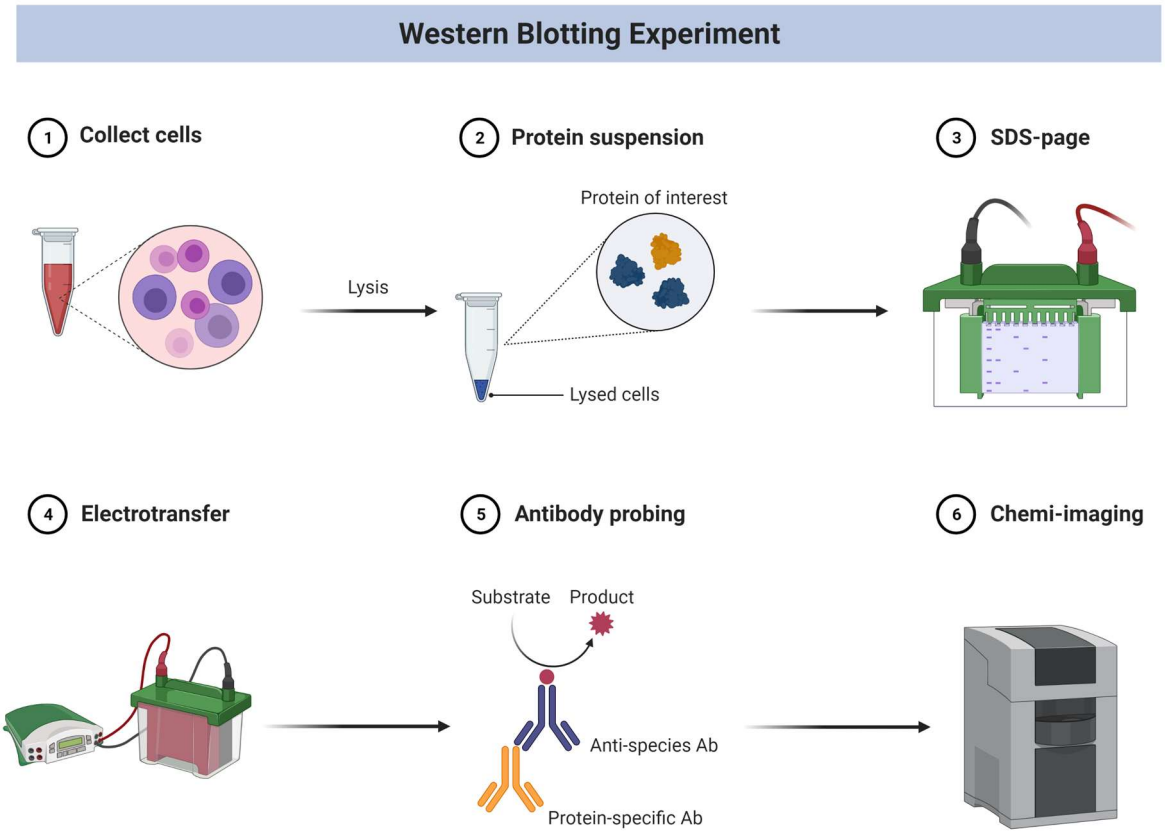

Figure 2.7: Overview of Western blotting procedure. Cells are treated, collected and lysed before to be subjected to separation according to their molecular weight in SDS-PAGE. Following electro transfer, the immunoreaction involved primary specific antibody and secondary antibody conjugated to HRP, allow to recognize the protein of interest. Images are acquired at ChemiDoc.

The membranes were stained with Ponceau solution to verify the correct transfer, washed with water to remove the staining. The membranes were blocked for 1 hour in a tris-buffered saline (TBST) solution containing 5% non-fat dry milk and 0.5% Tween 20, and then immunostained at 4°C overnight with anti-NF-κB/p65 (ab7970, Abcam, Cambridge, MA), anti-CIC [1], anti-ATP citrate lyase (ab157098, Abcam), anti-acetylated H3 (ab47915,

Abcam), anti-total H3 (ab1791, Abcam), anti-AnxA1 (GTX101070, GeneTex), anti-FPR2 or anti-β–actin (ab8227, Abcam) antibodies. The day after, the membranes were washed three times for 5 minutes in TBST and, following 1 hour incubation with HRP Goat anti-Rabbit IgG secondary antibody (Santa Cruz Biotechnology, Santa Cruz, CA, USA), the immunoreactions were detected by using the horseradish peroxidase substrate WesternBright™ ECL (Advansta, Menlo Park, CA, USA) at Chemidoc™ XRS detection system equipped with Image Lab Software for image acquisition and densitometric analysis (Bio-Rad Laboratories, Hercules, CA, USA) (**Figure 2.7**). The level of a specific protein from each sample was normalized against the respective β-actin signal. The protein expression level in the control sample was considered equal to 1. Each result from treated samples was expressed as proportion of the control sample.

2.14 Bradford protein assay

To measure the concentration of proteins, the Bradford assay was applied. Bradford protein assay is a colorimetric protein assay based on the shift in absorbance of Coomassie Brilliant Blue G-250. Under acidic conditions, when the dye binds to the protein being assayed is converted from the red form into its blue one. The shift in absorbance is from 465 nm to 595 nm, this is the value at absorbance readings are taken. Protein concentration in the sample was determined by using a standard curve built with known concentrations of bovine serum albumin (BSA, 0.25 - 0.5 - 1 - 2 μg/mL).

2.15 ACLY activity

ACLY activity was assessed by the coupled malic dehydrogenase method [101, 102], as previously described [100]. At the end of treatment with LPS alone or in presence of RWP_{FD}, cells were washed twice in ice-cold PBS, then the cell pellet was resuspended in ice-cold 0.1% NP40 in PBS and three freeze-melt cycles (-80°C for 8 minutes/40°C for 4 minutes) were made. On the supernatant collected after centrifugation, protein concentration was assessed by Bradford protein assay. One-hundred fifty micrograms of the cell lysate were added to the reaction mixture (50 mM Tris-HCl (pH 8.0), 10 mM $MgCl_2$, 1.9 mM DTT, 0.15 mM NADH, 0.07 mM CoA, 1 mM ATP, 2 mM potassium citrate, and 3.3 units/mL malic

dehydrogenase). The reaction was carried out in a quartz cuvette and absorbance at 340 nm at 25°C was monitored with a spectrophotometer. To determine the specific ACLY activity, changes in absorbance values in the absence of exogenous ATP were subtracted from variations observed in the presence of ATP and normalized to the protein concentration.

2.16 Chromatin immunoprecipitation (ChIP)

Chromatin immunoprecipitation (ChIP) is a powerful and versatile technique that allows to detect a protein (even if it is present in few quantities) at its *in vivo* binding site on chromatin. ChIP experiment is made of different phases: it begins with cell lysis and chromatin solubilization (**Figure 2.8**). The chromatin fragments, which are released from the cells, are subjected to numerous sonication cycles to obtain smaller fragments then subjected to immunoprecipitation by using specific antibodies that recognize the factors/proteins of interest (**Figure 2.8**). Obviously, together with these factors, the DNA sequences are also immunoprecipitated. Immunoprecipitation reactions were performed by using Dynabeads® Protein G, magnetic beads uniformly coated with recombinant protein G. During incubation, the antibody binds to Dynabeads® through its Fc (crystallizable fragment) domain. The tube is placed on a magnet, which attracts the beads, so that the supernatant can be removed by aspiration. This is followed by digestion of RNA, with RNase, and of proteins, including that of interest which was recognized by the antibody, with proteinase K and analysis by PCR, after appropriate purification of the DNA fragments (**Figure 2.8**).

If the protein under study is associated with a specific DNA region *in vivo*, the fragments of DNA that include this region will be enriched in the immunoprecipitated with respect to other portions of the genome. The presence and quantification of these genomic portions in the immunoprecipitated are determined by Real TIme PCR, in which the immunoprecipitated material is used as a template for amplifications with gene-specific primers (**Figure 2.8**).

Chromatin immunoprecipitation experiments were performed on human PBMC-derived macrophages (5×10^6 cells) treated with LPS for 3 hours in the presence or absence of SB-204990 (SB), a specific ACLY inhibitor [103].

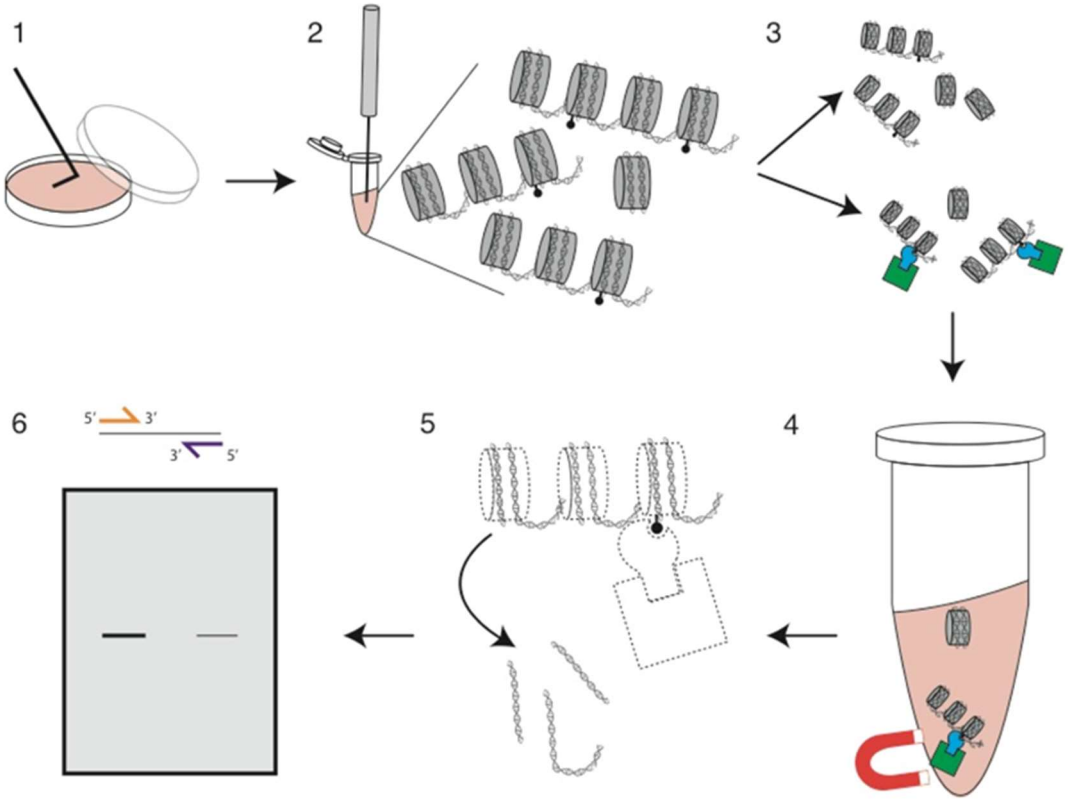

Figure 2.8: ChIP experiment. (1) Cells are collected, centrifuged and the cell pellet is lysed. (2) Chromatin, released from cells, is fragmented at the sonicator. (3) Protein G, linked to magnetic beads, and the primary antibody against the protein of interest are added to the DNA fragments. For the negative control (mock) the incubation is done in the absence of antibody. (4) With magnetic separation, the immunoprecipitated of the DNA fragments linked to the protein of interest is isolated, which is eliminated by treatment with proteinase K (5). The precipitate is analyzed by PCR (6).

A native ChIP was performed to analyze H3 acetylation levels. Cells were lysed in 0.1% NP-40-PBS buffer plus protease inhibitors, put on ice for 10 min and centrifuged at 1000 g for 2 min at 4ºC. The cell pellet was suspended in 0.1% NP-40-PBS buffer and sonicated at power 70%, cycle 9 for 25 min to have bands of 500-1000 bp. 20 µg of chromatin were immunoprecipitated in incubation buffer (10 mM Tris-HCl pH=8; 150 mM NaCl; 10 mM KCl; 1 mM EDTA; 0.1% NP40) plus 30 µL of Dynabeads Protein G (ThermoFisher Scientific) overnight on rocking platform with Anti-H3 Acetylated (Ab 47915, Abcam) antibody. The day after, Input (total chromatin extract) and mock (immunoprecipitation without antibody) samples were recovered and then used for qPCR analysis. Protein/DNA complexes were retained and washed with PBS. After treatment with RNase and Protease K, DNA was purified by using gel Extraction PCR DNA Fragment Purification Miniprep Kit (DNA LAND SCIENTIFIC), as per manufacturer's instructions, and analyzed by qPCR

using the Fast SYBR Green Master Mix (Life Technologies) and the oligonucleotides reported below:

Name	**Oligonucleotide 5'-->3'**
Forward PTGS2 qPCR	CCGCTTCCTTTGTCCATCAG
Reverse PTGS2 qPCR	TTGGAAAGAGAGGCGGGAAA
Forward ACLY qPCR	CTTTCCAAAGTTGGGTCTTGTG
Reverse ACLY qPCR	CCTCAGCAATTCAGACTCCTT
Forward IL1β qPCR	GTCTTCCACTTTGTCCCACATA
Reverse IL1β qPCR	CTGACAATCGTTGTGCAGTTG

2.17 Wine Samples

Aglianico del Vulture red wine (*Vitis vinifera L.*) was provided by Cantine del Notaio (Rionero, Basilicata region, Italy).

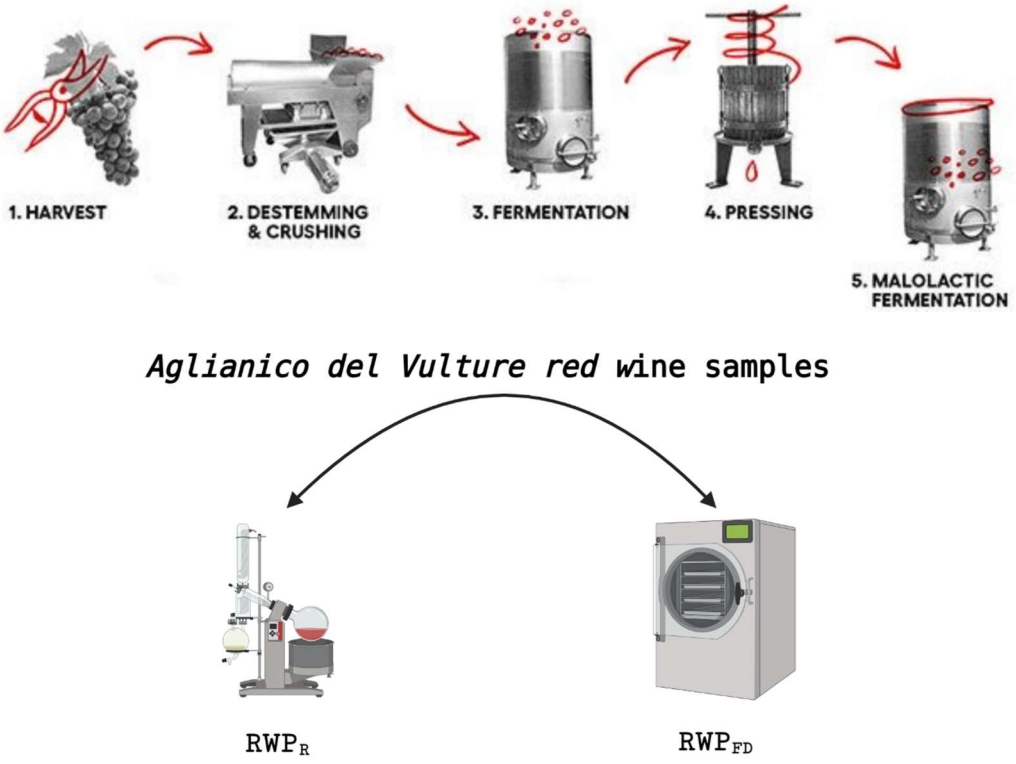

Figure 2.9: *Aglianico del Vulture* red wine samples. The wine tested in our experiment was obtained from harvest 2018. It was a wine with a malolactic fermentation. To remove solvents from wine rotary evaporator and freeze-dried were used to obtain RWP$_R$ and RWP$_{FD}$, respectively.

Grapes were harvested in September 2018 and samples used in our study were collected after grape pressing and when the fermentation was completed, so that no residual sugar was present into the wine (**Figure 2.9**). The samples were frozen and stored at -20 °C. To remove solvents from the samples and obtain red wine powders to use in our experiments, two methodologies were employed: freeze-drying or evaporation under reduced pressure. Therefore, the wine samples (500 mL) in glass cylinder were connected to a freeze-drying apparatus and freeze-dried under vacuum using a Stellar Millrock ST8S5-l lyophilizer (Millrock Technology, Kingston, NY, USA), RWP_{FD}, or evaporated under reduced pressure by using a rotary evaporator, RWP_R (**Figure 2.9**).

2.18 LC−MS and LC−MS/MS analyses

Part of whole and dealcoholized wine sample were dissolved in 100 µL of 40% MeOH with 0.1% (v/v) formic acid at a concentration of 10 mg/mL, centrifuged for 5 min at 13000 rpm and 1 µL aliquots were injected in an ultra-performance liquid chromatography-electrospray (UPLC–ESI)–Q-trap system. Mass spectrometry-based analyses were carried out to quantify specialized metabolites (Delphinidin-3-O-glucoside, Cyanidin-3-O-glucoside, Malvidin-3-O-glucoside, caffeic acid, coumaric acid, resveratrol, and quercetin). Quali-quantitative analysis was carried out using an API6500 Q-Trap spectrometer (AB Sciex, Foster City, CA, USA) coupled with a Nexerax2 UHPLC apparatus (Shimadzu, Kyoto, Japan), working in both positive and negative MRM (Multiple Reaction Monitoring) mode.

The instrumental parameters were optimized when solutions containing pure compounds were injected. A Kinetex column (Phenomenex) (C18 100 Å, 50 mm × 2.6 µm × 2.1 mm) was adopted for chromatographic analyses and compounds were separated using a linear gradient from 5% to 50% of acetonitrile (eluent B) and water containing 0.1% formic acid (eluent A) over 5 minutes followed by a faster gradient until to 95% of B. The flow rate was 0.35 mL/min, and the injection volume was 1 µL. To perform accurate quantitative analyses, 8 points (in the range 0.010-10 µg/mL) calibration curves were built for all the standard compounds. The mean values ± standard deviation (SD) from at least three experiments were reported. All data were processed using Analyst software (ABSciex), and identification of

compounds was based on retention times, accurate mass measurements, MS/MS data, exploration of specific spectral libraries and public repositories for MS-based metabolomic analysis [104], and comparison with data reported in the literature [105-109].

2.19 Cell count

Primary human monocytes were seeded into 96-well plate at a density of 2 x 10^4 cells/well and treated with a wide range of RWP_{FD} and RWP_R concentrations: 2.5, 5, 10, 20, 50, 100, 200, 400, 800, 1600 and 3200 µg/mL. At the end of 72-hour treatments, cell count was carried out by using the automated handheld Scepter 2.0 Cell Counter (Merck Millipore, Switzerland).

2.20 Quantification of cytokines

$CD14^+$ monocytes were seeded in 24-well plates at a density of 5 × 10^5 cells/well, treated with RWP_{FD} 20 or 200 µg/mL for 1 hour and then activated with 1 µg/mL of LPS. After 24 hours, cell-free supernatants were collected and assayed for the concentration of IL-1β, IL-6, TNF-α and IL-10 by Luminex® 100 System (R&D Systems, Inc., Minneapolis, MN, USA) using specific matched-pair antibodies and recombinant cytokines as standards following the manufacturer's recommendations.

2.21 Immunocytochemistry

Primary human monocytes were treated with LPS for 1 or 3 hours in the presence or not of RWP_{FD} 20 or 200 µg/mL. Cells were washed in PBS and fixed by cross-linking with 3% paraformaldehyde solution. Following permeabilization with PBS + 0,25% Triton X-100 (PBST) and blocking with PBST + 1% BSA (bovine serum albumin), cells were incubated with anti-p65 (ab7970, Abcam) primary antibody at 4°C overnight. The day after, we performed 2-hours incubation with the secondary antibody Alexa fluor 488 (Thermo Fisher Scientific). Fluoroshield Mounting Medium with DAPI (ab104139, Abcam) was employed as a counterstain for DNA and to preserve fluorescence. The images were obtained with the fluorescence microscope EVOS FLoid Cell Imaging Station (Thermo Fisher Scientific).

2.22 Quantification of citrate

The amount of cytosolic citrate was quantified by fluorometric method using the Citrate Colorimetric/Fluorometric Assay Kit (BioVision, Milpitas, CA, USA) as per manufacturer's instructions. In brief, monocytes-derived macrophages were treated with LPS in the presence or not of RWP_{FD} 20 or 200 µg/mL. Six hours later, cells were collected by centrifugation and washed twice in ice-cold water. Cell pellets were resuspended in ice-cold hypotonic buffer (20 mM Tris–HCl pH 7.4, 10 mM NaCl, 0.5% Nonidet P40, 3 mM $MgCl_2$) to ensure cell lysis. Cytosolic fractions were collected by centrifugation at 4°C at 12000 rpm for 10 minutes and deproteinized by Amicon Ultra Centrifugal Filters (Millipore). The quantification of citrate followed. In the assay, citrate is converted to oxaloacetate and oxaloacetate to pyruvate. The pyruvate is determined thanks to conversion of a nearly colorless probe to a fluorescent (Ex/Em, 535/587 nm) product.

2.23 ROS assay

To evaluate ROS levels, $CD14^+$ monocytes were triggered by LPS in the presence or not of RWP_{FD} 20 or 200 µg/mL. Where indicated, cells were treated also with 5 mM sodium malate (Sigma-Aldrich) or 500 µM NADPH (Sigma-Aldrich).

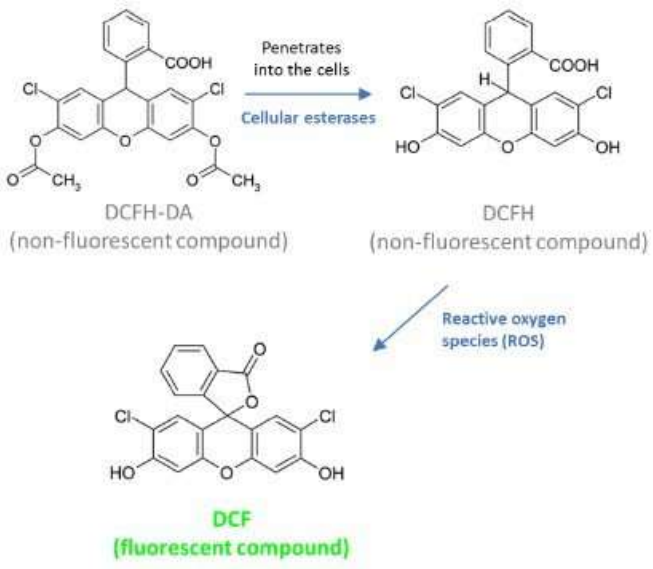

Figure 2.10: DCFH-DA reaction in ROS Assay. 2'-7'dichlorofluorescin diacetate (DCFH-DA), a cell permeant reagent, is deacetylated by cellular esterases to a non-fluorescent compound, DCFH, which is then oxidized by ROS into the fluorescent compound DCF.

Following 24 hours, cells were collected, washed with PBS, and incubated in the dark at 37°C for 30 minutes with 10 μM of 6-Carboxy-2',7'-Dichlorodihydrofluorescein Diacetate (DCFH-DA, Thermo Fisher Scientific) to determine intracellular ROS concentration.
DCFH-DA is cell-permeant. In cells, upon cleavage of the acetate groups by intracellular esterases and oxidation by reactive oxygen species, the nonfluorescent DCF-DA is converted to the highly fluorescent DCF, a chemically reduced form of fluorescein used as an indicator for ROS in cells (**Figure 2.10**).

2.24 NO• assay

To evaluate NO• levels, $CD14^+$ monocytes were triggered by LPS in the presence or not of RWP_{FD} 20 or 200 μg/mL. In some experiments, cells were treated also with 5 mM sodium malate or 500 μM NADPH. Following 24 hours, cells were collected, washed with PBS, and incubated in the dark at 37°C for 30 minutes to measure intracellular NO• concentration by using 4-Amino-5-Methylamino-2',7'-Difluorofluorescein Diacetate (DAF-FM Diacetate, Thermo Fisher Scientific). DAF-FM is essentially nonfluorescent until it reacts with NO• to form a fluorescent benzotriazole (**Figure 2.11**).

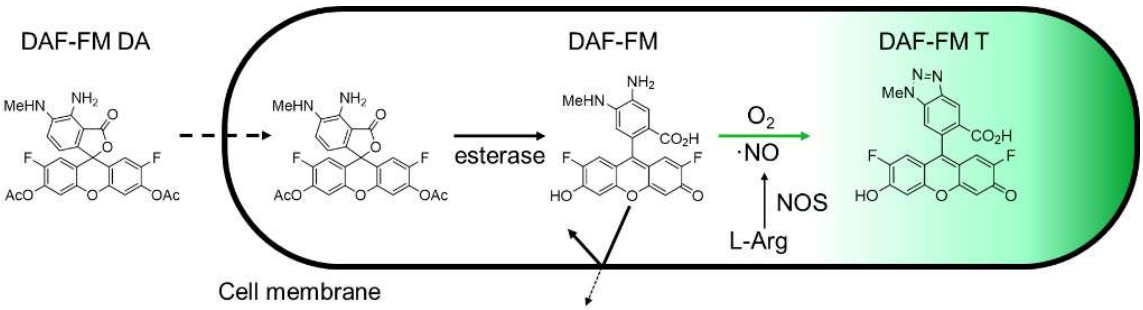

Figure 2.11: DAF-FM diacetate reaction in NO assay. Diaminofluorescein-FM diacetate (DAF-FM DA) is non-fluorescent and cell permeable reagent that in cells is deacetylated by esterases in cell impermeable DAF-FM, which is reacts with NO to generate the fluorescent compound DAF-FM T.

2.25 PGE2 detection

For PGE2 quantification cells were pre-treated with RWP_{FD} 20 or 200 µg/mL for 1 hour and, where indicated, exposed also to 5 mM sodium acetate (Sigma-Aldrich); then inflammation was induced by LPS. At the end of 48 hours LPS-treatment, cell supernatants were collected and PGE_2 concentration was measured by using DetectX® Prostaglandin E2 High Sensitivity Immunoassay Kit (Arbor Assays, Ann Arbor, MI, USA). The kit uses a mouse monoclonal antibody. Standards and samples were pipetted into a clear microtiter plate coated with an antibody direct to mouse IgG. A PGE2-peroxidase conjugate was added in the wells. The binding reaction was initiated by the addition of the monoclonal antibody that captures PGE2. After overnight incubation, the plate was washed, and substrate was added. The substrate reacted with the bound PGE2-peroxidase conjugate. After a short incubation, stop solution was added and absorbance quantified at 450 nm (**Figure 2.12**). The concentration of the PGE2 in the sample was calculated using calibration curve after making suitable correction for the dilution of the sample.

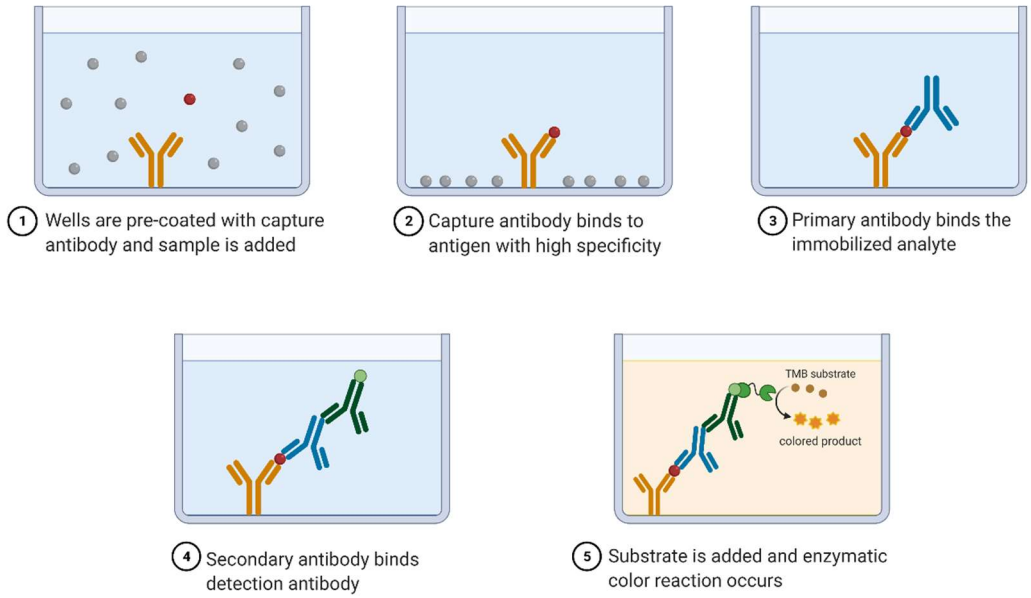

Figure 2.12: Sandwich ELISA for PGE2 detection. Wells are pre-coated with a known quantity of capture antibody. The antigen-containing sample is applied to the plate and captured by antibody. A specific primary antibody is added and binds to antigen. This primary antibody could also be in the serum of a donor to be tested for reactivity towards the antigen. Secondary antibodies are applied as detection antibodies. Substrate is added to be converted by the enzyme into a color signal.

2.26 Statistical analysis

Results are shown as mean values ± standard deviation (SD) of at least three independent experiments, carried out in triplicate. *One-way ANOVA* followed by *Dunnett's* or *Tukey's* tests for multiple comparisons were performed to determine statistical significance of differences. The statistical techniques used for data analysis are detailed in figure legends. Asterisks in figures denote statistical significance: *$p<0.05$, **$p<0.01$ and ***$p<0.001$. When *Tukey's* post hoc test was performed, different letters indicate significant differences between treatments at $p<0.05$.

3 RESULTS

3.1 Human *ACLY* gene promoter contains an active NF-κB responsive element

ATP citrate lyase plays a central role in energy metabolism and is essential in inflammatory response following macrophage activation by pro-inflammatory stimuli such as LPS, TNFα, IFNγ or a combination of TNFα and IFNγ [51], as previously described. Indeed, mRNA and protein levels of ACLY are increased in the presence of these stimuli and metabolites derived from the cleavage of citrate by ACLY contributes to chemical mediators of inflammation production [51]. Moreover, ACLY is upregulated in pathologies characterized by a strong inflammatory component, such as Down syndrome or Beçhet syndrome [76, 77].

TLR4 signaling pathway plays an important role in initiating the innate immune response and its activation by LPS is responsible for chronic and acute inflammatory disorders. As consequence of LPS binding to TLR4, the intracellular signal cascade of NF-κB transcription factor is triggered [110].

Taken into consideration the relevant role of ACLY in inflammation and that the main pathway reported for LPS-TLR4-induced signaling acts through NF-κB, we wondered if the human ACLY gene promoter had a κB site, the consensus DNA sequence for NF-κB binding.

Therefore, in order to clarify the molecular mechanisms responsible for ACLY gene upregulation during LPS activation, we performed *in silico* analysis of the human ACLY gene promoter.

The entire sequence of human *ACLY* gene promoter (-3145/+3) was subjected to computational analysis using AliBaba2.1 program (http://gene-regulation.com/pub/programs/alibaba2/).

Through this analysis, several potential biding sites for transcriptional factors were identified, among them we identified one NF-κB responsive element with a score of 85.7 localized at −2048/−2038 bp (**Figure 3.1**).

Figure 3.1: Sequence of human *ACLY* gene promoter. The nucleotide A of ATG start sequence corresponds to +1 while nucleotides upstream this position are indicated with negative numbers. The underlined sequence represents the consensus DNA sequence for NF-κB transcription factor. Sequence indicated with "FOR 3000", "FOR 1000" and "REV" were used for primers to obtain deletion fragments.

By using the primers indicated in **Figure 3.1** (FOR 3000, FOR 1000 and REV) and human genomic DNA as template, we performed PCR reactions to obtain two deletion fragments of human *ACLY* gene promoter and constructs obtained were indicated as "3000", which contains NF-κB responsive element (**Figure 3.2a**), and "1000", that lacks the DNA consensus sequence for NF-κB (**Figure 3.2b**). These fragments, containing at the ends the restriction sites recognized by the enzymes Bgl II and Hind III, were cloned into the pGL3 Basic vector (**Figure 2.1**) upstream of the luciferase reporter gene. To verify that orientation of the fragment was correct and the absence of errors during the amplification PCR, each fragment was subjected to automatic sequencing. The constructs were transformed in bacterial cells, purified, and used in transient transfection experiments.

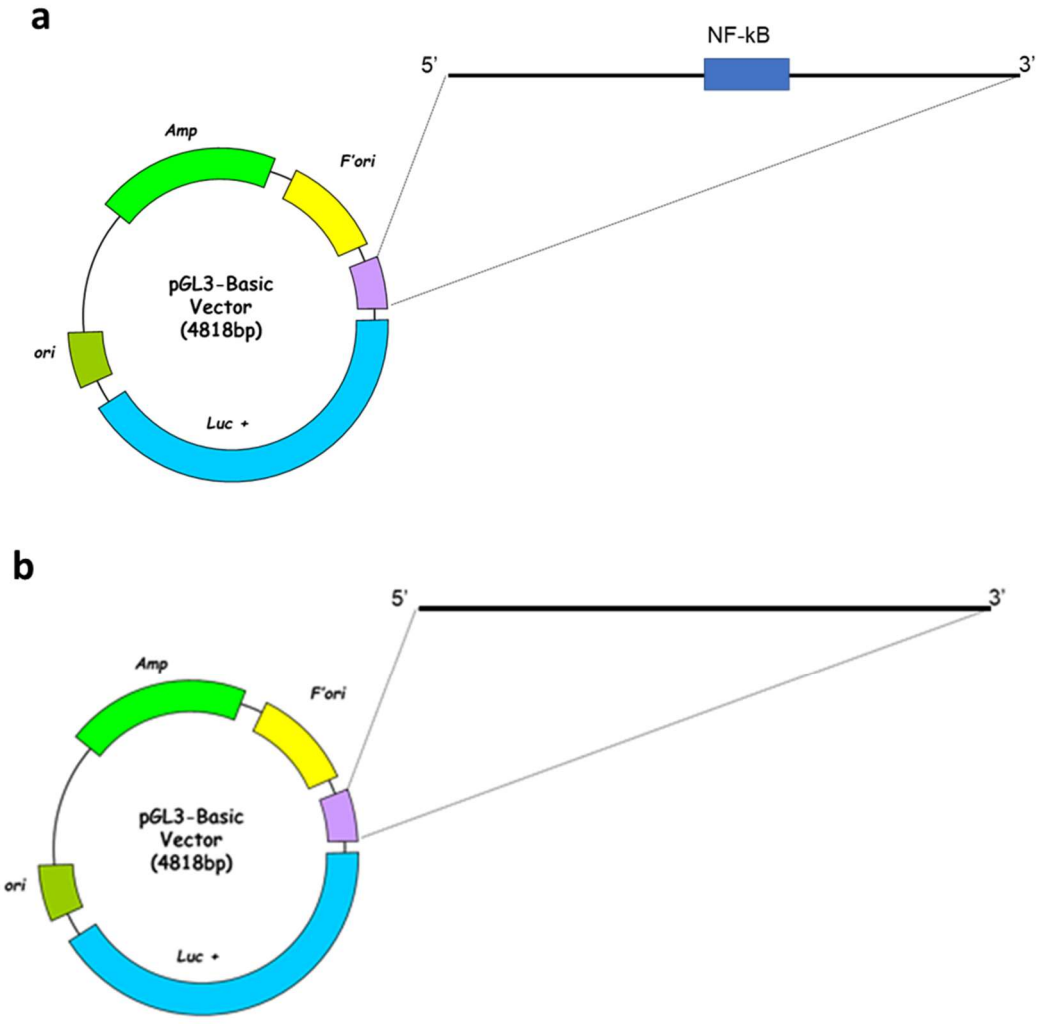

Figure 3.2: Schematic representation of construct "3000" and "1000". In pGL3-Basic vector (a) −3116/−82 bp region of the *ACLY* gene promoter, containing NF-κB responsive element, or (b) a deletion fragment of this region, without NF-κB responsive element, was cloned.

3.2 LPS and TNFα modulate ACLY via NF-κB transcription factor

To evaluate the putative role of NF-κB transcription factor in modulating ACLY during macrophage activation, HEK293 cells were transiently transfected with constructs "3000", "1000", obtained as described in section 3.1, or empty pGL3 vector (pGL3) as negative control (**Figure 3.3**). Forty-eight hours after transfection, cells were treated with LPS or TNFα for 24 hours. Then cells were lysed, and luciferase activity was evaluated. The choice to evaluate also the effect of TNFα was dictated to the fact that it is known that TNFα binds to TNF receptors and leads to NF-κB activation [111].

The value of luciferase activity for cells transfected with empty pGL3 vector (pGL3) (**Figure 3.3**) was set equal to 1, so the values for other treatments were calculated as proportion of pGL3. We observed an increase in luciferase activity when cells were transfected with "1000" and "3000" alone (**Figure 3.3**). LPS and TNFα tripled luciferase activity in HEK293 cells transfected with "3000", but they did not affect luciferase activity in the presence of "1000". Since construct "3000" contained the responsive element to NF-κB, we can conclude that LPS and TNFα modulate ACLY through NF- κB.

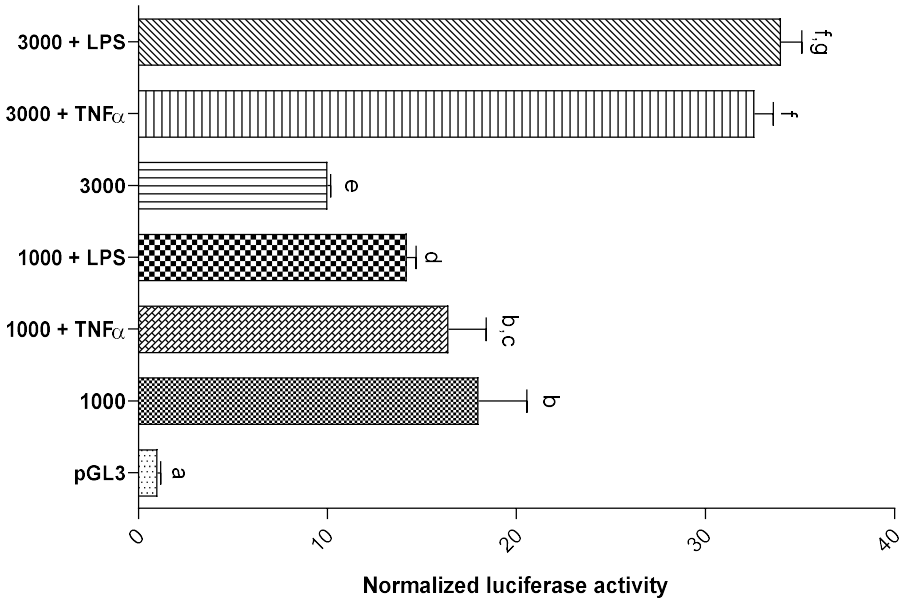

Figure 3.3: LPS and TNFα modulate ACLY expression through NF-κB. HEK293 cells were transiently transfected with pGL3 basic vectors: empty (pGL3), containing the −3116/−82 bp region of the *ACLY* gene promoter (3000) or a truncated version of this region (1000). Then, cells were triggered with LPS or TNFα. Cells transfected with empty pGL3-Basic vector were used as negative control. The luciferase gene reporter activity was assessed after 24 hours.

3.3 ACLY is upregulated very early in LPS-triggered macrophages

It is known that in macrophages differentiated from peripheral blood mononuclear cells LPS produced a rapid increase in ACLY mRNA and protein levels [51]. To shed more light on the early activation of ACLY, we treated human PBMC-derived macrophages with LPS and performed ACLY gene expression time courses to evaluate mRNA and protein levels.

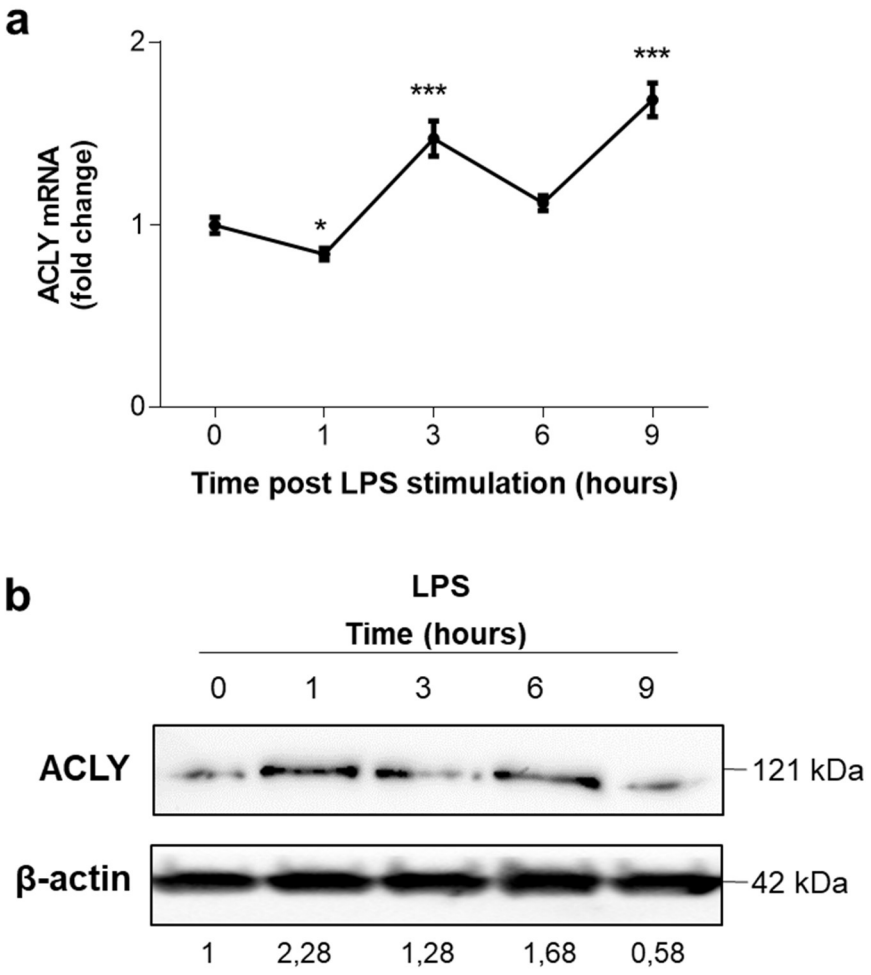

Figure 3.4: ACLY is early upregulated in PBMC-derived macrophages upon LPS stimulation. In the presence of LPS, in human PBMC-derived macrophages, ACLY mRNA and protein levels increase very early and change continuously in the first hours of activation. Real time PCR and Western blot were performed to evaluate ACLY mRNA (a) and protein (b) levels, respectively. In (b) specific antibodies detected the expression levels of ACLY and β-actin. The intensities of immunolabeled protein bands were measured by a quantitative software and normalized to β-actin; values obtained are reported under western blot images. Protein expression levels in untreated cells (0) were taken as 1 and other samples were expressed in proportion to untreated cells.

While ACLY mRNA increased 3 hours after LPS addition (**Figure 3.4a**), an early upregulation was observed within 1 hours after LPS stimulation when we analyzed ACLY protein. At this time point a double amount of ACLY protein was found followed by a decline at 3 hours and another increase at 6 hours post LPS addition (**Figure 3.4b**). ACLY mRNA decreased at 6 hours from the beginning of LPS treatment and reached a second peak after 3 hours, when it was 9 hours of treatment with LPS (**Figure 3.4a**). Conversely, ACLY protein levels declined at 9 hours reaching a value a lower than one of untreated cells (0, **Figure 3.4b**). Therefore, the trend in ACLY levels was not constant but fluctuated over time.

3.4 ACLY expression in immortalized bone marrow derived macrophages

Taking into consideration the technical impossibility of always working with macrophages deriving from PBMC as well as the interest in evaluating effects of the various treatments on the citrate pathway in cellular models derived from other species, we carried out experiments also in murine macrophages: immortalized bone marrow derived macrophages. Firstly, we treated iBMDM with LPS and evaluated ACLY protein levels. As reported in **Figure 3.5**, ACLY protein reached a peak after 3 hours-treatment with LPS to then declined. In iBMDM the maximum increase in ACLY expression is reached later -3 hours - than in macrophages derived from PBMC -1 hour- after LPS addition (**Figure 3.4b**). In iBMDM ACLY expression changes continuously in the first hours of LPS stimulation, too.

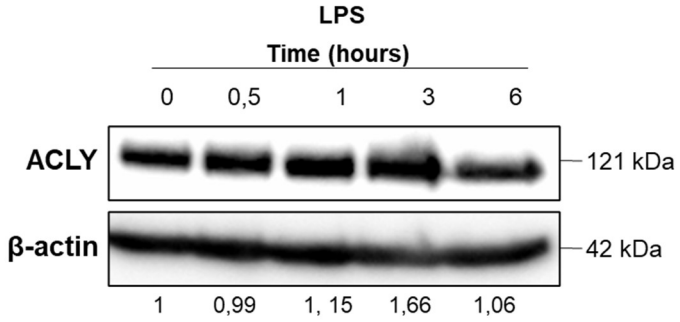

Figure 3.5: ACLY is early upregulated in iBMDM upon LPS stimulation. In the presence of LPS, in iBMDM, ACLY protein levels increase early and change continuously in the first hours of activation. Western blot experiments were performed to evaluate ACLY protein levels. Specific antibodies detected the expression levels of ACLY and β-actin. The intensities of immunolabeled protein bands were measured by a quantitative software and normalized to β-actin; values obtained are reported under western blot images. Protein expression levels in untreated cells (0) were taken as 1 and other samples were expressed in proportion to untreated cells.

3.5 LPS affects ACLY activity

Although it is well known that LPS modulates ACLY mRNA and protein [51] and time courses performed confirmed those data underling that ACLY upregulation is one of the fastest events during macrophage activation, effect of LPS on ACLY functional activity have never been investigated. Therefore, in PBMC-derived macrophages and iBMDM we evaluated ACLY activity after different times of LPS treatment. Surprisingly, the trend in ACLY activity was the same of protein levels in both human and murine macrophages. In PBMC-derived macrophages, ACLY showed two peaks at 1 and 6 hours, respectively, after LPS treatment (**Figure 3.6a**), similarly to protein levels, with the increase at 1 hour strongest that one at 6 hours (**Figure 3.4b**). The pattern of ACLY activity was like that of the protein in iBMDM where only one peak was observed at 3 hours of LPS stimulation (**Figure 3.6b**). Of note the peak of ACLY activity reached in human macrophages is more intense than in murine macrophages (**Figure 3.6**).

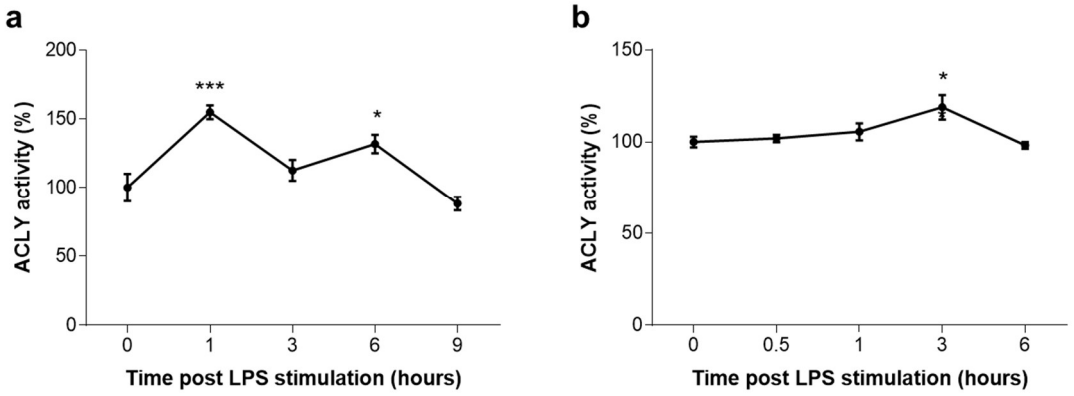

Figure 3.6: Effect of LPS on ACLY activity in PBMC-derived macrophages and iBMDM. Human (a) and murine (b) macrophages were triggered with LPS and ACLY enzymatic activity was evaluated. Values represent means ± SD of three independent experiments. Statistical significance of differences was evaluated by *one-way ANOVA* followed by *Dunnett's test* for multiple comparisons (*p<0.05, ***p<0.001).

3.6 Short-term ACLY activation supports histone acetylation

Recent studies have highlighted the key role of ACLY in promoting histone acetylation in LPS-triggered murine BMDMs [112, 113]. Therefore, we investigated on the existence of the same relationship between the short-term ACLY activation and histone acetylation status in human macrophages derived from PBMCs. To this end, we quantified the levels of acetylated histone H3 in human LPS-treated PBMC-derived macrophages in the presence or

absence of SB-204990 [103]. Of note, we observed a strong and early decrease of acetylated H3 histone in SB-treated macrophages at all the times tested from the beginning of LPS stimulation (1-3-6 hours) (**Figure 3.7**).

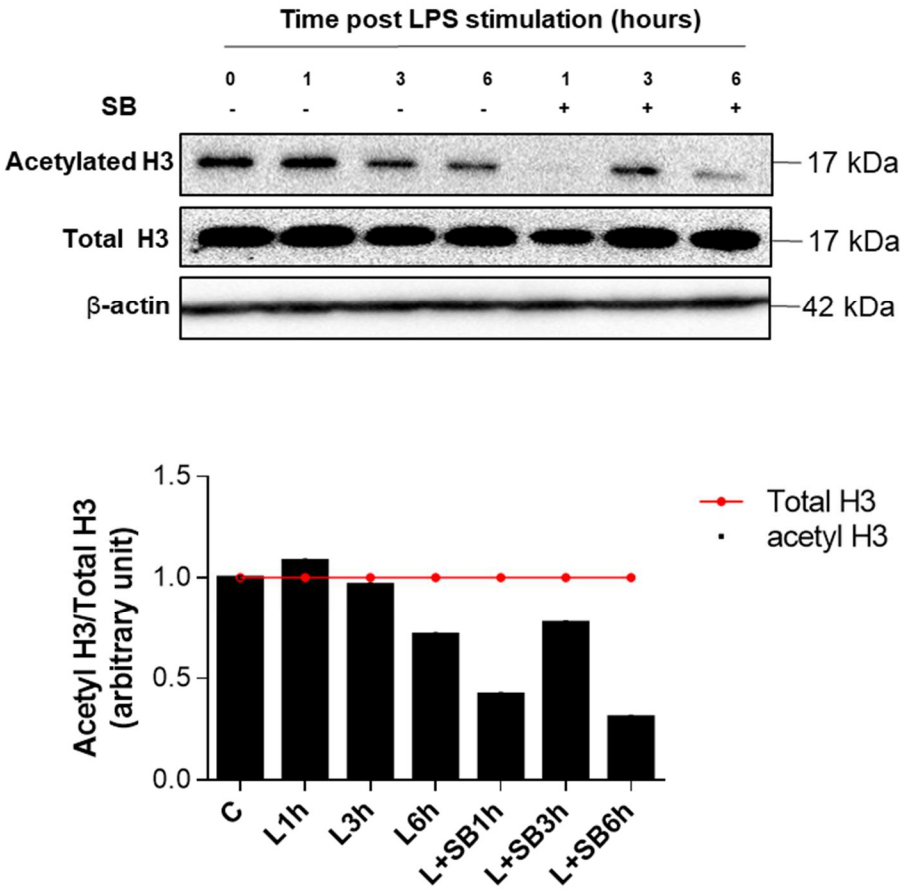

Figure 3.7. Short-term ACLY activation sustains histone acetylation Human PBMC-derived macrophages were treated with LPS for 1, 3 and 6 hours in the presence or not of SB-204990 (SB) and used to quantify H3 acetylated histone, total H3 and β-actin The intensities of immunolabeled protein bands were measured by using a quantitative software and normalized to total H3 levels (lower panel). Protein expression levels in control sample were taken as 1 and other samples were expressed in proportion of the control.

3.7 Short-term ACLY activation sustains the transcription of *IL-1β*, *IL6* and *PTGS2* proinflammatory genes

Afterwards, we treated human LPS-treated PBMC-derived macrophages with SB-204990 to analyze the effect of ACLY inhibition on *IL-1β, IL6* and *PTGS2* proinflammatory gene expression. To this end, ChIP experiments were performed by using specific antibody

against the acetylated histone H3. As shown in **Figure 3.8**, LPS induced a strong increase of the histone H3 acetylation levels in the promoter regions of *IL-1β, IL6* and *PTGS2* proinflammatory genes. SB addition completely abolished this effect at all the promoters analyzed, which suggests that ACLY activation by LPS is required to model chromatin structure to allow for the transcription of abovementioned proinflammatory genes.

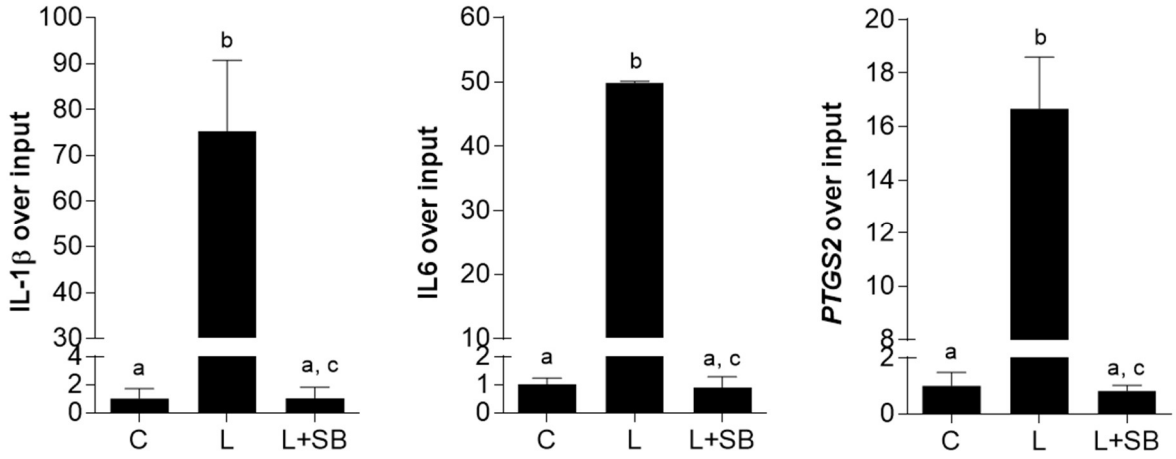

Figure 3.8. Short-term ACLY activation sustains transcription of *IL-1β, IL6* and *PTGS2* proinflammatory genes Human PBMC-derived macrophages were treated with LPS for 3 hours in the presence or not of SB-204990 (SB) and used to carry out chromatin immunoprecipitation (ChIP) analysis with an antibody against acetylated hystoneH3; then specific primers were used in Real-Time PCR experiments to analyze *IL-1β, IL6* and *PTGS2* gene promoters. Data are representative of three independent experiments and are presented as means ± SD. According to *one-way ANOVA*, differences were significant. Therefore, *Tukey's* post hoc test was performed, and different letters indicate significant differences between treatments at $p<0.05$.

As confirmation of this first result, IL-1β, IL6 and COX2 protein levels were quantified. We recorded reduced levels of IL-1β, IL6 and COX2 expression in the presence of ACLY inhibition by SB (**Figure 3.9**).

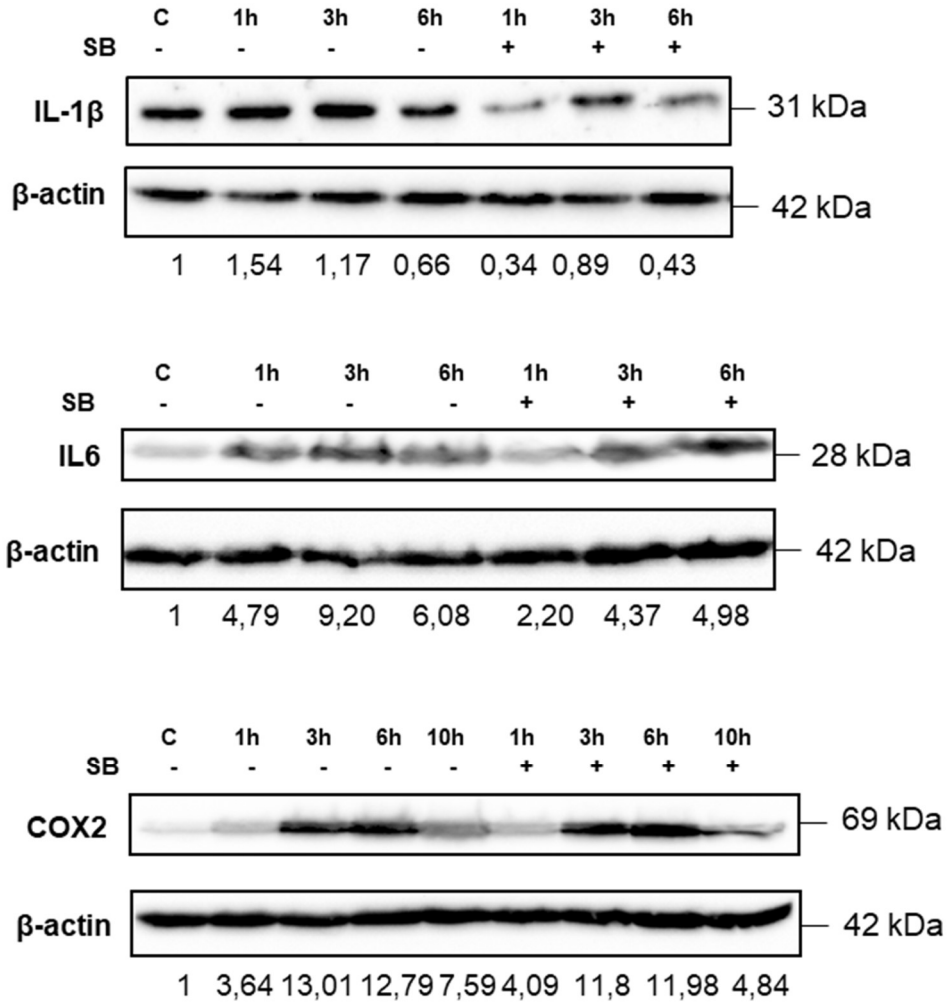

Figure 3.9. ACLY inhibition reduces IL-1β, IL6 and COX2 proinflammatory genes expression. Human PBMC-derived macrophages were treated with LPS for different times in the presence or not of SB-204990 (SB) and used to quantify IL-1β, IL6 and COX2 protein levels. Western blotting data presented are representative of at least 3 independent experiments. The intensities of immunolabeled protein bands were measured by using a quantitative software and normalized to β-actin: values obtained are reported under western blot images. Protein expression levels in control sample were taken as 1 and other samples were expressed in proportion of the control.

A parallel reduction was observed when the secretion of IL-1β, IL6 and PGE2 was measured in LPS-treated human macrophages in the presence of SB (**Figure 3.10**).

All these data confirm that LPS-induced human macrophages require a short-term ACLY activation to switch on the chromatin structure and trigger transcription of proinflammatory genes.

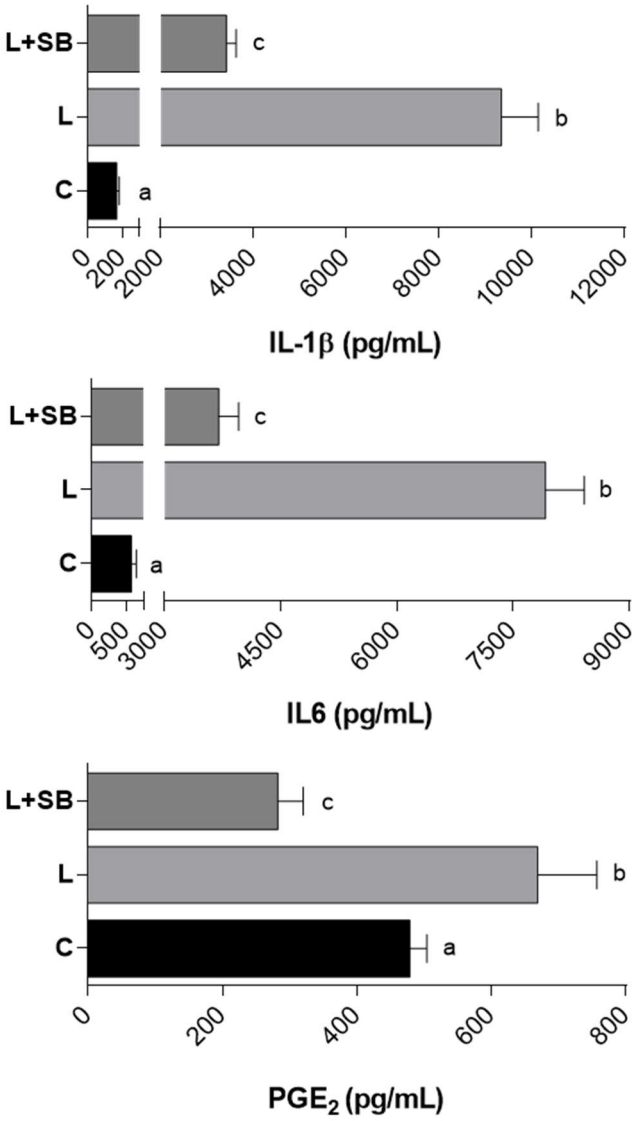

Figure 3.10. ACLY inhibition by SB reduces IL-1β, IL6 and PGE2 secretion. Human PBMC-derived macrophages were treated with LPS for different times in the presence or not of SB-204990 (SB) and used to quantify IL-1β, IL6 and PGE2 secretion. Data are representative of three independent experiments and are presented as means ± SD. According to one-way ANOVA, differences were significant. Therefore, Tukey's post hoc test was performed and different letters indicate significant differences between treatments at $p<0.05$.

3.8 Identification and quantification of *Aglianico del Vulture* red wine powder components

Aglianico del Vulture red wine samples were freeze-dried under vacuum (RWP_{FD}) or evaporated under reduced pressure (RWP_R) to obtain the red wine powder on which LC-

ESI-QTrap-MS/MS and LC-ESI-QTrap-MS analyses were performed. The simultaneous separation and identification of all compounds have been guaranteed using the Kinetex column and LC-ESI-MS/MS (alternating positive and negative ionization modes). In the optimized chromatographic column, the identified compounds displayed great results since retention times were very short, from 1.21 to 2.51 minutes (**Figure 3.11**).

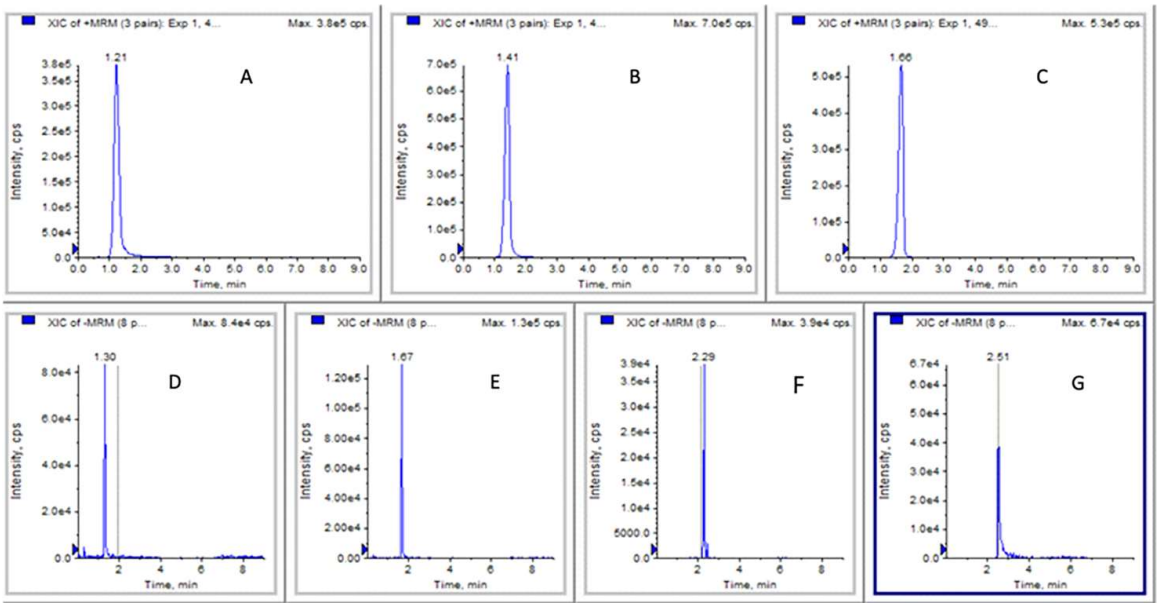

Figure 3.11: MRM data in both positive and negative ions of a mix standard solution A: delphinidin 3-*O*-glucoside; B: cyanidin 3-*O*-glucoside; C: malvidin 3-*O*-glucoside; D: caffeic acid; E: coumaric acid; F: resveratrol and G: quercetin.

Each component was identified by comparison of its *m/z* (mass to charge ratio) value in the total ion current (TIC) profile with that described in the literature. Seven secondary metabolites were identified (**Table 3.1**) belonging to a wide variety of structurally different classes: anthocyanidins (delphinidin 3-O-glucoside, cyanidin-3-O-glucoside, and malvidin 3-O-glucoside), phenolic acids (caffeic acid and p-coumaric acid), stilbenes (resveratrol), and flavonols (quercetin).

Aglianico del Vulture red wine powders revealed good content of anthocyanidins. Specifically, in RWP_{FD} malvidin 3-*O*-glucoside was the most abundant (14.00 ± 0.23 mg/100 mL), followed by cyanidin 3-*O*-glucoside (1.30 ± 0.218 mg/100 mL) and delphinidin 3-*O*-glucoside (0.072 ± 0.003 mg/100 mL) (**Table 3.1**). Those results are similar to the characteristic anthocyanidin profile of *Aglianico* wine: as reported in literature, 60%

of total anthocyanidins is represented by malvidin 3-*O*-glucoside while cyanidin 3-*O*-glucoside and delphinidin 3-*O*-glucoside are around 5% [114]. The content of resveratrol in *Aglianico del Vulture* was similar to other Italian red wines: 0.053 ± 0.01 mg/100 mL [115-117]. Concentrations of caffeic acid and *p*-coumaric acid were 0.218 ± 0.047 mg/100 mL and 0.078 ± 0.002 mg/100 mL, respectively. Quercetin was determined equal to 0.785 ± 0.02 mg/100 mL.

The extraction method employed influenced the amount of the specialized metabolites found in the red wine powders, as is evident from **Table 3.1**. The extract obtained by using rotary evaporator, RWP_R, showed lower amounts of all analyzed compounds with respect to RWP_{FD}.

	RWP_{FD} mg/100 mL ± SD	**RWP_R** mg/100 mL ± SD
Phenolic acids		
Caffeic acid	0.218 ± 0.047	0.118 ± 0.04
Coumaric acid	0.078 ± 0.002	0.057 ± 0.01
Stilbenes		
Resveratrol	0.053 ± 0.01	0.033 ± 0.01
Anthocyanidins		
Delphinidin-3-O-Glucoside	0.072 ± 0.003	0.054 ± 0.002
Cyanidin-3-O-Glucoside	1.30 ± 0.18	0.92 ± 0.11
Malvidin-3-O-Glucoside	14.00 ± 0.23	8.58 ± 0.07
Flavonols		
Quercetin	0.785 ± 0.02	0.419 ± 0.02

Table 3.1: Composition of red wine powders obtained from *Aglianico del Vulture*. Mass spectrometry-based analyses were carried out to identify and quantify specialized metabolites in RWP_{FD} and RWP_R. The mean values ± standard deviation (SD) from at least three independent experiments are reported.

3.9 Evaluation of cytotoxic effect of *Aglianico del Vulture* red wine powder on primary human monocytes

Primary human monocytes were treated for 72 hours with increasing concentrations of RWP_{FD} and RWP_R (2.5, 5, 10, 20, 50, 100, 200, 400, 800, 1600 and 3200 µg/mL). As shown in **Figure 3.12**, the extraction method employed also influenced the cell viability. When cell counts were performed, RWP_{FD} did not affect cell number until at dose of 800 µg/mL (**Figure 3.12a**). A slight cytotoxicity was observed at the highest tested concentrations of 1600 and 3200 µg/mL, where reductions in cell number compared with untreated cells (0) were about 20% and 40%, respectively (***$p<0.001$, *Dunnett's multiple comparisons test*) (**Figure 3.12a**). On the other hand, RWP_R halved the cell number at 800 µg/mL and at 3200 µg/mL only 15% of cells were viable (**Figure 3.12b**).

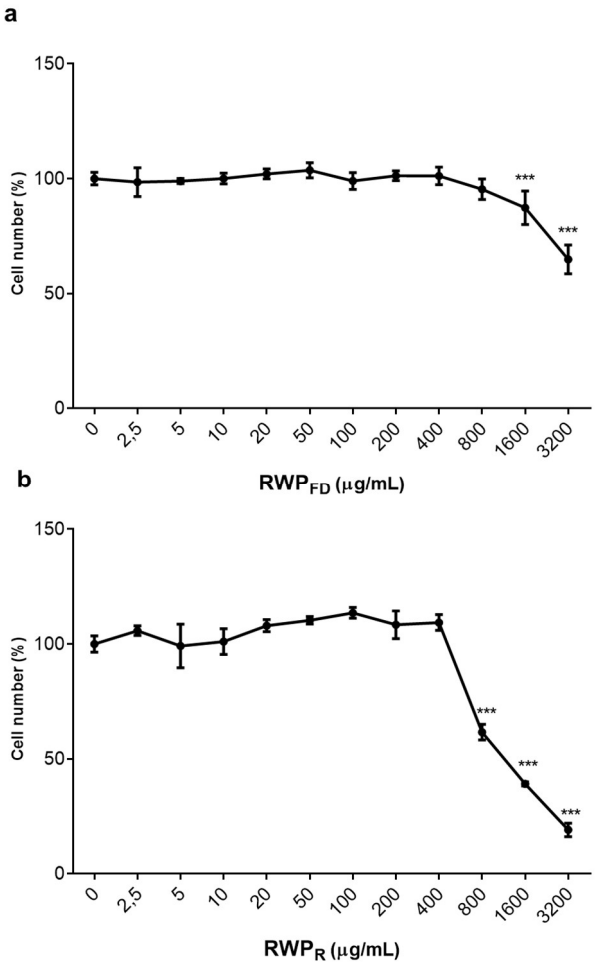

Figure 3.12: Effect of RWP_{FD} and RWP_R on primary human monocytes cell number. Primary human monocytes were treated with increasing concentrations of RWP_{FD} and RWP_R, ranging from 2.5 to 3200 µg/mL,

and cell viability was assessed by cell count after 72 hours exposure. The mean values ± SD of three independent experiments with four replicates in each are shown. Differences were significant ($p<0.001$) according to *one-way ANOVA*. *Dunnett's multiple comparisons test* was run as *post-hoc* test to compare treatment groups with control group (0, set at 100%); where indicate, differences were statistically significant (*** $p<0.001$).

These first results have highlighted that the extraction method affected both the amount of the specialized metabolites and the cell viability. Taking into consideration that RWP_R was less rich in phenolic compounds and more cytotoxic, we decided to perform all the subsequent experiments, aimed to evaluate anti-inflammatory and immunomodulatory properties of *Aglianico del Vulture* wine, with RWP_{FD}. Therefore, we have chosen two intermediate and non-toxic concentrations, one 10 times higher than the other one: 20 and 200 μg/mL.

3.10 *Aglianico del Vulture* red wine powder reduces the secretion of pro-inflammatory cytokines IL-1β, IL-6 and TNF-α

The health promoting properties of red wines in many pathological conditions may include their ability to fight inflammation since phenolic compounds act as positive modulators of inflammatory biomarkers (e.g. cytokines) and oxidative stress. Therefore, the start point of our analysis in defining the immunomodulatory effects of *Aglianico del Vulture* red wine powder was the quantification of cytokines. We treated primary human monocytes with LPS in the presence or not of RWP_{FD} 20 (R20) and 200 μg/mL (R200) and focused on the secretion of pro-inflammatory cytokines IL-1β, IL-6 and TNF-α. Since LPS leads to the rapid activation of pro-inflammatory cytokines IL-1β, IL-6 and TNF-α [2], we assessed the release of these inflammatory mediators after 24 hours of stimulation with LPS. LPS induced marked and significant increases in the levels of all the cytokines analyzed (**Figure 3.13:** C *vs.* L, $p<0.001$, *Tukey's test*). We observed a dose-dependent manner reduction in IL-1β, IL-6 and TNF-α secretion in the presence of RWP_{FD} (**Figure 3.13**). Specifically, at a dose of 200 μg/mL, RWP_{FD} reduced significantly of almost by half the levels of IL-6 and TNFα pro-inflammatory cytokines released after stimulation with LPS (**Figure 3.13b-c**), while IL-1β of 40%. Whereas RWP_{FD} used as 20 μg/mL decreased levels of IL-1β, IL-6 and TNF-α (**Figure 3.13**: L *vs.* L + R20, $p<0.001$, *Tukey's test*) by about 35%.

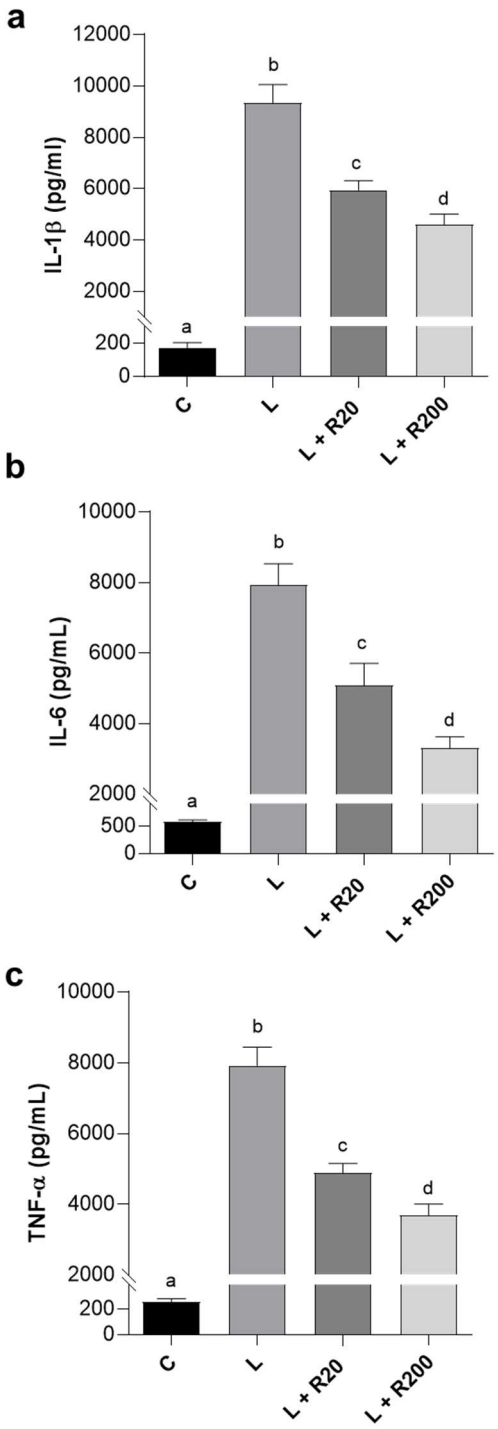

Figure 3.13: RWP affected the secretion of IL-1β, IL-6 and TNF-α pro-inflammatory cytokines. Primary human monocytes were incubated with RWP_{FD} and activated to macrophages with 1 µg/mL LPS. Twenty-four hours later, the concentrations of the pro-inflammatory IL-1β (a), IL-6 (b) and TNF-α (c) cytokines in cell culture supernatants were measured. Values represent the means ± SD of three independent experiments with four replicates in each. According to *one-way ANOVA*, differences in IL-1β (a), IL-6 (b), TNF-α (c) levels were significant ($p<0.001$). Therefore, *Tukey's post hoc test* was performed, and different letters indicate significant differences between treatments at $p<0.05$. Abbreviations: C, control; L, LPS; R20, RWP_{FD} 20 µg/mL; R200, RWP_{FD} 200 µg/mL.

3.11 *Aglianico del Vulture* red wine powder increases the production of pro-inflammatory cytokine IL-10

Excessive secretion of pro-inflammatory cytokines could be deleterious for the host since they could induce systemic metabolic and hemodynamic problems. To dampen excessive inflammation during infection, macrophages produce IL-10 anti-inflammatory cytokine as a negative-feedback mechanism. LPS leads to the production of IL-10, necessary to initiate host defence against microbial invasion [2]. We assessed IL-10 release after 24 hours of stimulation with LPS in the presence of RWP_{FD}. IL-10 anti-inflammatory cytokine levels increased significantly in a concentration-dependent manner when cells were treated with RWP_{FD} compared to being triggered only with LPS (**Figure 3.14**: L *vs.* L+R20 – L+R200, $p<0.001$, *Tukey's test*). At the dose of 200 µg/mL, IL-10 amount was almost the double.

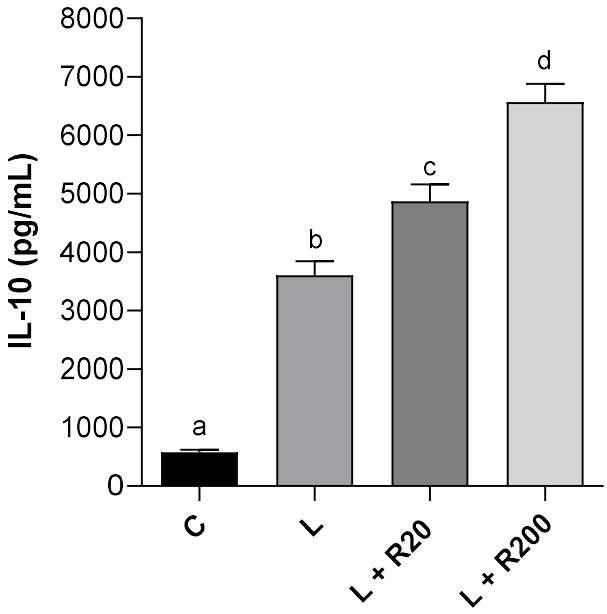

Figure 3.14: RWP affected the secretion of IL-10 anti-inflammatory cytokine. Primary human monocytes were incubated with RWP_{FD} and activated to macrophages with 1 µg/mL LPS. Twenty-four hours later, the concentration of IL-10 was evaluated. Values represent the means ± SD of three independent experiments with four replicates in each. According to *one-way ANOVA*, differences were significant ($p<0.001$). Therefore, *Tukey's post hoc test* was performed, and different letters indicate significant differences between treatments at $p<0.05$. Abbreviations: C, control; L, LPS; R20, RWP_{FD} 20 µg/mL; R200, RWP_{FD} 200 µg/mL.

3.12 NF-κB pathway is a critical target of *Aglianico del Vulture* red wine powder

NF-κB pathway plays keys roles both in inflammatory process and for the protective properties of a moderate wine consumption [118] . Indeed NF-κB regulates the expression of several immunoregulatory genes encoding for enzymes (e.g. COX2), inflammatory cytokines, and chemokines [119].

We analyzed if the red wine powder from *Aglianico del Vulture* will affect NF-κB pathway beginning from the evaluation of NF-κB protein levels. For this, LPS-triggered macrophages were treated RWP_{FD} 20 or 200 μg/mL and western blot analyses were performed. As was to be expected, LPS induced a marked over-expression of subunit p65 of NF-κB (**Figure 3.15a**). RWP_{FD}, regardless of the dose, reduced p65/NF-κB protein levels to about 40% (**Figure 3.15a**).

Similar results were obtained when the attention was focused on NF-κB signal transduction pathway. HEK293 cells were transfected with a NF-κB reporter plasmid containing a firefly luciferase gene driven by five copies of NF-κB responsive element located upstream of TATA box: pro-inflammatory stimuli induce endogenous NF-κB to bind to the DNA responsive elements and thus the transcription of luciferase reporter gene with consequent increase in luciferase activity. In cells treated only with LPS we observed a significant increase in luciferase activity, when compared to untreated cells (**Figure 3.15b**, C *vs.* LPS, $p<0.001$, *Tukey's test*); RWP_{FD} reported the levels of luciferase activity at values like those of untreated cells. Even if significant (*Tukey's test*), no strong differences were found between RWP_{FD} 20 μg/mL and RWP_{FD} 200 μg/mL in inhibit NF-κB pathway (**Figure 3.15b**).

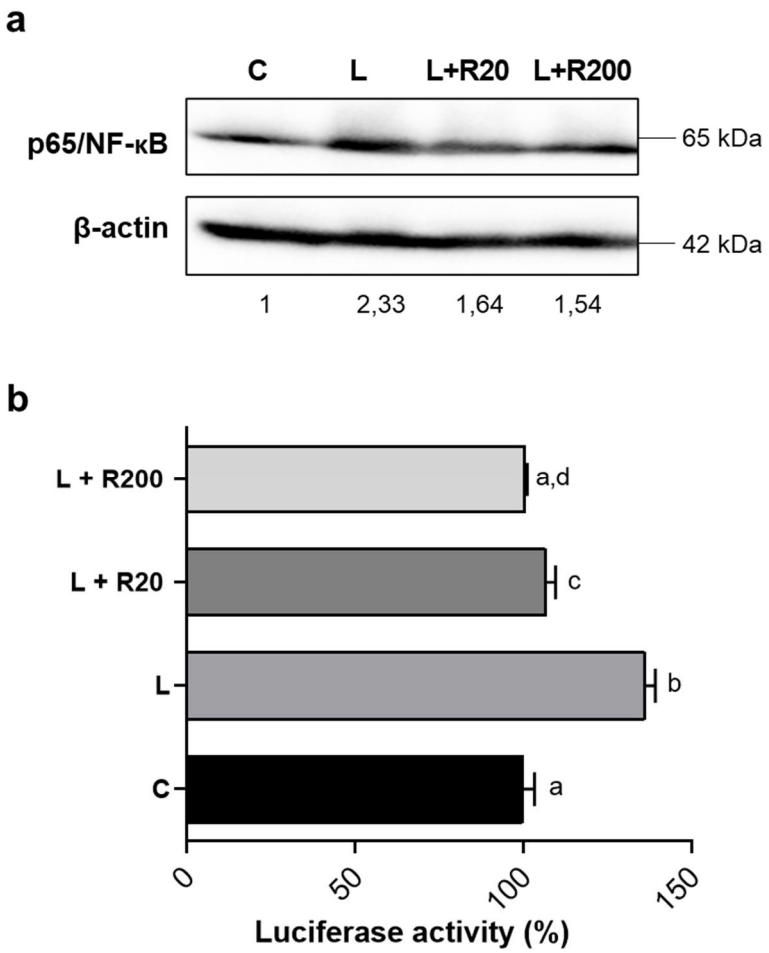

Figure 3.15. RWP reduced NF-κB expression and promoter activity. (a) Primary human monocytes were incubated with RWP_{FD} 20 µg/mL or RWP_{FD} 200 µg/mL and activated to macrophages with 1 µg/mL LPS. Specific antibodies detected the expression levels of p65 and β-actin. The intensities of immunolabeled protein bands were measured by a quantitative software and normalized to β-actin; values obtained are reported under western blot images. Protein expression levels in control sample were taken as 1 and other samples were expressed in proportion to the control. (b) HEK293 cells were transfected with NF-κB luciferase reporter plasmid and treated with LPS in the presence or not of RWP_{FD} 20 µg/mL or RWP_{FD} 200 µg/mL. Bar chart reports the mean values ± SD of three independent experiments, each in triplicate. According to *one-way ANOVA*, differences were significant ($p<0.001$). Therefore, *Tukey's post hoc test* was performed, and different letters indicate significant differences between treatments at $p<0.05$. Abbreviations: C, control; L, LPS; R20, RWP_{FD} 20 µg/mL; R200, RWP_{FD} 200 µg/mL.

3.13 *Aglianico del Vulture* red wine powder inhibits p65 nuclear translocation

NF-κB is made of two subunits (p65 and p50) and, when associated with an I-κB protein, is sequestered in the cytoplasm. The binding to cell surface receptors of activation signals such as endotoxins (i.e. LPS) or tumor necrosis factor-α (TNF-α) induces the phosphorylation of

I-κB protein and its ubiquination. Once being freed from its association with I-κB, the NF-κB complex moves from cytoplasm to the nucleus where it binds to specific sequences in the promoter/enhancer regions of its target genes. Taking into consideration that RWP_{FD} affected the expression levels of p65, we analyzed the cellular localization of NF-κB after treatment with *Aglianico del Vulture* powder. In monocytes triggered only with LPS, we observed the translocation of subunit p65 of NF-κB from cytosol to nucleus after 1 hour and 3 hours (**Figure 3.16**). In presence of RWP_{FD}, the main NF-κB localization was cytosolic (**Figure 3.16**).

These data, with previously described in section 3.10, suggest that RWP plays a role in inhibiting the NF-κB pathway.

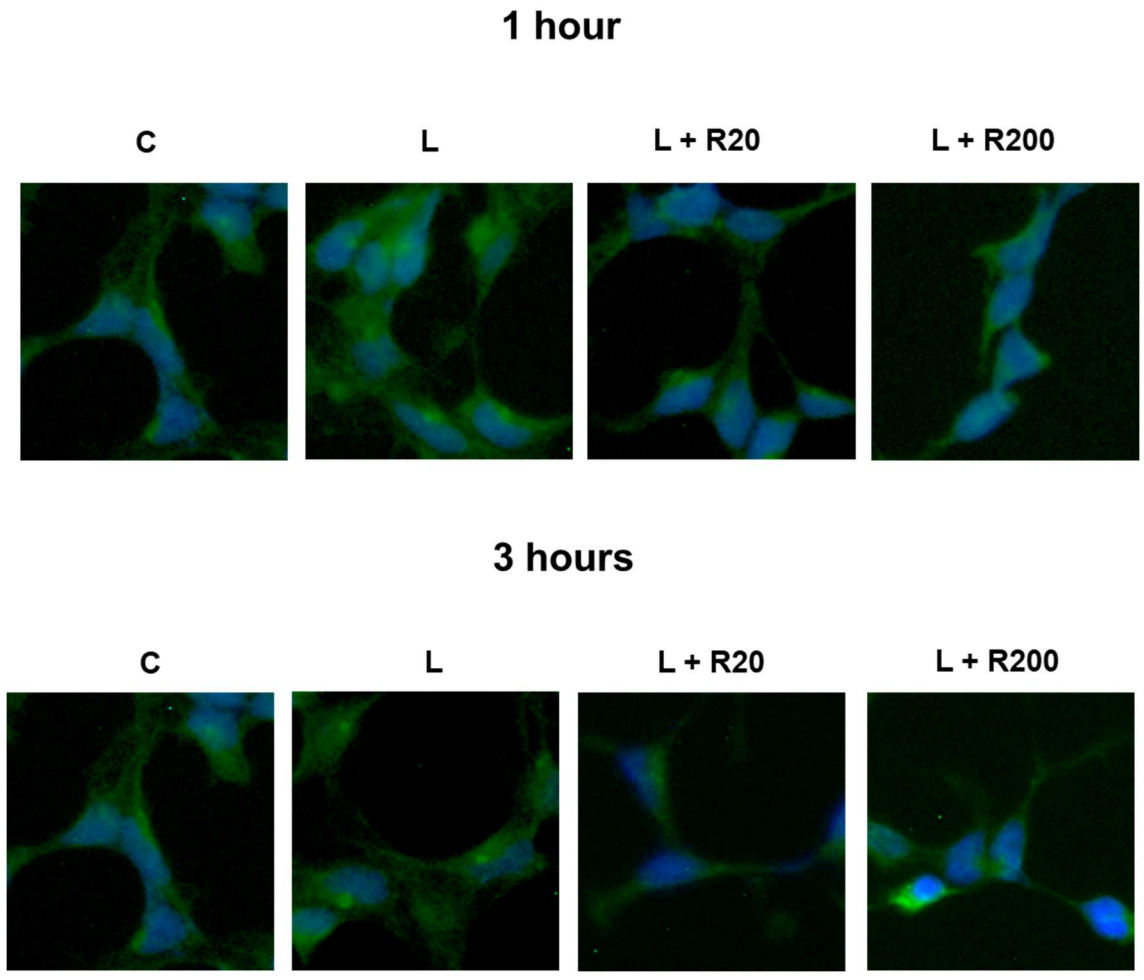

Figure 3.16. RWP inhibited NF-κB nuclear translocation. Primary human monocytes were incubated with RWP_{FD} 20 µg/mL or RWP_{FD} 200 µg/mL and activated to macrophages with 1 µg/mL LPS. Immunocytochemistry experiments were performed to identify the cellular localization of p65, recognized by a specific antibody. Abbreviations: C, control; L, LPS; R20, RWP_{FD} 20 µg/mL; R200, RWP_{FD} 200 µg/mL.

3.14 *Aglianico del Vulture* red wine powder modulates citrate carrier expression through NF-κB

NF-κB modulates *SLC25A1* gene, which encodes the mitochondrial citrate carrier, one of the components of the citrate pathway [1, 70]. Indeed, the human *SLC25A1* promoter contains two NF-κB response elements at positions −414/−405 bp and −1314/−1305 bp. To verify if RWP induced alterations in the transcription rate of the *SLC25A1* promoter through NF-κB, HEK293 cells were transfected with SLC25A1pGL3 - the previously described pGL3 basic-LUC vector encompassing the −1785/−20 bp promoter region of the *SLC25A1* gene cloned upstream of the luciferase reporter gene [99].

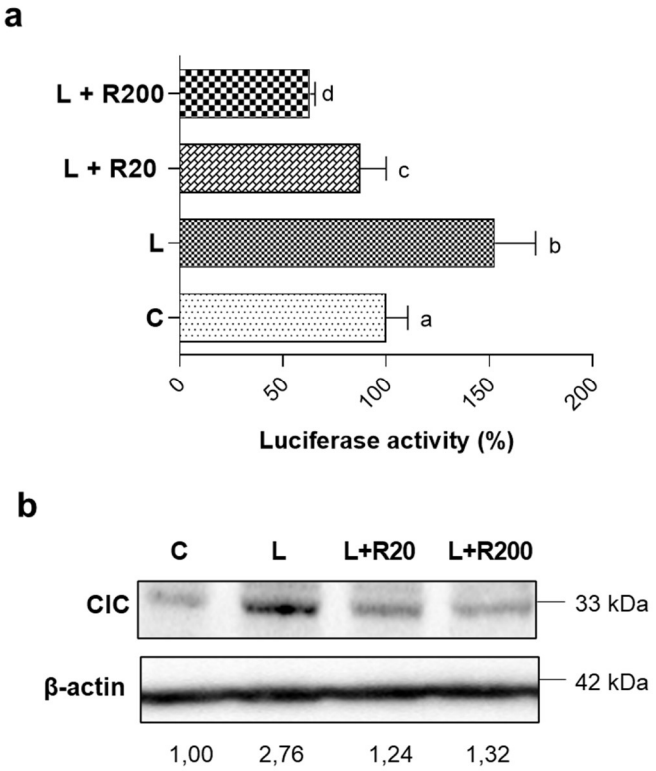

Figure 3.17. Effect of RWP on CIC transcription rate and expression. (a) HEK293 cells were transfected with SLC25A1pGL3. Then, cells were triggered with LPS in absence (L) or in presence of RWP_{FD} 20 µg/mL or RWP_{FD} 200 µg/mL. Unstimulated cells (C) were used as negative control. The luciferase gene reporter activity was assessed after 24 hours. Values represent means ± SD of three experiments made in triplicate. Statistical analysis was performed by o*ne-way ANOVA* followed by *Tukey's test* for multiple comparisons. Different letters indicate significant differences at $p<0.05$. (b) Primary human monocytes, pre-incubated for 1 hour with RWP_{FD} 20 µg/mL or RWP_{FD} 200 µg/mL, were activated to macrophages with LPS and CIC and β-actin protein levels were evaluated. CIC, and β-actin proteins were immunodecorated with specific antibodies. The intensities of immunolabeled protein bands were measured by using a quantitative software and normalized to β-actin: values obtained are reported under western blot images. Protein expression levels in control sample were taken as 1 and other samples were expressed in proportion of the control. Abbreviations: C, control; L, LPS; R20, RWP_{FD} 20 µg/mL; R200, RWP_{FD} 200 µg/mL.

Thus, cells were treated with LPS, in the presence or absence of RWP_{FD}. We observed that RWP_{FD} significantly reduced luciferase activity in a dose dependent manner by 50% (RWP_{FD} 20 µg/mL) and 60% (RWP_{FD} 200 µg/mL) in cells upon LPS stimulation (*Tukey's test*, **Figure 3.17a**).

We also performed western blot analyses to evaluate CIC expression and we found, as was to be expected, reduced CIC protein levels after RWP_{FD} treatment (**Figure 3.17b**). However, no dose dependent effect at the protein level was observed. LPS induced a threefold increase of CIC with respect to untreated cells (C, **Figure 3.17b**) and RWP_{FD}, as both 20 µg/mL and 200 µg/mL, reported CIC levels to values similar to those of control (**Figure 3.17b**).

3.15 *Aglianico del Vulture* red wine powder affects the cytosolic citrate levels

The mitochondrial citrate carrier is upregulated in inflammation being responsible for the export of citrate from mitochondria to cytosol after isocitrate dehydrogenase inhibition induced by activating stimuli. We have demonstrated that *Aglianico del Vulture* powder could affect CIC expression through NF-κB. In human monocytes treated with LPS, in the presence or absence of $RWP_{FD,}$ we detected a correspondent lowering in cytosolic citrate levels: RWP_{FD} either as 20 µg/mL or as 200 µg/mL reduced cytosolic citrate by around 40% with respect to LPS-triggered cells (**Figure 3.18**).

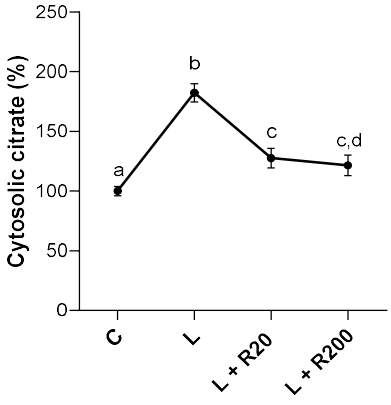

Figure 3.18: Effect of RWP_{FD} on cytosolic citrate levels. Primary human monocytes, pre-incubated for 1 hour with RWP_{FD} 20 µg/mL or RWP_{FD} 200 µg/mL, were activated to macrophages with LPS and the cytosolic citrate concentration was measured by a fluorometric method. Values represent means ± SD of three experiments, each in triplicate. Statistical analysis was performed by o*ne-way ANOVA* followed by *Tukey's test* for multiple comparisons. Different letters indicate significant differences at $p<0.05$. Abbreviations: C, control; L, LPS; R20, RWP_{FD} 20 µg/mL; R200, RWP_{FD} 200 µg/mL.

3.16 *Aglianico del Vulture* red wine powder regulates ACLY through NF-κB transcription factor

HEK293 cells were transiently transfected with pGL3-Basic vector containing the −3165/−20 bp region of the human *ACLY* gene promoter (called "3000", **Figure 3.19**), including the NF-κB responsive element, and with the mutant construct without the NF-κB responsive element (called "1000", **Figure 3.19**), The absence of the binding site for NF-κB was responsible for the lower *ACLY* gene promoter activity in cells transfected with 1000 than 3000 (**Figure 3.19**). Following 24 hours of LPS treatment, the strongest promoter activity was registered in 3000 transfected cells (3000 + LPS, **Figure 3.19**). The luciferase gene reporter activity was significantly reduced to levels like unstimulated cells (3000, **Figure 3.19**) by RWP_{FD} 20 µg/mL and to even lower levels by RWP_{FD} 200 µg/mL (**Figure 3.19**).

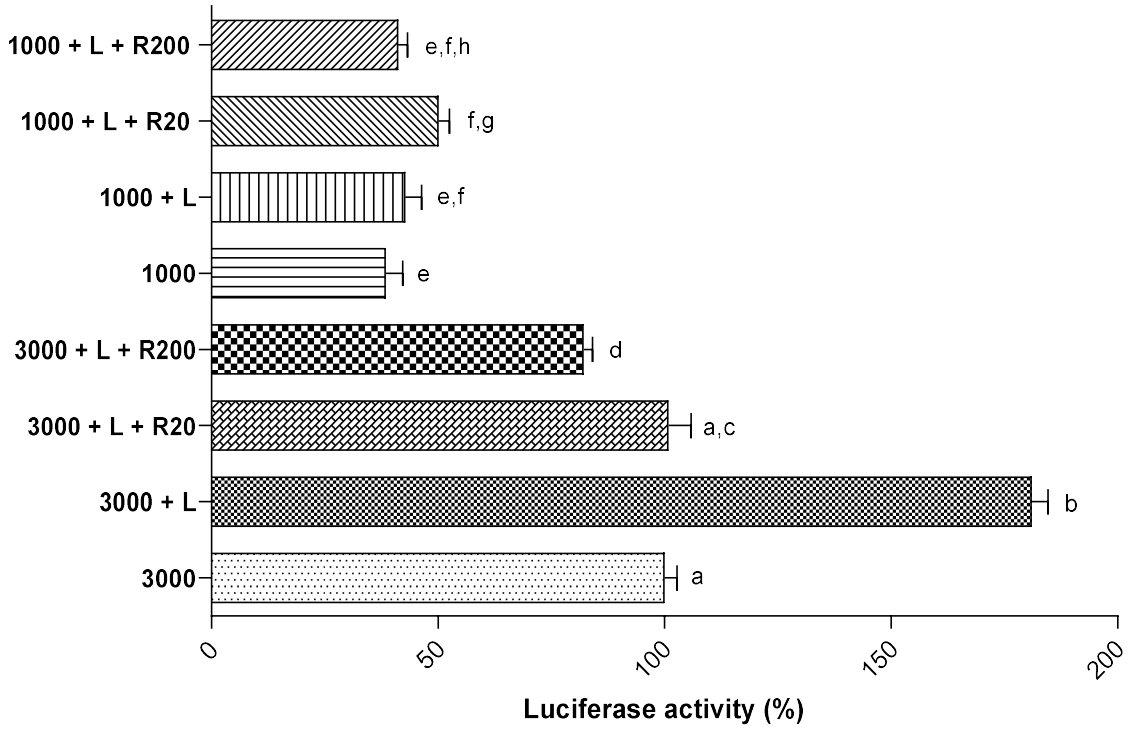

Figure 3.19. RWP_{FD} modulated ACLY through NF-κB. HEK293 cells were transiently transfected with 3000 or 1000. Then, cells were triggered with LPS in absence (L) or in presence of RWP_{FD} 20 µg/mL or RWP_{FD} 200 µg/mL. Unstimulated cells were used as negative control. The luciferase gene reporter activity was assessed after 24 hours. Values represent means ± SD of three experiments conducted in triplicate. Statistical analysis was performed by o*ne-way ANOVA* followed by *Tukey's test* for multiple comparisons. Different letters indicate significant differences at $p<0.05$. Abbreviations: C, control; L, LPS; R20, RWP_{FD} 20 µg/mL; R200, RWP_{FD} 200 µg/mL.

3.17 *Aglianico del Vulture* red wine powder reduces ACLY expression and activity

RWP_{FD} induced decreases in ACLY protein levels and enzymatic activity in LPS-triggered macrophages parallel to luciferase activity reduction as consequence of NF-κB inhibition (**Figure 3.20**). More in detail, LPS induced a two-fold increase in ACLY expression levels (**Figure 3.20a**) and a 35% rise in ACLY activity (**Figure 3.20b**). No significant differences were observed between the two tested concentrations of RWP_{FD} in bringing ACLY protein levels (**Figure 3.20a**) and activity (**Figure 3.20b**) down. These results, together with CIC and cytosolic citrate depletion, define a crucial role of RWP in immunometabolism as inhibitor of the citrate pathway.

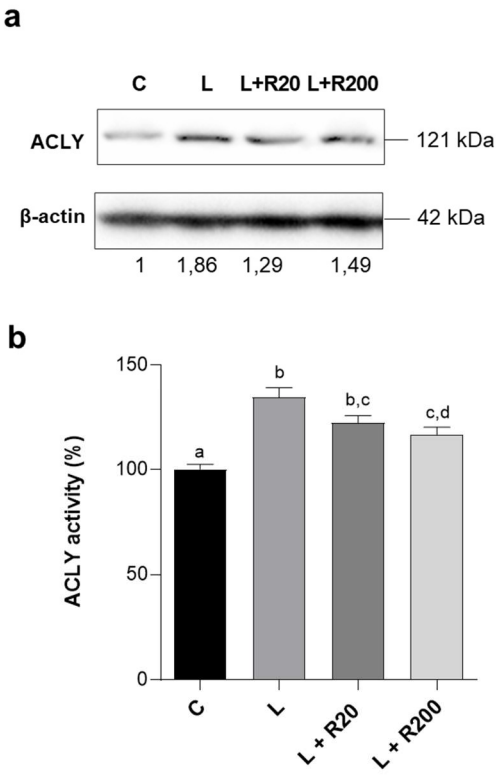

Figure 3.20. Effect of RWP_{FD} on ACLY protein and activity. (a) Primary human monocytes, pre-incubated for 1 hour with RWP_{FD}, were activated to macrophages with LPS and protein levels of ACLY and β-actin were evaluated. The intensities of immunolabeled protein bands, immunodecorated with specific antibodies, were measured by using a quantitative software and normalized to β-actin: values obtained are reported under western blot images. Protein expression levels in control sample were taken as 1 and other samples were expressed in proportion of the control. (b) In cells treated as in (a) ACLY enzymatic activity was quantified. In (b) values represent means ± SD of three experiments performed in triplicate. Statistical analysis was performed by o*ne-way ANOVA* followed by *Tukey's test* for multiple comparisons. Different letters indicate significant differences at $p<0.05$. Abbreviations: C, control; L, LPS; R20, RWP_{FD} 20 µg/mL; R200, RWP_{FD} 200 µg/mL.

3.18 *Aglianico del Vulture* red wine powder reduces histone acetylation via ACLY

It has been recently demonstrated that rapid metabolic changes in LPS-induced macrophages are important to increase acetyl-CoA derived from citrate following ACLY cleavage. Acetyl-CoA contributes in turn to histone acetylation [79, 113], epigenetic modification critical in regulation if global chromatin accessibility and gene transcription. Changes in histone acetylation have a great impact in inflammation since transcriptional regulation of genes involved in macrophages activation and inactivation or determination of their polarization state occurs through histone modifications [72].

We have shown that after LPS stimulation the levels of acetylated H3 histone increased (**Figure 3.21**) while no changes were observed in total H3 levels. Conversely, the treatment of cells with RWP_{FD} lowered acetylated H3 in a dose dependent manner (**Figure 3.21**), suggesting an epigenetic activity of *Aglianico del Vulture* red wine powder.

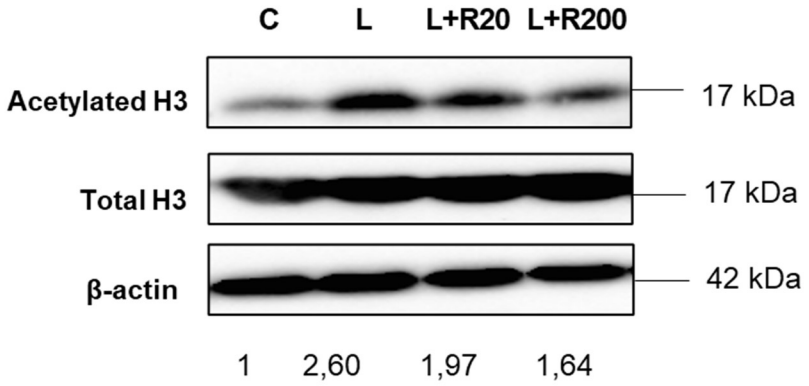

Figure 3.21. Effect of RWP_{FD} on H3 histone acetylation. Primary human monocytes, pre-incubated for 1 hour with RWP_{FD}, were activated to macrophages with LPS and protein levels of acetylated H3, total H3 and β-actin were evaluated. The intensities of immunolabeled protein bands were measured by using a quantitative software and normalized to β-actin: values obtained are reported under western blot images. Protein expression levels in control sample were taken as 1 and other samples were expressed in proportion of the control. Abbreviations: C, control; L, LPS; R20, RWP_{FD} 20 µg/mL; R200, RWP_{FD} 200 µg/mL**.**

3.19 *Aglianico del Vulture* red wine powder lowers ROS levels

The previous results clearly indicated that RWP_{FD} downregulated the citrate pathway. Indeed, reduced levels of CIC and ACLY and cytosolic citrate were observed in the presence of RWP_{FD} in LPS-triggered macrophages. Citrate cleavage made by ACLY supplies intermediaries for the biosynthesis of three inflammatory mediators: ROS, $NO^{\bullet}$ and

prostaglandin E_2 [95]. In LPS-triggered macrophages, the accumulated citrate is exported by CIC from mitochondria to the cytosol where it is converted by ACLY into oxaloacetate and acetyl-CoA. OAA is converted to pyruvate with consequent production of NADPH [120], used for ROS and $NO^{\bullet}$ synthesis. Our analysis showed enhanced and significant releases of ROS when human primary monocytes were activated only with LPS (**Figure 3.22**).

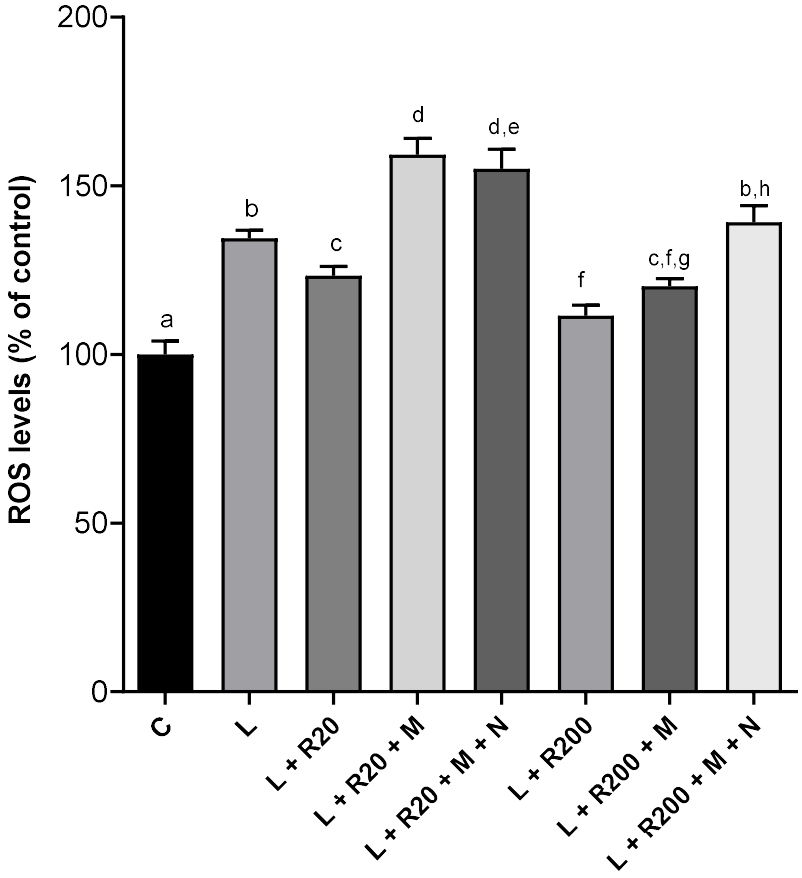

Figure 3.22. RWP lowered ROS levels, which were restored by addition of exogenous malate and NADPH. Primary human monocytes were treated with LPS (L) in absence or in presence of RWP_{FD} alone or plus malate and NADPH. Following 24 hours, ROS levels were evaluated and expressed as percentage of unstimulated cells (C, set at 100 %). Mean values ± SD of three replicate independent experiments with five replicates in each are shown. According to *one-way* ANOVA, differences were significant ($p<0.001$). Therefore, *Tukey's post hoc test* was performed and different letters indicate significant differences between treatments at $p<0.05$. Abbreviations: C, control; L, LPS; R20, RWP_{FD} 20 µg/mL; R200, RWP_{FD} 200 µg/mL; M, malate; N, NADPH.

Conversely, RWP_{FD} reduced the levels of reactive oxygen species in a dose dependent manner. More in detail, RWP_{FD} 20 µg/mL decreased the levels of ROS - with respect to cells treated only with LPS - by 10% and RWP_{FD} 200 µg/mL by 20% (**Figure 3.22**). Malate and NADPH are two metabolites downstream the citrate pathway: malate is produced by MDH1,

while NADPH derived from ME1 cleavage of malate in pyruvate. Exogenous malate used alone or in combination with NADPH reverts ACLY inhibition phenotype leading to a huge increase in ROS levels, as evident from **Figure 3.22**.

3.20 *Aglianico del Vulture* red wine powder affects NO• concentration

Nitric oxide is another metabolite whose production could be influenced by the activation or inhibition of the citrate pathway. When we quantified NO• levels in LPS-triggered human macrophages treated RWP_{FD} we found a dose dependent reduction.

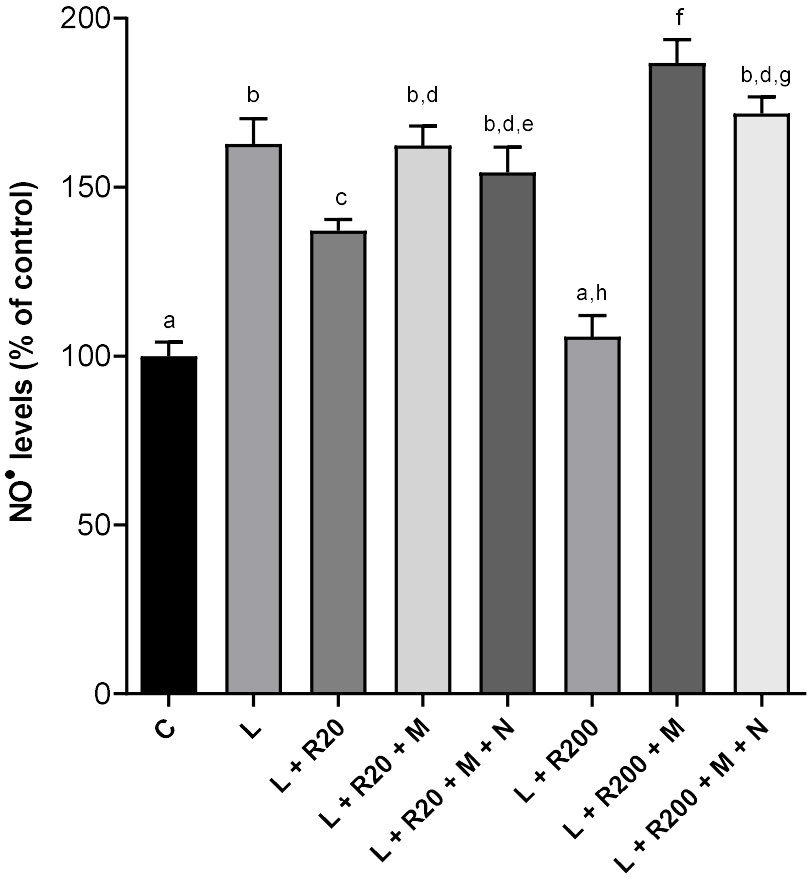

Figure 3.23. RWP lowered NO• levels, which were restored by addition of exogenous malate and NADPH. Primary human monocytes were treated with LPS (L) in absence or in presence of RWP_{FD} alone or plus malate and NADPH. Following 24 hours, NO• levels were evaluated and expressed as percentage of unstimulated cells (C, set at 100 %). Mean values ± SD of three replicate independent experiments with five replicates in each are shown. According to *one-way* ANOVA, differences were significant ($p<0.001$). Therefore, *Tukey's post hoc test* was performed and different letters indicate significant differences between treatments at $p<0.05$. Abbreviations: C, control; L, LPS; R20, RWP_{FD} 20 µg/mL; R200, RWP_{FD} 200 µg/mL; M, malate; N, NADPH.

In particular, RWP_{FD} 20 µg/mL decreased by 15% the levels of $NO^{\bullet}$ while RWP_{FD} 200 µg/mL of about 35% with respect to cells activated only with LPS (**Figure 3.23**). When malate and NADPH were added, $NO^{\bullet}$ levels increased in LPS-triggered cells treated with RWP_{FD} (**Figure 3.23**). Taken into consideration these results and ones illustrated in section 3.18, the effect of *Aglianico del Vulture* red wine powder on ROS and $NO^{\bullet}$ levels could occur through the citrate pathway suppression together with a direct inhibition of NF-κB, which controls the expression of ACLY, but also the expression of *NADPH oxidase* and *iNOS* genes respectively [121, 122].

3.21 *Aglianico del Vulture* red wine powder reduces PGE_2 levels: involvement of the citrate pathway

Then, the focus was set on the other inflammatory mediator downstream the citrate pathway, the prostaglandin E_2. PGE_2 levels were measured in cell culture supernatants after 48 hours of incubation with LPS (**Figure 3.24**).

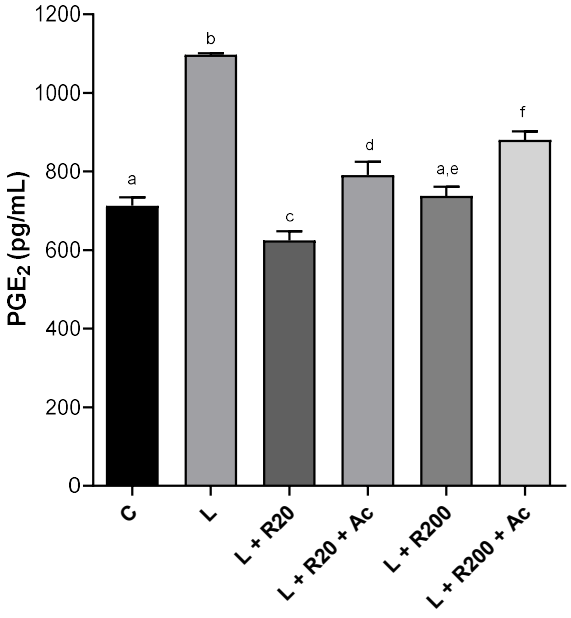

Figure 3.24. RWP lowered PGE_2 levels. Primary human monocytes were activated to macrophages with LPS (L) in absence or in presence of RWP_{FD} alone or plus acetate. Following 48 hours, PGE_2 levels were evaluated and expressed as percentage of the levels in untreated cells (set at 100%). Mean values ± SD of three replicate independent experiments with three replicates in each are shown. According to *one-way* ANOVA, differences were significant ($p<0.001$). Therefore, *Tukey's post hoc test* was performed and different letters indicate significant differences between treatments at $p<0.05$. Abbreviations: C, control; L, LPS; R20, RWP_{FD} 20 µg/mL; R200, RWP_{FD} 200 µg/mL; Ac, acetate.

3.22 *Aglianico del Vulture* red wine powder inhibits COX2

Taking into consideration the ability of RWP to reduce PGE_2 inflammatory mediator, the attention was then placed on the enzyme COX2 responsible for its synthesis. It is well known that wine polyphenols inhibit COX2 in LPS-induced inflammation, indeed we found an increase in COX2 protein levels after activation with LPS (**Figure 3.25a**).

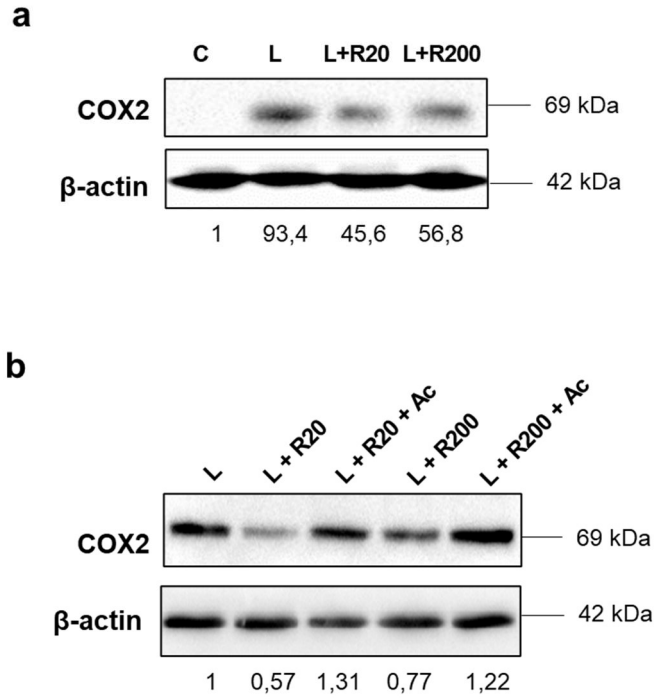

Figure 3.25. RWP lowered COX2 levels. Primary human monocytes were activated to macrophages with LPS (L) in absence or in presence of RWP_{FD} alone or plus acetate and COX2 levels were quantified. COX2 and β-actin proteins were immunodecorated with specific antibodies. The intensities of immunolabeled protein bands were measured by using a quantitative software and normalized to β-actin; values obtained are reported under western blot images. Protein expression levels in control sample were taken as 1 and other samples were expressed in proportion to the control. Abbreviations: C, control; L, LPS; R20, RWP_{FD} 20 µg/mL; R200, RWP_{FD} 200 µg/mL; Ac, acetate.

The powder of *Aglianico del Vulture* at 20 µg/mL as well as 200 µg/mL reduced COX2 expression levels almost the half with respect to macrophages activated only with LPS (**Figure 3.25a**). The strongest reduction was observed with the lowest tested concentration of RWP_{FD}, 20 µg/mL (**Figure 3.25a**). Interestingly, acetate, a metabolite downstream of the citrate pathway, reverted the inhibition of COX2 induced by RWP_{FD} (**Figure 3.25b**), with a trend similar to those observed in PGE_2 levels and illustrated in the previous paragraph.

3.23*Aglianico del Vulture* red wine powder modulates expression of pro-resolutive AnxA1/FPR2 axis

Finally, our attention was placed on the effect of RWP_{FD} on AnxA1/FPR2 axis in LPS-induced macrophages. AnnexinA1 is a pro-resolutive protein induced and activated during inflammation with the scope to limit tissue damage and to restore homeostasis through activation of Formyl Peptide Receptor 2 [93].

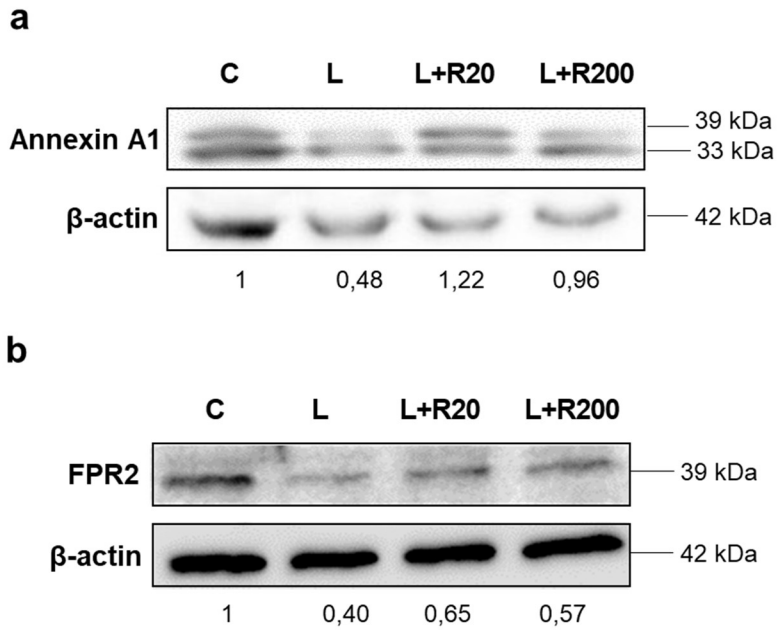

Figure 3.26. RWP_{FD} significantly restored AnxA1 expression. Primary human monocytes were incubated with RWP_{FD} 20 µg/mL or RWP_{FD} 200 µg/mL and activated with 1 µg/mL LPS. Expression of AnxA1 (a) and FPR2 (b) was assessed following 24 hours treatment with LPS. The intensities of immunolabeled protein bands were measured by using a quantitative software and normalized to β-actin; values obtained are reported under western blot images. Protein expression levels in control sample were taken as 1 and other samples were expressed in proportion to the control. Abbreviations: C, control; L, LPS; R20, RWP_{FD} 20 µg/mL; R200, RWP_{FD} 200 µg/mL.

We observed that the treatment with LPS reduced total AnxA1 expression. RWP_{FD}, at both concentrations tested, was able to restore AnxA1 physiological amount, thus preventing cells to undergo excessive inflammation (**Figure 3.26a**). In addition, FPR2 was downregulated by LPS administration (**Figure 3.26b**). Although not significantly, RWP slightly increased FPR2 expression (**Figure 3.26b**).

4 DISCUSSION

Immune response and metabolism have been considered for a long time as two independent cell functions. During the last decades, increasing amount of evidence has demonstrated a strong interaction between immunity and energy metabolism such as the new field ‘‘immunometabolism’’ has born. In LPS-activated macrophages, the inflammatory response is characterized by a metabolic reprogramming affecting both the release of pro-inflammatory mediators and activation of the transcription of numerous pro-inflammatory genes. Among them, the mitochondrial citrate carrier and ATP citrate lyase, both involved in the metabolism of citrate, are upregulated as well as the concentration of cytosolic citrate is increased [1, 51, 54, 70]. The gene silencing or inhibition of CIC or ACLY causes a reduction of inflammatory mediators, namely ROS, NO and PGE2 [1, 51, 70]. ACLY acts immediately downstream to CIC, but in activated macrophages unexpectedly ACLY is activated earlier than CIC. Indeed, CIC is activated 24 hours after LPS-stimulation in macrophages from peripheral blood as well as in U937 cells [7].

We found that ACLY reached a peak in its protein level after only 1 hour of LPS stimulation while the first increase in mRNA was after 3 hours. It could be hypnotized that CIC function needs only when the cytosolic citrate is depleted following the quick ACLY activation, although molecular mechanisms need to be clarified. One hypothesis could be related to a possible involvement of acetyl-CoA derived from the citrate cleavage in acetylation; thus, ACLY could generate acetyl-CoA for epigenetic modifications on protein involved in inflammatory cascade. In fact, we demonstrated that human macrophages derived from PBMCs, when activated by LPS, require a short-term ACLY activation to sustain histone acetylation and switch on the chromatin structure in order to trigger the transcription of several proinflammatory genes, namely *IL-1β, IL6* and *PTGS2*.

Interestingly, we found an early upregulation of ACLY in murine macrophages. It means that the citrate pathway has a key role also in immune cells from other species. Although there is still much to do to have a complete overview of the molecular mechanism of citrate pathway and immunometabolism.

For the first time we have investigated the biological activity of *Aglianico del Vulture* red wine. We have demonstrated its health promoting features exerted by phenolic compounds with well-known immunomodulatory and anti-inflammatory properties [87-92, 123-126]. The most abundant secondary metabolites identified in *Aglianico del Vulture* were malvidin

3-*O*-glucoside and cyanidin 3-*O*-glucoside. These results are in accordance with the typical anthocyanin profiling of *Aglianico* red wine in which malvidin 3-*O*-glucoside is about 60% while cyanidin 3-*O*-glucoside and delphinidin 3-*O*-glucoside represent 5% of total anthocyanidins [114]. Each wine has its typical profile of phenolic compounds that defines its characteristics. When we compared the composition of *Aglianico del Vulture* with one of other wine we found several differences. For example, malvidin 3-*O*-glucoside, cyanidin 3-*O*-glucoside and delphinidin 3-*O*-glucoside were present in higher concentration with respect to *Carignano del Sulcis* DOC red wine, cultivated in the southwestern region of Sardinia (Italy) [108]. In our sample, the concentration of resveratrol was lower (0.053 ± 0.01 mg/100 mL) than that of red wines from Veneto region (Italy), in which resveratrol averaged 0.083 mg/100 mL [127], and Campania region (Italy) [117]. On the other hand, quercetin was more abundant in *Aglianico del Vulture* red wine, compared to red wines from Campania, in particular with respect to *Aglianico del Benevento* [117]. Finally, higher levels of caffeic acid were found in *Aglianico del Vulture* in comparison with wines renowned for anti-inflammatory properties for their content in phenolic compounds such as Cabernet Sauvignon, Merlot, Syrah and Carménère [124].

Experiments aimed to evaluate immunomodulatory proprieties of *Aglianico del Vulture* powder were performed on human macrophages derived from PBMCs activated with LPS. *Aglianico del Vulture* powder reduced the secretion of pro-inflammatory cytokines IL-1β, IL-6 and TNF-α. On the other hand, RWP induced an increased release of IL-10, necessary to initiate host defence against microbial invasion [2]. These data are according to the rescuing effect exerted by RWP on AnxA1 levels, which were decreased upon LPS activation. AnxA1/FPR2 axis is implicated in resolution of inflammation, thus RWP could modulate inflammatory response with an alternative mechanism to fight against uncontrolled inflammation resulting in chronic disease following unbalance between inflammation and resolution [128].

Different studies reported that polyphenols from red grapes and wines could abrogate the LPS-mediated activation of NF-κB with consequent attenuation of the storm of pro-inflammatory cytokines released by monocytes [129]. NF-κB pathway is a critical target for the protective properties of a moderate wine consumption. When we evaluated the effect of RWP on NF-κB transcription factor, as was to be expected, we found that RWP reduced-the

expression of p65 subunit of NF-κB, promoter activity and nuclear translocation of NF-κB. As consequence of NF-κB inhibition, *SLC25A1* and *ACLY* gene promoter activities lowered with consequent reduction in CIC and ACLY protein levels; a parallel decrease in cytosolic citrate concentration and inflammatory mediators linked to the citrate pathway (ROS, $NO^{\bullet}$ and PGE2) was observed. Obviously, the effect of the tested powder on ROS, $NO^{\bullet}$ and PGE2 could also be a consequence of the direct inhibition of NF-κB since under its transcriptional controls are genes encoding for iNOS and COX2, responsible for their synthesis. However, the role of the citrate pathway is noteworthy. Indeed, treatments with metabolites downstream the citrate pathway removed RWP inhibitory effects on pro-inflammatory mediators: exogenous malate alone or in combination with NADPH reverted the reduction of ROS and $NO^{\bullet}$ levels; acetate did the same on PGE_2 concentration and COX2 expression levels. Analogous involvement of the citrate pathway was found in Down syndrome, where hydroxycitrate – a natural ACLY inhibitor – reduced the typical pro-oxidant status, but the addition of malate or NADPH abolished its antioxidant effect [76].

Interestingly, RWP reduced the acetylation of H3 histone. Acetyl-CoA, a product of the citrate pathway needed for histone acetylation [96], represents a key node in metabolism due to its intersection with many metabolic pathways and transformations, influencing the regulation of numerous life processes.

In addition to the effect on the citrate pathway, compounds contained in *Aglianico del Vulture* red wine might have other beneficial effect. In fact, it is known that increasing of cytokines IL-1β and TNF-α, with subsequent increased expression of adhesion molecules, contributes to lipid accumulation within the atheroma and dysregulated activity of vascular smooth muscle cells [130]. Thus, reduction of pro-inflammatory cytokines by RWP might also positively affect the cardiovascular system. Furthermore, since inflammation and ROS may regulate several miRNAs determining the increase/decrease (i.e. oxidative stress-responsive miRNAs) [131], it could also be hypothesized that these phenolic compounds may also control the expression of some target miRNAs in both physiological and pathological conditions [132]. For example, the phytochemical epigallocatechin gallate may act as epigenetic modulator of DNA methylation and chromatin remodelling, leading to the alteration of gene expression and modification of miRNA activities [133]. Other beneficial effects, such as glucose homeostasis, mitochondrial function, energy metabolism, stress

responses, have been ascribed to phenolic compounds [134]. However, further investigations are needed to elucidate these and other potential beneficial effects of RWP.

In short, this PhD thesis study highlighted the contribution of red wine *Aglianico del Vulture* phenolic compounds in modulation of inflammatory response. Notably, this red wine has an own phenolic profile. RWP exerted its immunomodulatory activity through different pathways, including the suppression of inflammatory mediators and the inhibition of NF-κB transcription factor and the citrate pathway. Different bioactive compounds from red wines have been shown to inhibit inflammatory mediators via NF-κB [123, 125, 126].

The involvement of the citrate pathway is the strongest novelty of our study since this pathway has never been investigated so far as a possible mechanism of action for any kind of wine. We demonstrated that this pathway mediates several anti-inflammatory effects of *Aglianico del Vulture* wine. In the recent years, different studies clarified that ACLY and CIC are overexpressed in several inflammatory conditions. Therefore, the citrate pathway seems a new hopeful target of inflammation. In this context, its inhibition by phenolic compounds from red wine *Aglianico del Vulture* - as a molecular mechanism underlying the regulation of macrophage function - could reveal interesting applications in the prevention and treatment of inflammatory chronic diseases.

5 CONCLUSIONS

The anti-inflammatory and immunomodulatory proprieties of *Aglianico del Vulture* red wine have never been investigated so far. Therefore, for the first time, we revealed the capacity a red wine powder obtained from *Aglianico del Vulture* to dampen the inflammatory process and to activate pro-resolutive pathway with the aim to restore the homeostasis. Phenolic compounds identified in *Aglianico del Vulture* red wine powder were anthocyanidins (delphinidin 3-O-glucoside, cyanidin-3-O-glucoside, and malvidin 3-O-glucoside), phenolic acids (caffeic acid and p-coumaric acid), stilbenes (resveratrol), and flavonols (quercetin) (**Figure 5.1**).

In LPS-triggered macrophages, RWP reduces the secretion of pro-inflammatory cytokines IL-1β, IL-6 and TNF-α while increases anti-inflammatory IL-10 cytokine production (**Figure 5.1**).

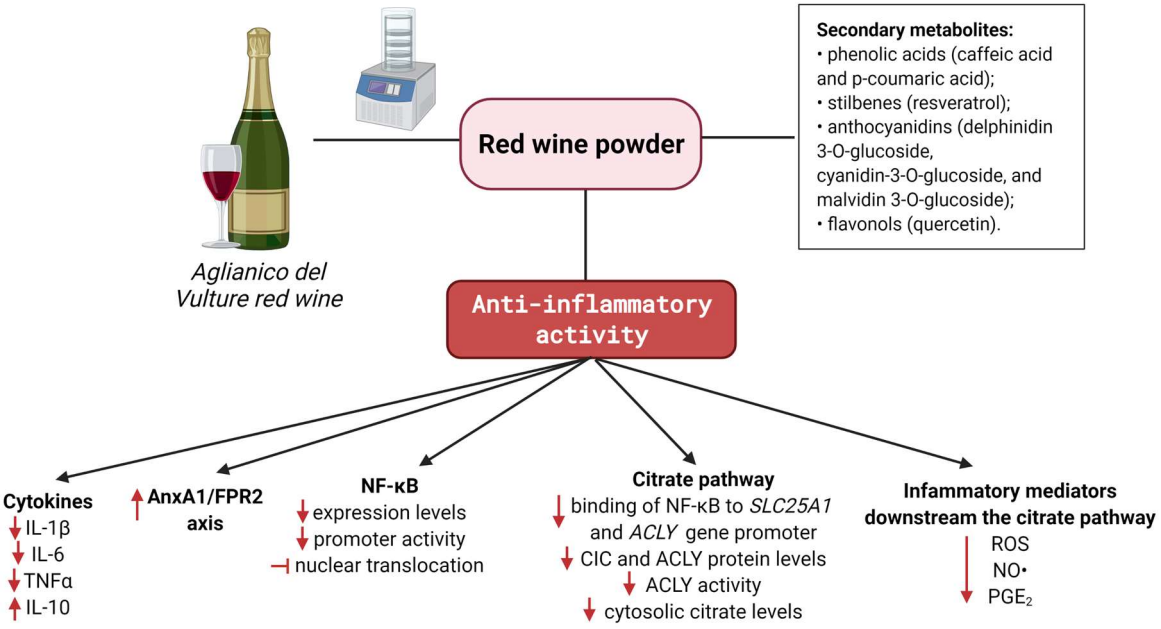

Figure 5.1: *Aglianico del Vulture* red wine powder suppresses inflammatory pathway and activates pro-resolutive processes. *Aglianico del Vulture* red wine powder was obtained by freeze-drying. Once determined its own phenolic profiles, immunomodulatory properties were evaluated in LPS-triggered human macrophages derived from PBMCs. Beyond RWP ability to modulate classical pathway of macrophage function, such as NF-κB and AnxA1/FPR2 axis, we identified the citrate pathway as target of RWP in carrying out its anti-inflammatory activity.

Secondary metabolites from *Aglianico del Vulture* modulate NF-κB signaling pathway by inhibition of p65 expression and nuclear translocation as well as NF-κB promoter activity

(**Figure 5.1**). Moreover, RWP activates pro-resolutive pathways by restoring Annexin A1 levels (**Figure 5.1**).

Beyond these two classical pathways of macrophage function, we also identify the citrate pathway as a RWP target since it reduces CIC and ACLY protein levels, ACLY enzymatic activity, ROS, $NO^{\bullet}$, PGE2 inflammatory mediators and histone acetylation levels (**Figure 5.1**).

Overall results suggest that *Aglianico del Vulture* powder suppresses inflammation and activates pro-resolutive processes hinting the potential value of RWP in the prevention and treatment of inflammatory conditions as well as inflammatory chronic diseases.

REFERENCES

1. Infantino, V.; Convertini, P.; Cucci, L.; Panaro, M. A.; Di Noia, M. A.; Calvello, R.; Palmieri, F.; Iacobazzi, V., The mitochondrial citrate carrier: a new player in inflammation. *Biochem J* **2011,** 438, (3), 433-6.

2. Medzhitov, R., Origin and physiological roles of inflammation. *Nature* **2008,** 454, (7203), 428-35.

3. Medzhitov, R., Inflammation 2010: new adventures of an old flame. *Cell* **2010,** 140, (6), 771-6.

4. Channon, K. M.; Qian, H.; George, S. E., Nitric oxide synthase in atherosclerosis and vascular injury: insights from experimental gene therapy. *Arterioscler Thromb Vasc Biol* **2000,** 20, (8), 1873-81.

5. Ferrero-Miliani, L.; Nielsen, O. H.; Andersen, P. S.; Girardin, S. E., Chronic inflammation: importance of NOD2 and NALP3 in interleukin-1beta generation. *Clin Exp Immunol* **2007,** 147, (2), 227-35.

6. Panayi, G. S.; Corrigall, V. M.; Henderson, B., Stress cytokines: pivotal proteins in immune regulatory networks; Opinion. *Curr Opin Immunol* **2004,** 16, (4), 531-4.

7. Scheibner, K. A.; Lutz, M. A.; Boodoo, S.; Fenton, M. J.; Powell, J. D.; Horton, M. R., Hyaluronan fragments act as an endogenous danger signal by engaging TLR2. *J Immunol* **2006,** 177, (2), 1272-81.

8. Schonthaler, H. B.; Guinea-Viniegra, J.; Wagner, E. F., Targeting inflammation by modulating the Jun/AP-1 pathway. *Ann Rheum Dis* **2011,** 70 Suppl 1, i109-12.

9. Wang, A.; Al-Kuhlani, M.; Johnston, S. C.; Ojcius, D. M.; Chou, J.; Dean, D., Transcription factor complex AP-1 mediates inflammation initiated by Chlamydia pneumoniae infection. *Cellular Microbiology* **2013,** 15, (5), 779-794.

10. Ghosh, S.; May, M. J.; Kopp, E. B., NF-kappa B and Rel proteins: evolutionarily conserved mediators of immune responses. *Annu Rev Immunol* **1998,** 16, 225-60.

11. Beg, A. A.; Finco, T. S.; Nantermet, P. V.; Baldwin, A. S., Jr., Tumor necrosis factor and interleukin-1 lead to phosphorylation and loss of I kappa B alpha: a mechanism for NF-kappa B activation. *Mol Cell Biol* **1993,** 13, (6), 3301-10.

12. Takeuchi, O.; Akira, S., Pattern recognition receptors and inflammation. *Cell* **2010,** 140, (6), 805-20.

13. Kelly, B.; O'Neill, L. A., Metabolic reprogramming in macrophages and dendritic cells in innate immunity. *Cell Res* **2015,** 25, (7), 771-84.

14. Pearce, E. J.; Everts, B., Dendritic cell metabolism. *Nat Rev Immunol* **2015,** 15, (1), 18-29.

15. Wynn, T. A.; Chawla, A.; Pollard, J. W., Macrophage biology in development, homeostasis and disease. *Nature* **2013,** 496, (7446), 445-55.

16. Gordon, S., Alternative activation of macrophages. *Nat Rev Immunol* **2003,** 3, (1), 23-35.

17. Sica, A.; Mantovani, A., Macrophage plasticity and polarization: in vivo veritas. *J Clin Invest* **2012,** 122, (3), 787-95.

18. Mackaness, G. B., Cellular resistance to infection. *J Exp Med* **1962,** 116, 381-406.

19. Nathan, C. F.; Murray, H. W.; Wiebe, M. E.; Rubin, B. Y., Identification of interferon-gamma as the lymphokine that activates human macrophage oxidative metabolism and antimicrobial activity. *J Exp Med* **1983,** 158, (3), 670-89.

20. Stein, M.; Keshav, S.; Harris, N.; Gordon, S., Interleukin 4 potently enhances murine macrophage mannose receptor activity: a marker of alternative immunologic macrophage activation. *J Exp Med* **1992,** 176, (1), 287-92.

21. Mills, C. D.; Kincaid, K.; Alt, J. M.; Heilman, M. J.; Hill, A. M., M-1/M-2 macrophages and the Th1/Th2 paradigm. *J Immunol* **2000,** 164, (12), 6166-73.

22. Nahrendorf, M.; Swirski, F. K., Abandoning M1/M2 for a Network Model of Macrophage Function. *Circ Res* **2016,** 119, (3), 414-7.

23. Martinez, F. O.; Gordon, S., The M1 and M2 paradigm of macrophage activation: time for reassessment. *F1000Prime Rep* **2014,** 6, 13.

24. Saqib, U.; Sarkar, S.; Suk, K.; Mohammad, O.; Baig, M. S.; Savai, R., Phytochemicals as modulators of M1-M2 macrophages in inflammation. *Oncotarget* **2018,** 9, (25), 17937-17950.

25. Mosser, D. M.; Edwards, J. P., Exploring the full spectrum of macrophage activation. *Nat Rev Immunol* **2008,** 8, (12), 958-69.

26. Ley, K., M1 Means Kill; M2 Means Heal. *J Immunol* **2017,** 199, (7), 2191-2193.

27. Xue, J.; Schmidt, S. V.; Sander, J.; Draffehn, A.; Krebs, W.; Quester, I.; De Nardo, D.; Gohel, T. D.; Emde, M.; Schmidleithner, L.; Ganesan, H.; Nino-Castro, A.; Mallmann, M. R.; Labzin, L.; Theis, H.; Kraut, M.; Beyer, M.; Latz, E.; Freeman, T. C.; Ulas, T.; Schultze, J. L., Transcriptome-based network analysis reveals a spectrum model of human macrophage activation. *Immunity* **2014,** 40, (2), 274-88.

28. Mathis, D.; Shoelson, S. E., Immunometabolism: an emerging frontier. *Nat Rev Immunol* **2011,** 11, (2), 81.

29. O'Neill, L. A.; Kishton, R. J.; Rathmell, J., A guide to immunometabolism for immunologists. *Nat Rev Immunol* **2016,** 16, (9), 553-65.

30. O'Neill, L. A.; Pearce, E. J., Immunometabolism governs dendritic cell and macrophage function. *J Exp Med* **2016,** 213, (1), 15-23.

31. Galvan-Pena, S.; O'Neill, L. A., Metabolic reprograming in macrophage polarization. *Front Immunol* **2014,** 5, 420.

32. Krawczyk, C. M.; Holowka, T.; Sun, J.; Blagih, J.; Amiel, E.; DeBerardinis, R. J.; Cross, J. R.; Jung, E.; Thompson, C. B.; Jones, R. G.; Pearce, E. J., Toll-like receptor-induced changes in glycolytic metabolism regulate dendritic cell activation. *Blood* **2010,** 115, (23), 4742-9.

33. Warburg, O., On the origin of cancer cells. *Science* **1956,** 123, (3191), 309-14.

34. Freemerman, A. J.; Johnson, A. R.; Sacks, G. N.; Milner, J. J.; Kirk, E. L.; Troester, M. A.; Macintyre, A. N.; Goraksha-Hicks, P.; Rathmell, J. C.; Makowski, L., Metabolic reprogramming of macrophages: glucose transporter 1 (GLUT1)-mediated glucose metabolism drives a proinflammatory phenotype. *J Biol Chem* **2014,** 289, (11), 7884-96.

35. Nagy, C.; Haschemi, A., Time and Demand are Two Critical Dimensions of Immunometabolism: The Process of Macrophage Activation and the Pentose Phosphate Pathway. *Front Immunol* **2015,** 6, 164.

36. Medzhitov, R.; Horng, T., Transcriptional control of the inflammatory response. *Nat Rev Immunol* **2009,** 9, (10), 692-703.

37. Jha, A. K.; Huang, S. C.; Sergushichev, A.; Lampropoulou, V.; Ivanova, Y.; Loginicheva, E.; Chmielewski, K.; Stewart, K. M.; Ashall, J.; Everts, B.; Pearce, E. J.; Driggers, E. M.; Artyomov, M. N., Network integration of parallel metabolic and transcriptional data reveals metabolic modules that regulate macrophage polarization. *Immunity* **2015,** 42, (3), 419-30.

38. O'Neill, L. A., A broken krebs cycle in macrophages. *Immunity* **2015,** 42, (3), 393-4.

39. Michelucci, A.; Cordes, T.; Ghelfi, J.; Pailot, A.; Reiling, N.; Goldmann, O.; Binz, T.; Wegner, A.; Tallam, A.; Rausell, A.; Buttini, M.; Linster, C. L.; Medina, E.; Balling, R.; Hiller, K., Immune-responsive gene 1 protein links metabolism to immunity by catalyzing itaconic acid production. *Proc Natl Acad Sci U S A* **2013,** 110, (19), 7820-5.

40. Mills, E. L.; Kelly, B.; Logan, A.; Costa, A. S. H.; Varma, M.; Bryant, C. E.; Tourlomousis, P.; Dabritz, J. H. M.; Gottlieb, E.; Latorre, I.; Corr, S. C.; McManus, G.; Ryan, D.; Jacobs, H. T.; Szibor, M.; Xavier, R. J.; Braun, T.; Frezza, C.; Murphy, M. P.; O'Neill, L. A., Succinate Dehydrogenase Supports Metabolic Repurposing of Mitochondria to Drive Inflammatory Macrophages. *Cell* **2016,** 167, (2), 457-470 e13.

41. Blouin, C. C.; Page, E. L.; Soucy, G. M.; Richard, D. E., Hypoxic gene activation by lipopolysaccharide in macrophages: implication of hypoxia-inducible factor 1alpha. *Blood* **2004,** 103, (3), 1124-30.

42. Chen, C.; Pore, N.; Behrooz, A.; Ismail-Beigi, F.; Maity, A., Regulation of glut1 mRNA by hypoxia-inducible factor-1. Interaction between H-ras and hypoxia. *J Biol Chem* **2001,** 276, (12), 9519-25.

43. Semenza, G. L.; Jiang, B. H.; Leung, S. W.; Passantino, R.; Concordet, J. P.; Maire, P.; Giallongo, A., Hypoxia response elements in the aldolase A, enolase 1, and lactate dehydrogenase A gene promoters contain essential binding sites for hypoxia-inducible factor 1. *J Biol Chem* **1996,** 271, (51), 32529-37.

44. Tannahill, G. M.; Curtis, A. M.; Adamik, J.; Palsson-McDermott, E. M.; McGettrick, A. F.; Goel, G.; Frezza, C.; Bernard, N. J.; Kelly, B.; Foley, N. H.; Zheng, L.; Gardet, A.; Tong, Z.; Jany, S. S.; Corr, S. C.; Haneklaus, M.; Caffrey, B. E.; Pierce, K.; Walmsley, S.; Beasley, F. C.; Cummins, E.; Nizet, V.; Whyte, M.; Taylor, C. T.; Lin, H.; Masters, S. L.; Gottlieb, E.; Kelly, V. P.; Clish, C.; Auron, P. E.; Xavier, R. J.; O'Neill, L. A., Succinate is an inflammatory signal that induces IL-1beta through HIF-1alpha. *Nature* **2013,** 496, (7444), 238-42.

45. Lampropoulou, V.; Sergushichev, A.; Bambouskova, M.; Nair, S.; Vincent, E. E.; Loginicheva, E.; Cervantes-Barragan, L.; Ma, X.; Huang, S. C.; Griss, T.; Weinheimer, C. J.; Khader, S.; Randolph, G. J.; Pearce, E. J.; Jones, R. G.; Diwan, A.; Diamond, M. S.; Artyomov, M. N., Itaconate Links Inhibition of Succinate Dehydrogenase with Macrophage Metabolic Remodeling and Regulation of Inflammation. *Cell Metab* **2016,** 24, (1), 158-66.

46. Mills, E. L.; Ryan, D. G.; Prag, H. A.; Dikovskaya, D.; Menon, D.; Zaslona, Z.; Jedrychowski, M. P.; Costa, A. S. H.; Higgins, M.; Hams, E.; Szpyt, J.; Runtsch, M. C.; King, M. S.; McGouran, J. F.; Fischer, R.; Kessler, B. M.; McGettrick, A. F.; Hughes, M. M.; Carroll, R. G.; Booty, L. M.; Knatko, E. V.; Meakin, P. J.; Ashford, M. L. J.; Modis, L. K.; Brunori, G.; Sevin, D. C.; Fallon, P. G.; Caldwell, S. T.; Kunji, E. R. S.; Chouchani, E. T.; Frezza, C.; Dinkova-Kostova, A. T.; Hartley, R. C.; Murphy, M. P.; O'Neill, L. A., Itaconate is an anti-inflammatory metabolite that activates Nrf2 via alkylation of KEAP1. *Nature* **2018,** 556, (7699), 113-117.

47. Everts, B.; Amiel, E.; van der Windt, G. J.; Freitas, T. C.; Chott, R.; Yarasheski, K. E.; Pearce, E. L.; Pearce, E. J., Commitment to glycolysis sustains survival of NO-producing inflammatory dendritic cells. *Blood* **2012,** 120, (7), 1422-31.

48. Pell, V. R.; Chouchani, E. T.; Frezza, C.; Murphy, M. P.; Krieg, T., Succinate metabolism: a new therapeutic target for myocardial reperfusion injury. *Cardiovasc Res* **2016,** 111, (2), 134-41.

49. Feingold, K. R.; Shigenaga, J. K.; Kazemi, M. R.; McDonald, C. M.; Patzek, S. M.; Cross, A. S.; Moser, A.; Grunfeld, C., Mechanisms of triglyceride accumulation in activated macrophages. *J Leukoc Biol* **2012,** 92, (4), 829-39.

50. Im, S. S.; Yousef, L.; Blaschitz, C.; Liu, J. Z.; Edwards, R. A.; Young, S. G.; Raffatellu, M.; Osborne, T. F., Linking lipid metabolism to the innate immune response in macrophages through sterol regulatory element binding protein-1a. *Cell Metab* **2011,** 13, (5), 540-9.

51. Infantino, V.; Iacobazzi, V.; Palmieri, F.; Menga, A., ATP-citrate lyase is essential for macrophage inflammatory response. *Biochem Biophys Res Commun* **2013,** 440, (1), 105-11.

52. Thwe, P. M.; Pelgrom, L. R.; Cooper, R.; Beauchamp, S.; Reisz, J. A.; D'Alessandro, A.; Everts, B.; Amiel, E., Cell-Intrinsic Glycogen Metabolism Supports Early Glycolytic Reprogramming Required for Dendritic Cell Immune Responses. *Cell Metab* **2017,** 26, (3), 558-567 e5.

53. Loftus, R. M.; Finlay, D. K., Immunometabolism: Cellular Metabolism Turns Immune Regulator. *J Biol Chem* **2016,** 291, (1), 1-10.

54. Iacobazzi, V.; Infantino, V., Citrate--new functions for an old metabolite. *Biol Chem* **2014,** 395, (4), 387-99.

55. Yalcin, A.; Telang, S.; Clem, B.; Chesney, J., Regulation of glucose metabolism by 6-phosphofructo-2-kinase/fructose-2,6-bisphosphatases in cancer. *Exp Mol Pathol* **2009,** 86, (3), 174-9.

56. Palmieri, F., The mitochondrial transporter family (SLC25): physiological and pathological implications. *Pflugers Arch* **2004,** 447, (5), 689-709.

57. Gnoni, G. V.; Priore, P.; Geelen, M. J.; Siculella, L., The mitochondrial citrate carrier: metabolic role and regulation of its activity and expression. *IUBMB Life* **2009,** 61, (10), 987-94.

58. Kaplan, R. S., Structure and function of mitochondrial anion transport proteins. *J Membr Biol* **2001,** 179, (3), 165-83.

59. Wellen, K. E.; Hatzivassiliou, G.; Sachdeva, U. M.; Bui, T. V.; Cross, J. R.; Thompson, C. B., ATP-citrate lyase links cellular metabolism to histone acetylation. *Science* **2009,** 324, (5930), 1076-80.

60. Iacobazzi, V.; Lauria, G.; Palmieri, F., Organization and sequence of the human gene for the mitochondrial citrate transport protein. *DNA Seq* **1997,** 7, (3-4), 127-39.

61. Stoffel, M.; Karayiorgou, M.; Espinosa, R., 3rd; Beau, M. M., The human mitochondrial citrate transporter gene (SLC20A3) maps to chromosome band 22q11 within a region implicated in DiGeorge syndrome, velo-cardio-facial syndrome and schizophrenia. *Hum Genet* **1996,** 98, (1), 113-5.

62. Kaplan, R. S.; Mayor, J. A.; Wood, D. O., The mitochondrial tricarboxylate transport protein. cDNA cloning, primary structure, and comparison with other mitochondrial transport proteins. *J Biol Chem* **1993,** 268, (18), 13682-90.

63. Zara, V.; Dolce, V.; Capobianco, L.; Ferramosca, A.; Papatheodorou, P.; Rassow, J.; Palmieri, F., Biogenesis of eel liver citrate carrier (CIC): negative charges can substitute for positive charges in the presequence. *J Mol Biol* **2007,** 365, (4), 958-67.

64. Zara, V.; Ferramosca, A.; Papatheodorou, P.; Palmieri, F.; Rassow, J., Import of rat mitochondrial citrate carrier (CIC) at increasing salt concentrations promotes presequence binding to import receptor Tom20 and inhibits membrane translocation. *J Cell Sci* **2005,** 118, (Pt 17), 3985-95.

65. Zara, V.; Ferramosca, A.; Palmisano, I.; Palmieri, F.; Rassow, J., Biogenesis of rat mitochondrial citrate carrier (CIC): the N-terminal presequence facilitates the solubility of the preprotein but does not act as a targeting signal. *J Mol Biol* **2003,** 325, (2), 399-408.

66. Ferramosca, A.; Zara, V., Dietary fat and hepatic lipogenesis: mitochondrial citrate carrier as a sensor of metabolic changes. *Adv Nutr* **2014,** 5, (3), 217-25.

67. Chypre, M.; Zaidi, N.; Smans, K., ATP-citrate lyase: a mini-review. *Biochem Biophys Res Commun* **2012,** 422, (1), 1-4.

68. Pinkosky, S. L.; Groot, P. H. E.; Lalwani, N. D.; Steinberg, G. R., Targeting ATP-Citrate Lyase in Hyperlipidemia and Metabolic Disorders. *Trends Mol Med* **2017,** 23, (11), 1047-1063.

69. Wei, J.; Leit, S.; Kuai, J.; Therrien, E.; Rafi, S.; Harwood, H. J., Jr.; DeLaBarre, B.; Tong, L., An allosteric mechanism for potent inhibition of human ATP-citrate lyase. *Nature* **2019,** 568, (7753), 566-570.

70. Infantino, V.; Iacobazzi, V.; Menga, A.; Avantaggiati, M. L.; Palmieri, F., A key role of the mitochondrial citrate carrier (SLC25A1) in TNFalpha- and IFNgamma-triggered inflammation. *Biochim Biophys Acta* **2014,** 1839, (11), 1217-1225.

71. Williams, N. C.; O'Neill, L. A. J., A Role for the Krebs Cycle Intermediate Citrate in Metabolic Reprogramming in Innate Immunity and Inflammation. *Front Immunol* **2018,** 9, 141.

72. Daskalaki, M. G.; Tsatsanis, C.; Kampranis, S. C., Histone methylation and acetylation in macrophages as a mechanism for regulation of inflammatory responses. *J Cell Physiol* **2018,** 233, (9), 6495-6507.

73. Li, T.; Garcia-Gomez, A.; Morante-Palacios, O.; Ciudad, L.; Ozkaramehmet, S.; Van Dijck, E.; Rodriguez-Ubreva, J.; Vaquero, A.; Ballestar, E., SIRT1/2 orchestrate acquisition of DNA methylation and loss of histone H3 activating marks to prevent premature activation of inflammatory genes in macrophages. *Nucleic Acids Res* **2020,** 48, (2), 665-681.

74. Rhee, J.; Solomon, L. A.; DeKoter, R. P., A role for ATP Citrate Lyase in cell cycle regulation during myeloid differentiation. *Blood Cells Mol Dis* **2019,** 76, 82-90.

75. Zaslona, Z.; Palsson-McDermott, E. M.; Menon, D.; Haneklaus, M.; Flis, E.; Prendeville, H.; Corcoran, S. E.; Peters-Golden, M.; O'Neill, L. A. J., The Induction of Pro-IL-1beta by Lipopolysaccharide Requires Endogenous Prostaglandin E2 Production. *J Immunol* **2017,** 198, (9), 3558-3564.

76. Convertini, P.; Menga, A.; Andria, G.; Scala, I.; Santarsiero, A.; Castiglione Morelli, M. A.; Iacobazzi, V.; Infantino, V., The contribution of the citrate pathway to oxidative stress in Down syndrome. *Immunology* **2016,** 149, (4), 423-431.

77. Santarsiero, A.; Leccese, P.; Convertini, P.; Padula, A.; Abriola, P.; D'Angelo, S.; Bisaccia, F.; Infantino, V., New Insights into Behcet's Syndrome Metabolic Reprogramming: Citrate Pathway Dysregulation. *Mediators Inflamm* **2018,** 2018, 1419352.

78. Santarsiero, A.; Onzo, A.; Pascale, R.; Acquavia, M. A.; Coviello, M.; Convertini, P.; Todisco, S.; Marsico, M.; Pifano, C.; Iannece, P.; Gaeta, C.; D'Angelo, S.; Padula, M. C.; Bianco, G.; Infantino, V.; Martelli, G., Pistacia lentiscus Hydrosol: Untargeted Metabolomic Analysis and Anti-Inflammatory Activity Mediated by NF-kappaB and the Citrate Pathway. *Oxid Med Cell Longev* **2020,** 2020, 4264815.

79. Lauterbach, M. A.; Hanke, J. E.; Serefidou, M.; Mangan, M. S. J.; Kolbe, C. C.; Hess, T.; Rothe, M.; Kaiser, R.; Hoss, F.; Gehlen, J.; Engels, G.; Kreutzenbeck, M.; Schmidt, S. V.; Christ, A.; Imhof, A.; Hiller, K.; Latz, E., Toll-like Receptor Signaling Rewires Macrophage Metabolism and Promotes Histone Acetylation via ATP-Citrate Lyase. *Immunity* **2019,** 51, (6), 997-1011 e7.

80. Tan, M.; Mosaoa, R.; Graham, G. T.; Kasprzyk-Pawelec, A.; Gadre, S.; Parasido, E.; Catalina-Rodriguez, O.; Foley, P.; Giaccone, G.; Cheema, A.; Kallakury, B.; Albanese, C.; Yi, C.; Avantaggiati, M. L., Inhibition of the mitochondrial citrate carrier, Slc25a1, reverts steatosis, glucose intolerance, and inflammation in preclinical models of NAFLD/NASH. *Cell Death Differ* **2020,** 27, (7), 2143-2157.

81. O'Neill, L. A. J.; Artyomov, M. N., Itaconate: the poster child of metabolic reprogramming in macrophage function. *Nat Rev Immunol* **2019,** 19, (5), 273-281.

82. Yu, X. H.; Zhang, D. W.; Zheng, X. L.; Tang, C. K., Itaconate: an emerging determinant of inflammation in activated macrophages. *Immunol Cell Biol* **2019,** 97, (2), 134-141.

83. Strelko, C. L.; Lu, W.; Dufort, F. J.; Seyfried, T. N.; Chiles, T. C.; Rabinowitz, J. D.; Roberts, M. F., Itaconic acid is a mammalian metabolite induced during macrophage activation. *J Am Chem Soc* **2011,** 133, (41), 16386-9.

84. Everts, B.; Amiel, E.; Huang, S. C.; Smith, A. M.; Chang, C. H.; Lam, W. Y.; Redmann, V.; Freitas, T. C.; Blagih, J.; van der Windt, G. J.; Artyomov, M. N.; Jones, R. G.; Pearce, E. L.; Pearce, E. J., TLR-driven early glycolytic reprogramming via the kinases TBK1-IKKvarepsilon supports the anabolic demands of dendritic cell activation. *Nat Immunol* **2014,** 15, (4), 323-32.

85. Assmann, N.; O'Brien, K. L.; Donnelly, R. P.; Dyck, L.; Zaiatz-Bittencourt, V.; Loftus, R. M.; Heinrich, P.; Oefner, P. J.; Lynch, L.; Gardiner, C. M.; Dettmer, K.; Finlay, D. K., Srebp-controlled glucose metabolism is essential for NK cell functional responses. *Nat Immunol* **2017,** 18, (11), 1197-1206.

86. Koivunen, P.; Hirsila, M.; Remes, A. M.; Hassinen, I. E.; Kivirikko, K. I.; Myllyharju, J., Inhibition of hypoxia-inducible factor (HIF) hydroxylases by citric acid cycle intermediates: possible links between cell metabolism and stabilization of HIF. *J Biol Chem* **2007,** 282, (7), 4524-4532.

87. Yahfoufi, N.; Alsadi, N.; Jambi, M.; Matar, C., The Immunomodulatory and Anti-Inflammatory Role of Polyphenols. *Nutrients* **2018,** 10, (11).

88. Hou, D. X.; Yanagita, T.; Uto, T.; Masuzaki, S.; Fujii, M., Anthocyanidins inhibit cyclooxygenase-2 expression in LPS-evoked macrophages: structure-activity relationship and molecular mechanisms involved. *Biochem Pharmacol* **2005,** 70, (3), 417-25.

89. Jeong, J. W.; Lee, W. S.; Shin, S. C.; Kim, G. Y.; Choi, B. T.; Choi, Y. H., Anthocyanins downregulate lipopolysaccharide-induced inflammatory responses in BV2 microglial cells by suppressing the NF-kappaB and Akt/MAPKs signaling pathways. *Int J Mol Sci* **2013,** 14, (1), 1502-15.

90. Vendrame, S.; Klimis-Zacas, D., Anti-inflammatory effect of anthocyanins via modulation of nuclear factor-kappaB and mitogen-activated protein kinase signaling cascades. *Nutr Rev* **2015,** 73, (6), 348-58.

91. Wang, H.; Cao, G.; Prior, R. L., Oxygen Radical Absorbing Capacity of Anthocyanins. *Journal of Agricultural and Food Chemistry* **1997,** 45, (2), 304-309.

92. Tsuda, T.; Shiga, K.; Ohshima, K.; Kawakishi, S.; Osawa, T., Inhibition of lipid peroxidation and the active oxygen radical scavenging effect of anthocyanin pigments isolated from Phaseolus vulgaris L. *Biochem Pharmacol* **1996,** 52, (7), 1033-9.

93. Perretti, M.; D'Acquisto, F., Annexin A1 and glucocorticoids as effectors of the resolution of inflammation. *Nat Rev Immunol* **2009,** 9, (1), 62-70.

94. Li, G.; He, S.; Chang, L.; Lu, H.; Zhang, H.; Zhang, H.; Chiu, J., GADD45α and annexin A1 are involved in the apoptosis of HL-60 induced by resveratrol. *Phytomedicine* **2011,** 18, (8), 704-709.

95. Infantino, V.; Pierri, C. L.; Iacobazzi, V., Metabolic Routes in Inflammation: The Citrate Pathway and its Potential as Therapeutic Target. *Curr Med Chem* **2019,** 26, (40), 7104-7116.

96. Shi, L.; Tu, B. P., Acetyl-CoA and the regulation of metabolism: mechanisms and consequences. *Curr Opin Cell Biol* **2015,** 33, 125-31.

97. Santarsiero, A.; Bochicchio, A.; Funicello, M.; Lupattelli, P.; Choppin, S.; Colobert, F.; Hanquet, G.; Schiavo, L.; Convertini, P.; Chiummiento, L.; Infantino, V., New synthesized polyoxygenated diarylheptanoids suppress lipopolysaccharide-induced neuroinflammation. *Biochem Biophys Res Commun* **2020,** 529, (4), 1117-1123.

98. Convertini, P.; Infantino, V.; Bisaccia, F.; Palmieri, F.; Iacobazzi, V., Role of FOXA and Sp1 in mitochondrial acylcarnitine carrier gene expression in different cell lines. *Biochem Biophys Res Commun* **2011,** 404, (1), 376-81.

99. Infantino, V.; Iacobazzi, V.; De Santis, F.; Mastrapasqua, M.; Palmieri, F., Transcription of the mitochondrial citrate carrier gene: role of SREBP-1, upregulation by insulin and downregulation by PUFA. *Biochem Biophys Res Commun* **2007,** 356, (1), 249-54.

100. Santarsiero, A.; Onzo, A.; Pascale, R.; Acquavia, M. A.; Coviello, M.; Convertini, P.; Todisco, S.; Marsico, M.; Pifano, C.; Iannece, P.; Gaeta, C.; D'Angelo, S.; Padula, M. C.; Bianco, G.; Infantino, V.; Martelli, G., Pistacia lentiscus Hydrosol: Untargeted Metabolomic Analysis and Anti-Inflammatory Activity Mediated by NF-κB and the Citrate Pathway. *Oxidative Medicine and Cellular Longevity* **2020,** 2020, 4264815.

101. Linn, T. C.; Srere, P. A., Identification of ATP citrate lyase as a phosphoprotein. *J Biol Chem* **1979,** 254, (5), 1691-8.

102. Migita, T.; Narita, T.; Nomura, K.; Miyagi, E.; Inazuka, F.; Matsuura, M.; Ushijima, M.; Mashima, T.; Seimiya, H.; Satoh, Y.; Okumura, S.; Nakagawa, K.; Ishikawa, Y.,

ATP citrate lyase: activation and therapeutic implications in non-small cell lung cancer. *Cancer Res* **2008,** 68, (20), 8547-54.

103. Pearce, N. J.; Yates, J. W.; Berkhout, T. A.; Jackson, B.; Tew, D.; Boyd, H.; Camilleri, P.; Sweeney, P.; Gribble, A. D.; Shaw, A.; Groot, P. H., The role of ATP citrate-lyase in the metabolic regulation of plasma lipids. Hypolipidaemic effects of SB-204990, a lactone prodrug of the potent ATP citrate-lyase inhibitor SB-201076. *Biochem J* **1998,** 334 (Pt 1), 113-9.

104. Horai, H.; Arita, M.; Kanaya, S.; Nihei, Y.; Ikeda, T.; Suwa, K.; Ojima, Y.; Tanaka, K.; Tanaka, S.; Aoshima, K.; Oda, Y.; Kakazu, Y.; Kusano, M.; Tohge, T.; Matsuda, F.; Sawada, Y.; Hirai, M. Y.; Nakanishi, H.; Ikeda, K.; Akimoto, N.; Maoka, T.; Takahashi, H.; Ara, T.; Sakurai, N.; Suzuki, H.; Shibata, D.; Neumann, S.; Iida, T.; Tanaka, K.; Funatsu, K.; Matsuura, F.; Soga, T.; Taguchi, R.; Saito, K.; Nishioka, T., MassBank: a public repository for sharing mass spectral data for life sciences. *J Mass Spectrom* **2010,** 45, (7), 703-14.

105. Aversano, R.; Contaldi, F.; Adelfi, M. G.; D'Amelia, V.; Diretto, G.; De Tommasi, N.; Vaccaro, C.; Vassallo, A.; Carputo, D., Comparative metabolite and genome analysis of tuber-bearing potato species. *Phytochemistry* **2017,** 137, 42-51.

106. Caddeo, C.; Nacher, A.; Vassallo, A.; Armentano, M. F.; Pons, R.; Fernandez-Busquets, X.; Carbone, C.; Valenti, D.; Fadda, A. M.; Manconi, M., Effect of quercetin and resveratrol co-incorporated in liposomes against inflammatory/oxidative response associated with skin cancer. *Int J Pharm* **2016,** 513, (1-2), 153-163.

107. Chirollo, C.; Vassallo, A.; Dal Piaz, F.; Lamagna, B.; Tortora, G.; Neglia, G.; De Tommasi, N.; Severino, L., Investigation of the Persistence of Penicillin G and Dihydrostreptomycin Residues in Milk of Lactating Buffaloes (Bubalus bubalis) Using Ultra-High-Performance Liquid Chromatography and Tandem Mass Spectrometry. *J Agric Food Chem* **2018,** 66, (25), 6388-6393.

108. Tuberoso, C. I. G.; Serreli, G.; Congiu, F.; Montoro, P.; Fenu, M. A., Characterization, phenolic profile, nitrogen compounds and antioxidant activity of Carignano wines. *Journal of Food Composition and Analysis* **2017,** 58, 60-68.

109. Tuberoso, C. I. G.; Serreli, G.; Montoro, P.; D'Urso, G.; Congiu, F.; Kowalczyk, A., Biogenic amines and other polar compounds in long aged oxidized Vernaccia di Oristano white wines. *Food Research International* **2018,** 111, 97-103.

110. Akira, S.; Takeda, K., Toll-like receptor signalling. *Nat Rev Immunol* **2004,** 4, (7), 499-511.

111. Schutze, S.; Wiegmann, K.; Machleidt, T.; Kronke, M., TNF-induced activation of NF-kappa B. *Immunobiology* **1995,** 193, (2-4), 193-203.

112. Lauterbach, M. A.; Hanke, J. E.; Serefidou, M.; Mangan, M. S. J.; Kolbe, C. C.; Hess, T.; Rothe, M.; Kaiser, R.; Hoss, F.; Gehlen, J.; Engels, G.; Kreutzenbeck, M.; Schmidt, S. V.; Christ, A.; Imhof, A.; Hiller, K.; Latz, E., Toll-like Receptor

Signaling Rewires Macrophage Metabolism and Promotes Histone Acetylation via ATP-Citrate Lyase. *Immunity* **2019,** 51, (6), 997-1011.e7.

113. Williams, N. C.; O'Neill, L. A., ACLY-matizing Macrophages to Histone Modification during Immunometabolic Reprogramming. *Trends Immunol* **2020,** 41, (2), 93-94.

114. Suriano, S.; Tarricone, L.; Savino, M.; Rossi, M. R., Caratterizzazione fenolica di Uve di Aglianico e Uva di Troia coltivate nel nord barese. *ENOLOGO-MILANO-* **2005,** 41, (12), 71.

115. Celotti, E.; Ferrarini, R.; Zironi, R.; Conte, L. S., Resveratrol content of some wines obtained from dried Valpolicella grapes: Recioto and Amarone. *Journal of Chromatography A* **1996,** 730, (1), 47-52.

116. Galgano, F.; Caruso, M.; Perretti, G.; Favati, F., Authentication of Italian red wines on the basis of the polyphenols and biogenic amines. *European Food Research and Technology* **2011,** 232, (5), 889-897.

117. Gambuti, A.; Strollo, D.; Ugliano, M.; Lecce, L.; Moio, L., trans-Resveratrol, quercetin, (+)-catechin, and (-)-epicatechin content in south Italian monovarietal wines: relationship with maceration time and marc pressing during winemaking. *J Agric Food Chem* **2004,** 52, (18), 5747-51.

118. Di Lorenzo, C.; Stockley, C.; Colombo, F.; Biella, S.; Orgiu, F.; Dell'Agli, M.; Restani, P., The Role of Wine in Modulating Inflammatory Processes: A Review. *Beverages* **2018,** 4, (4), 88.

119. Ghosh, S.; Hayden, M. S., New regulators of NF-kappaB in inflammation. *Nat Rev Immunol* **2008,** 8, (11), 837-48.

120. Todisco, S.; Convertini, P.; Iacobazzi, V.; Infantino, V., TCA Cycle Rewiring as Emerging Metabolic Signature of Hepatocellular Carcinoma. *Cancers (Basel)* **2019,** 12, (1).

121. Aktan, F., iNOS-mediated nitric oxide production and its regulation. *Life Sci* **2004,** 75, (6), 639-53.

122. Anrather, J.; Racchumi, G.; Iadecola, C., NF-kappaB regulates phagocytic NADPH oxidase by inducing the expression of gp91phox. *J Biol Chem* **2006,** 281, (9), 5657-67.

123. Decendit, A.; Mamani-Matsuda, M.; Aumont, V.; Waffo-Teguo, P.; Moynet, D.; Boniface, K.; Richard, E.; Krisa, S.; Rambert, J.; Merillon, J. M.; Mossalayi, M. D., Malvidin-3-O-beta glucoside, major grape anthocyanin, inhibits human macrophage-derived inflammatory mediators and decreases clinical scores in arthritic rats. *Biochem Pharmacol* **2013,** 86, (10), 1461-7.

124. Kekelidze, I.; Ebelashvili, N.; Japaridze, M.; Chankvetadze, B.; Chankvetadze, L., Phenolic antioxidants in red dessert wine produced with innovative technology. *Annals of Agrarian Science* **2018,** 16, (1), 34-38.

125. Ma, M. M.; Li, Y.; Liu, X. Y.; Zhu, W. W.; Ren, X.; Kong, G. Q.; Huang, X.; Wang, L. P.; Luo, L. Q.; Wang, X. Z., Cyanidin-3-O-Glucoside Ameliorates Lipopolysaccharide-Induced Injury Both In Vivo and In Vitro Suppression of NF-kappaB and MAPK Pathways. *Inflammation* **2015,** 38, (4), 1669-82.

126. Poulsen, M. M.; Fjeldborg, K.; Ornstrup, M. J.; Kjaer, T. N.; Nohr, M. K.; Pedersen, S. B., Resveratrol and inflammation: Challenges in translating pre-clinical findings to improved patient outcomes. *Biochim Biophys Acta* **2015,** 1852, (6), 1124-36.

127. Soleas, G. J.; Goldberg, D. M.; Ng, E.; Karumanchiri, A.; Tsang, E.; Diamandis, E. P., Comparative evaluation of four methods for assay of cis- and trans-resveratrol. *American journal of enology and viticulture* **1997,** 48, (2), 169-176.

128. Schett, G.; Neurath, M. F., Resolution of chronic inflammatory disease: universal and tissue-specific concepts. *Nature Communications* **2018,** 9, (1), 3261.

129. Magrone, T.; Jirillo, E., Polyphenols from red wine are potent modulators of innate and adaptive immune responsiveness. *Proc Nutr Soc* **2010,** 69, (3), 279-85.

130. von Scholten, B. J.; Reinhard, H.; Hansen, T. W.; Schalkwijk, C. G.; Stehouwer, C.; Parving, H. H.; Jacobsen, P. K.; Rossing, P., Markers of inflammation and endothelial dysfunction are associated with incident cardiovascular disease, all-cause mortality, and progression of coronary calcification in type 2 diabetic patients with microalbuminuria. *J Diabetes Complications* **2016,** 30, (2), 248-55.

131. Otton, R.; Bolin, A. P.; Ferreira, L. T.; Marinovic, M. P.; Rocha, A. L. S.; Mori, M. A., Polyphenol-rich green tea extract improves adipose tissue metabolism by down-regulating miR-335 expression and mitigating insulin resistance and inflammation. *J Nutr Biochem* **2018,** 57, 170-179.

132. Potenza, M. A.; Iacobazzi, D.; Sgarra, L.; Montagnani, M., The Intrinsic Virtues of EGCG, an Extremely Good Cell Guardian, on Prevention and Treatment of Diabesity Complications. *Molecules* **2020,** 25, (13).

133. Fang, M. Z.; Wang, Y.; Ai, N.; Hou, Z.; Sun, Y.; Lu, H.; Welsh, W.; Yang, C. S., Tea polyphenol (-)-epigallocatechin-3-gallate inhibits DNA methyltransferase and reactivates methylation-silenced genes in cancer cell lines. *Cancer Res* **2003,** 63, (22), 7563-70.

134. Meng, Q.; Velalar, C. N.; Ruan, R., Regulating the age-related oxidative damage, mitochondrial integrity, and antioxidative enzyme activity in Fischer 344 rats by supplementation of the antioxidant epigallocatechin-3-gallate. *Rejuvenation Res* **2008,** 11, (3), 649-60.